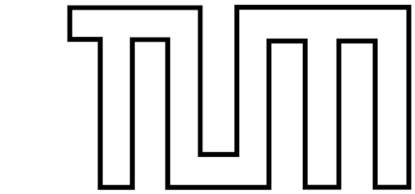

Fakultät für Chemie

Der Technischen Universität München

Tripartite Biosensors to Assess Protein Stability and Aggregation Propensity in Yeast

Veronika Sachsenhauser

Vollständiger Abdruck der von der Fakultät für Chemie der Technischen Universität München zur Erlangung des akademischen Grades eines Doktors der Naturwissenschaften (Dr. rer. nat.) genehmigten Dissertation.

Vorsitzender:		Prof. Dr. Bernd Reif
Prüfer der Dissertation:	1.	Prof. Dr. Johannes Buchner
	2.	Prof. Dr. James C. A. Bardwell

Die Dissertation wurde am 20.04.2020 bei der Technischen Universität München eingereicht und durch die Fakultät für Chemie am 26.05.2020 angenommen.

Meiner Familie

Summary

Despite the many methods available to study protein folding and aggregation in the test tube, there are relatively few tools available to study these processes in the cell. This is mainly due to the complexity of the crowded, cellular environment and its transient biochemical and biophysical changes, which make many methods, such as spectroscopic approaches, unsuitable. To enable the assessment of protein stability and solubility *in vivo*, we describe here a biosensor system that can be used in the cytosol of *Saccharomyces cerevisiae*. Our biosensor design consists of a tripartite fusion in which a protein of interest is inserted into a split antibiotic resistance protein. This approach directly links the *in vivo* stability and aggregation susceptibility of the inserted protein to the antibiotic sensitivity of the cell. We show a linear relationship between the thermodynamic stabilities of variants of the model folding protein immunity protein 7 (Im7) and the levels of antibiotic resistance conferred by tripartite fusions containing these variants in yeast. We demonstrate that the system can also be used to study the *in vivo* properties of yeast prion proteins Sup35 and Rnq1. Furthermore, we show the suitability of the biosensor for investigating proteins associated with neurodegenerative dysfunction diseases, such as the peptide amyloid beta 1-42 (Aβ42), which is involved in Alzheimer's disease, and the protein α-synuclein, which is associated with Parkinson's disease.

Zusammenfassung

Trotz der vielen Methoden, die zur Untersuchung der Proteinfaltung und -aggregation im Reagenzglas zur Verfügung stehen, gibt es relativ wenige Mittel, um diese Prozesse in der Zelle zu untersuchen. Dies liegt vor allem an der Komplexität der gedrängten, zellulären Umgebung und ihrer transienten biochemischen und biophysikalischen Veränderungen, die viele Methoden, wie z.B. spektroskopische Ansätze, ungeeignet machen. Um die Beurteilung der Proteinstabilität und -löslichkeit *in vivo* zu ermöglichen, beschreiben wir hier ein Biosensorsystem, das im Zytosol von *Saccharomyces cerevisiae* eingesetzt werden kann. Unser Biosensordesign besteht aus einer dreiteiligen Fusion, bei der ein interessierendes Protein in ein gespaltenes Antibiotikaresistenzprotein eingefügt wird. Dieser Ansatz stellt eine direkte Verbindung zwischen der *in vivo*-Stabilität und der Aggregationsanfälligkeit des eingefügten Proteins und der Antibiotika-Empfindlichkeit der Zelle her. Wir zeigen eine lineare Beziehung zwischen den thermodynamischen Stabilitäten von Varianten des Modells Faltungsprotein-Immunitätsprotein 7 (Im7) und dem Level der Antibiotikaresistenz, die durch dreigeteilte Fusionen, die diese Varianten in Hefe enthalten, verliehen wird. Wir zeigen, dass das System auch zur Untersuchung der *in vivo*-Eigenschaften der Hefeprion-Proteine Sup35 und Rnq1 verwendet werden kann. Darüber hinaus zeigen wir die Eignung des Biosensors zur Untersuchung von Proteinen, die mit neurodegenerativen Dysfunktionskrankheiten assoziiert sind, wie z.B. das Peptid Amyloid beta 1-42 (Aβ42), das bei der Alzheimer-Krankheit beteiligt ist, und das Protein α-Synuclein, das mit der Parkinson-Krankheit assoziiert ist.

Table of Contents

Index of Figures

Index of Tables

Abbreviations

Aβ42	amyloid beta 1-42
Amp	ampicillin
APH	aminoglycoside 3'-phosphotransferases
C-terminal	carboxyl-terminal
DMSO	dimethyl sulfoxide
DNA	deoxyribonucleic acid
DTT	dithiothreitol
E. coli	*Escherichia coli*
EDTA	ethylenediaminetetraacetic acid
ER	endoplasmic reticulum
FRET	Förster resonance energy transfer
FUS	fused in sarcoma
g	times gravity
g	gram
gDNA	genomic DNA
GdnHCl	guanidine hydrochloride
GFP	green fluorescent protein
Gly	glycine
GS	glycine-serine
h	hour
Hsp	heat shock protein
H_2O	water
HygMX	hygromycine B selection marker
IDP	intrinsically disordered protein
Im7	immunity protein 7
IPTG	isopropyl β-D-1-thiogalactopyranoside
Kan	kanamycin
KanMX	kanamycin selection marker
kDa	kilo Dalton
L	liter
leu	leucine
lys	lysine
m	milli
M	molar
MIC	minimum inhibitory concentration
min	minute
µ	micro
N-terminal	amino-terminal
NAT	nourseothricin N-acetyl transferase
NTC	nourseothricin

OD_{600}	optical density at 600 nm
PCR	polymerase chain reaction
PEG	polyethylene glycol
PMSF	phenylmethane sulfonyl fluoride
PQC	protein quality control
SC	synthetic complete
S. cerevisiae	*Saccharomyces cerevisiae*
SD	standard deviation
SDD-AGE	semi-denaturating detergent agarose gel electrophoresis
SDS	sodium dodecyl sulfate
SDS-PAGE	sodium dodecyl sulfate-polyacrylamide gel electrophoresis
Ser	serine
UPR	unfolded protein response
UPS	ubiquitin-proteasome system
ura	uracil
UV	ultraviolet
v v^{-1}	volume per volume
w v^{-1}	weight per volume
WT	wild type
YFP	yellow fluorescent protein
YPD	yeast extract peptone dextrose

1 Introduction

1.1 Relevance of biosensors to assess the protein folding state in the eukaryotic cell

Most proteins must fold into a well-defined three-dimensional conformation to perform their biological functions. Billions of years of evolution led to the correlation between conformational flexibility and function; however, trade-offs were apparently made to achieve this, as most proteins are only marginally stable and barely soluble when expressed under physiological conditions.[1–3] The conformation and expression level of each of the roughly 20,000 proteins in a human cell must be carefully regulated to maintain a balanced proteome.[4] Protein homeostasis, also referred to as proteostasis, is safeguarded by a network of molecular chaperones and proteolytic systems and their regulators. [5,6] Understanding the structure of this network and how it is regulated across various physiological conditions and in response to internal imbalances and exogenous insults is fundamental to a detailed understanding of how cellular life is maintained. The processes involved in protein quality control (PQC) are also medically significant since failure to maintain proteostasis is associated with several neurodegenerative illnesses, including Alzheimer's and Parkinson's disease.[4,5,7]

Protein misfolding and the formation of aggregates that cause cellular toxicity and contribute to proteostatic collapse are hallmarks of many neurodegenerative diseases.[4,5,7,8] The resulting imbalance in proteostasis can lead to cell death and hence neurodegeneration. Although different proteins have been implicated in neurodegenerative diseases, they seem to share many similarities at the subcellular level related to the abnormal protein misfolding and aggregation paradigms involved.[4,9] To date, no cure for these so called proteopathies has been found, partly because the complex molecular processes underlying pathologic misfolding and aggregation are poorly understood. *In vitro* studies on protein stability have provided valuable insight into the conformational changes underlying these pathologies. However, these experiments fall short in

replicating the transient chemical and physical changes in the cellular environment and cannot mimic the real impact of the complex cellular PQC machinery.[10,11]

One way to study neurodegenerative diseases *in vivo* is to use *Saccharomyces cerevisiae* as a model system. This unicellular organism is one of the best studied, easiest to analyze, and genetically tractable of eukaryotic organisms. Thanks to its high homology with mammals, yeast can provide mechanistic insights into the cell-autonomous mechanisms of neurodegeneration at an interactome-wide level.[12–16] Unlike with mammalian cells, a multitude of modern tools are available for this biological work horse, tools that enable systematic analysis of cellular processes and phenotypes.

Since methods to directly assess the folding state-associated function of a protein of interest are rarely available, several fusion-based approaches to indirectly assess *in vivo* stability and solubility have been devised.[15,17,18] Although valuable insights have been gained using these previously developed yeast protein misfolding reporters, their readouts for misfolding are typically indirect and commonly involve reporter-specific side effects. Limitations include overexpression-induced cytotoxicity, which may involve different mechanisms than the long-term toxicity often associated with neurodegenerative diseases, artifacts resulting from proteolysis of reporter fusions, and qualitative instead of quantitative readouts for protein stability.[19–23]

It has become clear that strategies relying on different biosensor principles provide overlapping but nevertheless different and incomplete measures for protein stability. This indicates that no single sensor can perfectly replicate the behavior of neurodegenerative-associated proteins in the cell. The inherent limitations of existing protein folding and aggregation sensors continues to drive the development of new methods based on different underlying principles. In this thesis, I describe a complementary approach—the optimization of a new protein folding biosensor platform for use in *S. cerevisiae*. By linking protein stability *in vivo* to antibiotic resistance, this biosensor allows for the sensitive assessment of protein misfolding and aggregation susceptibility in yeast. This biosensor advances the field by providing an appropriate platform for the high-throughput screening of factors affecting the folding or

aggregation propensity of multiple different neurodegeneration-associated proteins in a eukaryotic host.

1.2 Basic principles of protein folding

Protein folding is the physical process in which a polypeptide chain assumes its characteristic and functional three-dimensional structure from an unfolded state.[24] The process of folding often begins co-translationally at the ribosome when the amino acids of the newly synthesized, unfolded N terminus of the polypeptide chain start interacting with each other while the rest of the protein is still being synthesized. The intramolecular and intermolecular interactions that occur during and after biosynthesis result in the adoption of a defined, functional three-dimensional structure known as the native state.[25] The unique native structure that is adopted is defined by the protein's primary amino acid sequence, or primary sequence.[26] The native three-dimensional structure is essential for function. Since proteins evolved for function, which entails conformational flexibility, they are generally only marginally stable.[1,27] They are also typically expressed at levels close to their intrinsic solubility limits.[1,27]

1.2.1 Driving forces of protein folding

The physical process of protein folding is spontaneous and governed by intramolecular hydrophobic interactions, hydrogen bonds, and van der Waals forces, which are countered by conformational enthalpy. The folding process also depends on the interaction with and impact of surrounding factors such as binding partners, macromolecular crowding, the solvent, salt concentration, pH, and temperature.[28] An additional major driving force during folding of an amphiphilic molecule in an aqueous environment is the hydrophobic effect.[28] This phenomenon describes the tendency of non-polar surfaces to interact with each other in order to minimize their interaction with water molecules. Their interaction leads to the burial of non-polar side chains inside the protein and collapses the polypeptide into a compact, globular structure.

1.2.2 Protein folding dynamics and energy landscapes

Due to constant fluctuations, proteins populate an ensemble of conformational states.[29] The ensemble of conformations cluster into well-defined thermodynamic states that can be hierarchically arranged to form an energy landscape.[29] Increasing formation of native intramolecular contacts guides the folding path in an energetically downhill fashion on the protein's energy landscape. Protein folding results in a thermodynamically stable, native conformation with a minimized Gibbs free energy (G).[28,30] The Gibbs free energy is a thermodynamic potential that describes the maximum amount of non-expansion work that can be released through the reversible transformation from an initial to a final folding state at a constant pressure and temperature. The process of protein folding must be thermodynamically favorable, equaling a negative change in Gibbs free energy (ΔG), in order to proceed spontaneously. The change in Gibbs free energy (ΔG) is dependent on the change in enthalpy (ΔH), which is the sum of the heat released or taken up through bond formation or breakage.[28] ΔG is also dependent on the change in entropy (ΔS), which is the change in the number of possible energy distributions (adoptable conformations) in a system (disorder).[28] The relationship is defined by $\Delta G^\circ = \Delta H^\circ - T\Delta S^\circ$, where T is the temperature, where the superscript 0 indicates that the reaction is done under standard conditions.

The ensemble of conformations involves the intrinsic motions of a protein.[31] Molecular dynamics not only allow the protein to overcome small energy barriers along the folding pathway, but they often also enable the natively folded protein to execute its function. The solvent contributes to the protein's motions through dynamic interactions. Intrinsic movements like dynamic bond vibrations, side chain rotations, and loop motions proceed in the picosecond and nanosecond timescales.[29] Large-scale collective motions such as domain movements require microsecond, millisecond, and longer timescales. Most proteins fold in a timescale of milliseconds.[31] The slowest folding proteins involve proline isomerization and pass through a number of intermediate steps before they reach their native-state fold, which requires minutes to hours.

1.3 Protein misfolding and aggregation

1.3.1 Structural plasticity of proteins

As a result of billions of years of evolution for conformational flexibility to allow function, the native protein conformation is not always the most stable structure.[4,29] Some proteins appear to be fully or partially unfolded in their native state (so called intrinsically disordered proteins, or IDPs).[9] Unstable conformers can also be introduced by errors that occur during the folding process (off-pathway states) or by proteolytic cleavage fragments of larger protein complexes.[5,9] Misfolded or only partially folded proteins, commonly display hydrophobic residues and unstructured stretches that expose the polypeptide to the solvent. If they don't get refolded or proteolytically degraded, they can aggregate with other molecules in a concentration-dependent manner. These misfolded species can aggregate into different, interconvertible types of structures such as soluble oligomers, amorphous aggregates, and amyloid fibrils. A variety of distinct, self-propagating fibril structures can also be formed, which makes amyloid fibrils generally polymorphic at the molecular level.[9,32]

1.3.2 The structure and properties of amyloid fibrils

Amyloid fibrils are elongated structures that consist of parallel β-sheets oriented perpendicular to the long fibril axis.[4,9,29] An amyloid fibril is comprised of protofilaments formed by two flat β-sheets that are held together by hydrogen bonds within each β-sheet. The side chains of the parallel β-sheets inter-digitize due to van der Waals interactions between polar residues of the adjacent β-sheets (steric zipper).[9] A protofilament is typically 7–13 nm in diameter and several microns long. Amyloid fibrils form through hydrogen bonding between the β-sheets of the protofilaments, which leads to the twisting of protofilaments around one another or to their lateral association as flat ribbons.[9] The amyloid conformation of a protein can be even more stable than the native state due to extensive non-covalent bond formation within each amyloid fibril.

1.3.3 Mechanism of amyloid fibril formation

Different mechanisms of amyloid fibril formation have been described, including nucleated conformational conversion, native-like aggregation, and nucleated polymerization.[9] During the initial stages of the nucleated conformational conversion model, misfolded or metastable monomers aggregate into disordered oligomers that are soluble and only weakly stable.[9] If aggregation proceeds, the oligomers can internally reorganize and form β-sheet-rich structures. These β-sheet-rich oligomers can nucleate their growth into protofibrils through self-association and recruitment of more monomers. Further structural rearrangements within the protofibrils promotes bundling into mature fibrils with a cross-β-sheet structure. In the native-like aggregation model, early stages entail disordered aggregates or native-like aggregates that neither undergo structural rearrangements nor adopt β-sheet rich structural elements, but instead grow into large amorphous or native-like assemblies.[9] During a nucleated polymerization process, structural conversion of completely or partially disordered monomers through a thermodynamically unfavored process generates monomeric β-sheet nuclei that can directly promote fiber elongation.[9] These aggregation mechanisms should not be considered independently of each other, since certain types of conformations are involved in more than one mechanism.

1.3.4 Disease-associated protein misfolding and aggregation

Large protein aggregates, including amyloid, amorphous, or native-like assemblies, are well-defined pathological hallmarks of neurodegenerative diseases, including Alzheimer's or Parkinson's diseases.[9] Most of the aggregates associated with protein misfolding diseases consist of amyloid fibrils.[9] The pathological aggregates build up intracellularly and/or extracellularly, where the protein is normally located.[9] The involved proteins are usually small in size (< 100 amino acids) and variable in their folding state. Of the amyloid-associated proteins, ~40% fold into well-defined structures, ~25% are intrinsically disordered (in many cases, these result from proteolytic cleavage of larger proteins), ~22% of the structures are unknown, and one implicated protein adopts a globular structure with a disordered domain.[9] Amyloid aggregates are not only

able to conformationally template the conversion of other proteins of the cell into amyloids, but are also able to spread across cells. This infectious spreading ability is called prion-like behavior and is observed in the progression of many neurodegenerative diseases.[9,33,34]

1.3.5 The theory of toxic oligomers

Why amyloid formation is toxic and leads to cell death is currently not well understood. It seems likely that the toxicity associated with amyloid formation does not derive from the loss of function of the aggregated protein itself but is rather due to the structural properties of the aggregate or species on the pathway to amyloid formation.[29] Fibrillar structures were previously suspected to be responsible but now soluble oligomers are thought to be the primary toxic species due to their interactive potential—unpaired β-strands and hydrophobic residues generate a sticky surface on the oligomers that can disrupt phospholipid bilayers and interact with other cellular proteins to promote their misfolding and aggregation.[9,35] The stable oligomers are believed to be more damaging to the cell than the initially formed, unstable oligomers due to the stress level they induce in cell culture.[35,36] In the fibrillar conformation, the sticky surfaces of the molecules are buried into the interior of the fibril, making the amyloid structure less interactive. Nevertheless, fibrillar conformers do contribute to pathogenicity since they have been found to draw key cellular proteins that are themselves metastable into the assembly.[9,29] Through fragmentation, they generate monomers and oligomers, which in turn promote secondary nucleation events for fibril formation. The complex mechanisms of amyloid formation and structural amyloid polymorphisms have been well-characterized in *in vitro* studies. However, the initiation and formation of pathogenic aggregates in the cellular context is still poorly understood.

1.3.6 Mutations and altered environmental conditions can affect protein stability

The major event that facilitates the formation of potentially harmful aggregates is the loss of native state stability.[29] The native protein structure can be disturbed by a variety of intrinsic or

environmental factors.[26] Protein stability and solubility can be impacted through a change in pH, ionic strength (salt concentration), temperature, or the redox state of the cell, or via formation of biomolecular condensation phases.[19,26,37,38] Such contextual physical and chemical changes can be transient or last a long time in the cell.[38] Concerning protein misfolding diseases, it can be difficult to determine whether altered cellular conditions such as oxidative stress or altered liquid phase behavior are a cause of the amyloid cascade or a consequence of it.[19,39]

Protein stability and solubility can also be altered by intrinsic changes such as missense mutations in the amino acid sequence or mutations that alter the expression level of the protein itself, its binding partners, or components of the PQC machinery, such as chaperones.[29] Sequence mutations can also interfere with hydrogen bonding, electrostatic interactions, and post-translational-modifications, or lead to truncated products that cause decreased stability or increased aggregation susceptibility. Mutations that disrupt formation of the hydrophobic protein core are particularly destabilizing. The identification of specific point mutations in proteins associated with familial Parkinson's or Alzheimer's disease highlights the deleterious effect single mutations can have on the behavior of metastable, neurodegenerative misfolding disease-associated proteins.[40–42]

To help maintain the native protein fold, the crowded cellular environment contains a variety of factors that promote protein folding and stability, including molecular chaperones, ligands, and the PQC machinery. I describe this complex safety system in detail below.

1.4 Protein Quality Control

The initial misfolding events of many neurodegenerative disease-associated proteins result in a variety of consequences, including the accumulation of large deposits, such as amyloid plaques, and may eventually lead to the collapse of proteostasis.[29,43] Therefore, maintaining intracellular protein health by balancing folding and misfolding is of utmost importance in safeguarding the functionality of the proteome. To maintain proteostasis, the cell employs a constantly vigilant and active PQC system. Its roles include guarding and refolding metastable or

misfolded proteins, eliminating terminally misfolded or aggregated proteins, and clearing other damaged cellular components.[44–46]

The accumulation of misfolded proteins induces a highly conserved, compartment-dependent cellular stress response (called the heat shock response in the cytosol and nucleus, and the unfolded protein response in the endoplasmic reticulum (ER) and mitochondria).[47,48] Typically, the stress response includes the downregulation of protein synthesis and co-translationally acting chaperones, and on the transcriptional and post-translational level, the upregulation of the expression and activity of stress-inducible chaperones and degradation machinery.[49] In yeast, two transcription factors, heat shock factor 1 (HSF1) and Msn2/4, regulate the expression of heat shock response genes.[48]

The three major pathways involved in the PQC system are described in detail below. Many implicated PQC proteins can be part of more than one pathway.

1.4.1 Ubiquitin-proteasome system

One of the PQC pathways is governed by the ubiquitin-proteasome system (UPS). It functions to regulate the concentration of particular proteins and to degrade misfolded proteins in the cell.[29,50] The clearance pathway is composed of a hierarchical ubiquitination system and the 26S proteasome holoenzyme. Specific ubiquitin activating enzymes (E1), ubiquitin conjugating enzymes (E2), and ubiquitin ligases (E3) act sequentially to mediate the addition of ubiquitin chains to particular lysine residues of a misfolded substrate protein.[44] The linkage-specific ubiquitination pattern determines how the partitioning occurs in distinct proteostasis circuits.[51] The polyubiquitinated substrates are eventually recognized by the 19S proteasomal subunit where deubiquitinating enzymes (DUBs) mediate their deubiquitination, followed by their unfolding and translocation into the proteolytic chamber of the 20S proteasomal subunit.[29,44,50–52] The UPS plays an important role in many cellular processes, such as ribosomal PQC to remove and degrade unfinished translation products from stalled ribosomes.[53] Through cooperation with chaperones, the PQC system also functions to degrade terminally misfolded proteins.[50] Proteins

that misfold in the ER are recognized by resident chaperones, translocated to the cytosol, and degraded by the 26S proteasome through a process called ER-associated degradation (ERAD).[29]

Through gene co-expression analysis, the ubiquitin-proteasome pathway has been found to be one of the key components of the proteostasis system that constrains the pools of metastable proteins, such as neurodegenerative disease-associated proteins, in the cell.[54] For example, both Alzheimer's disease-associated proteins Aβ and tau are substrates of the UPS.[55,56] Since impaired function of the UPS has been closely linked to Alzheimer's disease, a causal relationship has been proposed to exist.[44,57] Others suspect that dysfunction of this clearance mechanism may also be an early consequence of the pathogenesis.[44] Given the enormous contribution of the UPS to the elimination of unstable and potentially neurotoxic protein species, the improvement of its efficiency is being investigated as a treatment option for neurodegenerative diseases.[58]

1.4.2 Molecular chaperones

Molecular chaperones constitute ~10% of the total protein mass in human cells, which highlights their biological significance.[59] Chaperones are highly interactive proteins that play key roles in all aspects of proteostasis.[60] These processes include assisting in *de novo* folding or refolding by allowing the protein to overcome non-native kinetic traps, facilitating protein assembly, preventing aggregation of unfolded proteins by binding to hydrophobic stretches, and promoting disaggregation.[5,29,60–62] Chaperones function as nodes in the complex PQC network since they often cooperate with other chaperones or components of the PQC system.[63] They interact with the UPS to promote the degradation of terminally misfolded substrates and together with the autophagy network assist in the degradation of misfolded oligomeric species and aggregates.[5] Due to their sequence similarity and function, the chaperones are categorized into major chaperone families.[29,63] In yeast, there are a total of 67 chaperones; the major chaperone families are Hsp90, Hsp70, Hsp40, CCT, Hsp60, Hsp10, prefoldin, ATPase-associated proteins with diverse cellular activities (AAA+), small heat shock proteins, and calnexin.[63] Additionally, Hsp90 and Hsp70 function is modulated through partnering with specific co-chaperones (in total, 15 co-chaperones).[63] The abundance of chaperones increases significantly

upon stress-induced protein misfolding and aggregation, and alludes to how they acquired their names as heat shock proteins (Hsp).[48] Despite the fact that most of the yeast chaperones' function and mechanisms of action are well-characterized, their comprehensive functions and the spectrum of cellular substrates they interact with are still largely unknown.[63]

Research on neural proteostasis has focused on the roles and the therapeutic targeting of chaperones in neurodegenerative diseases. In these illnesses, chaperones behave like a double-edged sword.[64] They can intervene at various stages of the aggregation process to impede or reverse abnormal protein folding and aggregation and promote the clearance of damaged protein species.[60,64] However, essential housekeeping functions of chaperones can also be hijacked for the propagation and distribution of amyloid aggregates.[64] Hence, to exploit the therapeutic potential of chaperones to suppress aggregation in neurodegenerative diseases, one must first decipher the complex chaperone mechanisms and identify chaperone factors with functional specificity.[64]

1.4.3 Autophagy

The third line of the PQC system is the autophagic lysosomal pathway.[29] The autophagy system involves the transport of cytoplasmic components into lysosomes (mammals) or vacuoles (yeast) for their elimination. This pathway is essential for basal proteostasis and is activated under stress conditions to degrade and remove damaged organelles and proteins.[61] It efficiently recycles cellular components, damaged organelles, and misfolded or aggregated proteins irrespective of their size and solubility.[49] Like the UPS, it utilizes ubiquitination to recruit target proteins.[61,65] The simplest form of autophagy involves the direct immersion of cytosolic damaged protein into lysosomes (microautophagy).[29] In chaperone-mediated autophagy, chaperones translocate damaged material across lysosomal membranes. To clear damaged material of larger size, a series of protein complexes cooperate to form autophagosomes that engulf the substrate. The autophagosomes are transported to and fuse with lysosomes (macroautophagy). The autophagic lysosomal pathway functionally supports the UPS when the UPS is functionally impaired or overwhelmed with the degradation of damaged proteins.

A malfunction in the autophagy pathway, including the disruption of the cytoskeletal network to transport endo- and autophagosomes to the lysosome, leads to their accumulation along with the accumulation of pathogenic proteins and damaged organelles.[61,66] Defects in autophagy and the consequent clearance of protein deposits are associated with the pathogenesis of many neurodegenerative diseases.[66] Controlled modifications of the autophagy system to promote the clearance of neurotoxic aggregates may prove useful in the development of possible therapeutic intervention strategies.[58,67]

Overload of the PQC system or it's malfunctioning has been strongly linked to neurodegenerative disease.[44,68] This evident relationship highlights the need to better understand the components of the complex PQC machinery that regulate proteostasis in the cell and may provide starting points for therapeutic targeting in neurodegenerative disease.

1.5 Strategies to assess protein stability in yeast

Identifying the cellular factors involved in the key processes responsible for the development and progression of neurodegenerative misfolding diseases is challenging. This is primarily due to limitations in detecting and quantifying changes in protein stability *in vivo*. The many biophysical and spectroscopic methods available for studying protein folding *in vitro* have provided a structural and mechanistic understanding of the native, misfolded, and aggregated states of misfolding disease-associated proteins.[69,70] However, it is unclear to what extent these findings can be transferred to the processes *in vivo* because of clear differences between the test tube and the cellular folding environment. Although the *in vivo* protease susceptibility generally correlates well with the thermodynamic *in vitro* stability of a protein,[71] as discussed earlier the tendency of a protein to aggregate is strongly influenced by environmental conditions.

The determination of the *in vivo* folding status of a protein by measuring the associated function is rarely possible due to a lack of appropriate assays or fundamental lack of knowledge about the protein's function. A number of different approaches to measure the *in vivo* stability of neurodegenerative-associated proteins have been developed for use in yeast. A detailed discussion on the general utility of yeast as a model for protein misfolding diseases can be found

in several excellent reviews.[13,15,18,23,72–74] Using yeast to model neurological misfolding disease has already proven to be a powerful approach for unraveling the complex mechanisms and pathways involved.[75] For example, several genetic modifiers (enhancers and suppressors) of the toxicity induced by the expression of the Parkinson's disease-associated protein α-synuclein were discovered using genetic screens in yeast.[76,77] Subsequently, some of the human orthologues of the discovered candidate genes were found to be closely associated with α-synuclein misfolding.[75,78] Moreover, the screens revealed several mechanisms implicated in the pathophysiology of Parkinson's disease.[75] Based on the results of the multitude of genome-wide gene deletion and overexpression screens in yeast, computational approaches were able to construct a "humanized" network that interconnects genetic forms of Parkinsonism, reveals druggable targets for α-synuclein, and predicts pathologies in patient-derived neurons.[79] It is clear that the different yeast models and yeast-based screening systems as a whole have tremendous potential to provide fundamental insights into disease pathologies.

Other methods to determine the protein stability and aggregation susceptibility of neurodegenerative disease-associated proteins involve different reporter systems. Depending on the reporter system used, different aspects of the misfolding or aggregation can be assessed. These reporter systems have been very useful in studying the *in vivo* protein stability of neurodegenerative disease-associated proteins.[17,18,72,74] Unfortunately, any reporter system also has specific inherent limitations. Commonly used approaches frequently involve a dose-dependent cytotoxic overexpression of neuropathogenic proteins in yeast, as already mentioned above.[80–83] Although the toxic phenotype is somewhat reminiscent of what is seen in human cells, the observed localization behavior of the protein in the yeast model can differ from the localization seen in the human pathology.[23,81] The observed toxicity may to some extent be unrelated to the misfolding of the protein since the high protein concentrations often used can result in the sequestration of native and non-native binding partners.[23] The high expression levels may also lead to transport of the protein into non-native cellular compartments or organelles.[23]

Additional methods to determine the folding of a protein of interest *in vivo* are frequently based on the fusion of a protein of interest to a reporter protein. These methods are based on

the assumption that the reporter protein will provide an accurate assessment for the folding of the fusion partner. Through quantification of the reporter readout, an indirect measure of the effective protein abundance can often be obtained.[84] Typically, green fluorescent protein (GFP) or other fluorescent proteins are used as fusion partners because they allow simple microscopic detection and quantifiable fluorescent readouts.[81,83,85] Other approaches involve the fusion to a functional protein, such as dihydrofolate reductase, these types of approaches enable yeast survival-based or colorimetric readouts for protein stability.[82,86,87] Major limitations of these fusion-based approaches are the propensity to obtain false readouts due to proteolytic cleavage of the fusion away from the protein that it is intended to monitor or truncation artifacts. Oftentimes altered solubility of the protein of interest is observed in the fusion context. To avoid such issues, one recent approach fuses the protein of interest to a relatively small transcriptional activator that regulates the expression of a fluorescent reporter protein in a solubility-dependent manner.[88] Förster resonance energy transfer (FRET)-based approaches also involve fusion of a protein of interest with fluorescent proteins. The changes in FRET efficiency are used as a measure for the degree of relative structural change in a protein of interest and therefore its folding.[89] Unfortunately, a low signal-to-noise ratio and limitations in the range of measurable distance change make this technique unattractive for practical use.[90] Nevertheless, the principle of FRET was exploited in a recent, clever approach to quantify the extent of a protein's self-assembly as a function of cellular concentration.[91] Complementation-based approaches based on the fusion of a split half of GFP to, for example, the Parkinson's disease-associated protein α-synuclein, allowed study of the oligomerization efficiency of different mutants of α-synuclein in yeast.[92] However, this interesting technique is characterized by a low signal-to-noise ratio, the tendency to increase non-specific interactions due to self-assembly propensities of the fragments alone, and proteolytic cleavage artifacts.

The multiple approaches employed to detect protein misfolding and aggregation in the cell demonstrate the dependence of the stability readout on the reporter strategy used. The reporter readouts fortunately all show at least partial agreement but all have their reporter-dependent limitations. The inherent constraints have spurred the development of new biosensor strategies. New tools may allow one to study different aspects of the misfolding and aggregation of

neurodegenerative disease-associated proteins and enable high-throughput screens to identify stability modifying factors. Ultimately, complementary biosensor systems could allow us to obtain a more complete understanding of neuropathological misfolding diseases.

2 Aims of the present work

In order to provide a versatile biosensor platform that allows the assessment of protein stability and aggregation propensity in a eukaryotic host, we decided to optimize a tripartite fusion system that links protein stability with an antibiotic resistance phenotype for use in yeast. The goal was to provide a versatile biosensor platform that would allow the sensitive determination of the protein misfolding and aggregation tendencies of neurodegenerative disease-associated proteins.

3 Materials and Methods

3.1 Materials

3.1.1 Technical equipment

Table 1. List of technical equipment used in this work.

Equipment	Vendor
Biomek® FX liquid handling robot	Beckman Coulter Life Sciences, Indianapolis, IN, USA
ChemiDoc MP Imaging System, BioRad	Bio-Rad Laboratories, Hercules, CA, USA
Eppendorf Centrifuge 5804R	Eppendorf, Hamburg, DE
Eppendorf Mastercycler epgradient S realplex2	Eppendorf, Hamburg, DE
Eppendorf small table top centrifuge 5415R	Eppendorf, Hamburg, DE
Eppendorf Thermomixer	Eppendorf, Hamburg, DE
Freezer -20°C Isotemp	Fisher Scientific, Hampton, NH, USA
Freezer -80°C	Thermo Fisher Scientific, Waltham, MA, USA
Fridge-Freezer Isotemp	Fisher Scientific, Hampton, NH, USA
Heating magnetic stirrer	Fisher Scientific, Hampton, NH, USA
Ice machine	Scotsman, Vernon Hills, IL, USA
Incubator 30 °C Isotemp	Fisher Scientific, Hampton, NH, USA
Incubator 34 °C Isotemp	Fisher Scientific, Hampton, NH, USA
Incubator 37 °C Heratherm	Thermo Fisher Scientific, Waltham, MA, USA
Microwave	Panasonic, Osaka, Japan
Mini-Centrifuge 100-240V, 50/60Hz	Fisher Scientific, Hampton, NH
Mini-PROTEAN Tetra Vertical Electrophoresis Cell	Bio-Rad Laboratories, Hercules, CA, USA
Mulit-vortexer IKA-VIBRAX-VXR	IKA Works, Wilmington, NC, USA
NanoDrop ND 1000 Spectrophotometer	Nanodrop technologies, Wilmington, DE
New Brunswick Innova 44 shaker	NewBrunswick Scientific, NJ, USA
Nikon Eclipse E800 microscope.	Nikon Inc., Melville, NY, USA
Odyssey CLx detection system	Li-cor, Lincoln, NE, USA
Owl™ EasyCast™ Mini Gel Electrophoresis System	Fisher Scientific, Hampton, NH, USA
pH meter accumet XL15	Fisher Scientific, Hampton, NH, USA
Photometer for OD	Thermo Fisher Scientific, Waltham, MA, USA
Pipetman, misc.	Eppendorf, Hamburg, DE
platform shaker, table top	Corning, NY, USA
Roller drum TC-7	NewBrunswick Scientific, NJ, USA
Scale, fine AB54-S	Mettler Toledo, OH, USA
TECAN M200 Infinite Pro	Tecan, Morrisville, NC, USA
Thermoblock, metal	VWR Scientific, IL, USA
Thermocycler	Eppendorf, Hamburg, DE
Trans-Blot Turbo Transfer System	Bio-Rad Laboratories, Hercules, CA, USA
Vortex Mixer	VWR Scientific, IL, USA
Water Bath	Lab-Line, Melrose Park, IL, USA

3.1.2 Chemicals

Table 2. List of chemicals used in this work.

Chemical	Company
1,2-dithiothreitol, DTT	Millipore Sigma, St. Louis, MO, USA
2-propanole	Fisher Scientific, Hampton, NH, USA
A	
Acetic acid, glacial	Mallinckrodt Baker, MO, USA
Acetone	ICN, Aurora, OH, USA
Acid phenol:$CHCl_3$	Calbiochem, San Diego, CA, USA
Agarose, low-electroendosmosis	Fisher Scientific, Hampton, NH, USA
Aminoadipic acid	Millipore Sigma, St. Louis, MO, USA
B	
Bacto-Agar	BD Biosciences, San Jose, CA, USA
Bacto-Tryptone	BD Biosciences, San Jose, CA, USA
Bacto-Yeast Extract	BD Biosciences, San Jose, CA, USA
β-mercaptoethanol	MP Biomedicals, Irvine, CA, USA
C	
Calcium chloride, $CaCl_2$	Thermo Fisher Scientific, Waltham, MA, USA
Chloroform (Sigma, C2432)	Millipore Sigma, St. Louis, MO, USA
Clorox household bleach	Clorox, Oakland, CA, USA
D	
D-(+)-Galactose	Millipore Sigma, St. Louis, MO, USA
D-(+)-Glucose	Millipore Sigma, St. Louis, MO, USA
D-(+)-Raffinose pentahydrate	Millipore Sigma, St. Louis, MO, USA
Dimethyl sulfoxide, DMSO	Millipore Sigma, St. Louis, MO, USA
E	
Ethanol	Mallinckrodt Baker, MO, USA
Ethylenediamine tetra acetic acid, EDTA	Millipore Sigma, St. Louis, MO, USA
G	
Glycerin	Fisher Scientific, Hampton, NH, USA
H	
Hydrochlorid acid, HCl	Fisher, Pittsburgh, PA, USA
Hydrogen peroxide, H_2O_2	Thermo Fisher Scientific, Waltham, MA, USA
I	
IPTG	GoldBio, St. Louis, MO, USA
L	
Lithium acetate dihydrate	Millipore Sigma, St. Louis, MO, USA
M	
Magnesium chloride, $MgCl_2$	Millipore Sigma, St. Louis, MO, USA
Magnesium sulfate, $MgSO_4$	Mallinckrodt Baker, Hazelwood, MO, USA
Methanol	EM Science, Gibbstown, NJ, USA
N	
N-(2-hydroxyethyl)-piperazine-N'-2-ethan sulfonic acid, Hepes	MP Biomedicals, Irvine, CA, USA
N-Ethylmaleimide	Millipore Sigma, St. Louis, MO, USA
Nonfat dry milk, instant	Kroger, OH, USA
P	
Phenol	MP Biomedicals, Irvine, CA, USA
PMSF	MP Biomedicals, Irvine, CA, USA

Polyethylene glycol 3350	Millipore Sigma, St. Louis, MO, USA
Potassium acetate	Millipore Sigma, St. Louis, MO, USA
Potassium chloride, KCl	Millipore Sigma, St. Louis, MO, USA
Potassium hydroxide, KOH	Merck, Whitehouse Station, NJ, USA
S	
SC Powder	Sunrise Science Products, San Diego, CA, USA
Sodium acetate	J.T. Baker, NJ, USA, USA
Sodium azide	MP Biomedicals, Irvine, CA, USA
Sodium chloride, NaCl	Fisher, Pittsburgh, PA, USA
Sodium dodecyl sulfate, SDS	Gibco, Rockville, MD, USA
Sodium hydroxide, NaOH	Millipore Sigma, St. Louis, MO, USA
T	
Trichloroacetic acid, TCA	Merck, Whitehouse Station, NJ, USA
Tris-(hydroxymethyl)-aminomethan, Tris	MP Biomedicals, Irvine, CA, USA
Trition X-100	MP Biomedicals, Irvine, CA, USA
Tween 20	MP Biomedicals, Irvine, CA, USA
U	
Urea, ultra pure	MP Biomedicals, Irvine, CA, USA
Y	
Yeast Synthetic Drop-out Medium Supplements without leucine	Millipore Sigma, St. Louis, MO, USA
Yeast Synthetic Drop-out Medium Supplements without uracil	Millipore Sigma, St. Louis, MO, USA
Yeast Synthetic Drop-out Medium Supplements without uracil, tryptophan	Millipore Sigma, St. Louis, MO, USA

3.1.3 Antibiotics, markers, dyes

Antibiotics listed in Table 3 were filter sterilized (0.2 µm filter) before use. Markers and dyes were used according to the manufacturer's instructions or as specified.

Table 3. List of antibiotics, markers, and dyes used.

Antibiotic or growth inhibitor compounds	**Company**	**Solvent**	**Stock [mg ml^{-1}]**	**Working concentration for selection [mg ml^{-1}]**
Ampicillin	GoldBio, St Louis, MO, USA	ddH_2O	200	0.2
G 418 disulfate salt	Millipore Sigma, St. Louis, MO, USA	ddH_2O	200	0.05-2
HG-80: Hygromycin B50 mg/mL	Omega Scientific, Tarzana, CA, USA	Phosphate buffered saline	50	0.3
Kanamycin Monosulfate	GoldBio, St Louis, MO, USA	ddH_2O	100	0.1
Nourseothricin Sulfate	GoldBio, St Louis, MO, USA	ddH_2O	100	0.1-2

Marker	Company
1 kb Plus DNA Ladder	Thermo Fisher Scientific, Waltham, MA, USA
PageRuler Prestained Protein Ladder	Thermo Fisher Scientific, Waltham, MA, USA
HiMark Standard	Thermo Fisher Scientific, Waltham, MA, USA

Dye	Company
Bromophenolblue	Millipore Sigma, St. Louis, MO, USA
Sybr Safe DNA Gel Stain	APExBio, Houston, TX, USA
Gel loading Dye, Purple (6x) for DNA	Promega, Madison, WI, USA
Gel loading Dye, Blue and Orange (6x) for DNA	Promega, Madison, WI, USA

3.1.4 Proteins

3.1.4.1 Enzymes and reaction master mixes

Enzymes were supplied in a readily usable master mix or otherwise the supplied buffers and additives of the corresponding enzymes (Table 4) were used. Restriction endonucleases were purchased from New England Biolabs, Ipswich, MA, USA. If available, the high-fidelity variant of a restriction enzyme was used.

Table 4. List of enzymes and master mixes used.

Protein/Enzyme	Company
Antarctic phosphatase	New England Biolabs, Ipswich, MA, USA
BamHI	New England Biolabs, Ipswich, MA, USA
Cloneamp HiFi PCR Premix	Takara Bio, Mountain View, CA, USA
DpnI restriction enzyme 10U/ul	New England Biolabs, Ipswich, MA, USA
EcoRI	New England Biolabs, Ipswich, MA, USA
Gibson Assembly Master Mix	New England Biolabs, Ipswich, MA, USA
GoTaq Green Master Mix	Promega, Madison, WI, USA
HindIII	New England Biolabs, Ipswich, MA, USA
In-Fusion HD Cloning Kit	Takara Bio, Mountain View, CA, USA
In-Fusion HD Enzyme Premix	Takara Bio, Mountain View, CA, USA
Lyticase from Arthrobacter luteus	Millipore Sigma, St. Louis, MO, USA
PacI	New England Biolabs, Ipswich, MA, USA
Pfu Ultra High-Fidelity DNA polymerase	Agilent Technologies, Santa Clara, CA, USA
PfuUltra High-Fidelity DNA polymerase 80 U	Agilent Technologies, Santa Clara, CA, USA

Phire Plant Direct PCR Master Mix	Thermo Fisher Scientific, Waltham, MA, USA
Phusion High-Fidelity DNA Polymerase	New England Biolabs, Ipswich, MA, USA
QuikChange II Site-Directed Mutagenesis Kit	Agilent Technologies, Santa Clara, CA, USA
SacI	New England Biolabs, Ipswich, MA, USA
SpeI	New England Biolabs, Ipswich, MA, USA
T4 DNA ligase	New England Biolabs, Ipswich, MA, USA
T4 DNA polynucleotide kinase	New England Biolabs, Ipswich, MA, USA
Zymolyase	Zymo Research, Irvine, CA, USA

3.1.4.2 Antibodies

Listed in Table 5 are the primary and secondary antibodies that were used in this work.

Table 5. List of antibodies used.

Antibody	Clonality	Supplier	Catalogue number	Working dilution
Primary antibodies				
Mouse anti-FLAG, M2	monoclonal	Millipore Sigma, St. Louis, MO, USA	F3165	1:2,000
Mouse anti-V5	monoclonal	Thermo Fisher Scientific, Waltham, MA, USA	R96025	1:2,000
Mouse anti-β-Amyloid, 1-16 (6E10)	monoclonal	BioLegend, San Diego, CA, USA	803004	1:1,000
Rabbit anti-Glucose-6-Phosphate Dehydrogenase (G-6-PDH)	polyclonal	Millipore Sigma, St. Louis, MO, USA	A9521	1:2,000
Rabbit anti-Rnq	polyclonal	Abnova, Taipei, Taiwan	PAB15579	1:1,000
Rabbit anti-Sup35	polyclonal	Abnova, Taipei, Taiwan	PAB15578	1:1,000
Secondary antibodies				
mouse anti-HA, stock concentration 0.5 mg mL^{-1}	monoclonal	Roche, Basel, Switzerland	12CA5	1:1,000
Goat anti-Mouse IgG (H+L) Alexa Fluor Plus 488	polyclonal	Thermo Fisher Scientific, Waltham, MA, USA	A32723	1:200
Goat anti-Mouse IgG IRDye® 800CW	N/A	LI-COR Biosciences, Lincoln, NE, USA	926-32210	1:15,000
Goat anti-Mouse IgG IRDye® 680RD	N/A	LI-COR Biosciences, Lincoln, NE, USA	926-68070	1:15,000
Goat anti-Rabbit IgG IRDye® 800CW	N/A	LI-COR Biosciences, Lincoln, NE, USA	926-32211	1:15,000
Goat anti-Rabbit IgG IRDye® 680RD	N/A	LI-COR Biosciences, Lincoln, NE, USA	926-68071	1:15,000

3.1.5 Kits and ready-to-use solutions

Table 6. List of kits and ready-to-use solutions.

Kit	**Company**
Wizard Genomic DNA Purification Kit	Promega, Madison, WI, USA
Mini-PROTEAN TGX Stain-Free Precast Gels	Bio-Rad Laboratories, Hercules, CA, USA
Trans-Blot Turbo Mini PVDF Transfer Packs	Bio-Rad Laboratories, Hercules, CA, USA
NucleoSpin Gel and PCR Clean-up	MACHEREY-NAGEL, Bethlehem, PA, USA
NucleoSpin Plasmid	MACHEREY-NAGEL, Bethlehem, PA, USA
DNA-free DNA Removal Kit AM1906	Thermo Fisher Scientific, Waltham, MA, USA
PrimeScript 1st strand cDNA Synthesis Kit 6110A	Takara Bio, Mountain View, CA, USA
Bullseye EvaGreen qPCR master Mix BEQPCR-R	Midwest Scientific, Valley Park, MO, USA
Solution	
Odyssey® Blocking Buffer in TBS	LI-COR Biosciences, Lincoln, NE, USA
EZBlock™ Protease Inhibitor Cocktail IV	BioVision, Milpitas, CA, USA
cOmplete™, EDTA-free Protease Inhibitor Cocktail	Millipore Sigma, St. Louis, MO, USA
SlowFade™ Diamond Antifade Mountant with DAPI	Thermo Fisher Scientific, Waltham, MA, USA
UltraPure™ Salmon Sperm DNA Solution	Thermo Fisher Scientific, Waltham, MA, USA

3.1.6 Consumables

Table 7. List of consumables used.

Consumables	**Company**
96 well plates	Corning, NY, USA
Axygen tips for BioMek	Corning, NY, USA
Breath-Easy film 9123-6100	USA Scientific, Ocala, FL, USA
GB002	MACHEREY-NAGEL, Bethlehem, PA, USA
GB004 blotting paper	MACHEREY-NAGEL, Bethlehem, PA, USA
Microscope Slides, Immunofluorescence	Polysciences, Warrington, PA, USA
Nitrocellulose membrane 0.45 µm	Thermo Fisher Scientific, Waltham, MA, USA
Petri-dishes	USA Scientific, Ocala, FL, USA
Pipette tips	USA Scientific, Ocala, FL, USA
serological pipettes	USA Scientific, Ocala, FL, USA
Sterile Polystyrene Disposable Serological Pipets	Corning, NY, USA
Super-frost™ Plus Microscope Slides	Fisher Scientific, Hampton, NH, USA

3.1.6 Buffers and solutions

3.1.6.1 Standard growth media

For solid medium 20% (w v^{-1}) bacto-agar was added to the liquid medium recipe components prior to autoclaving. Autoclaved media was cooled down at room temperature to about 60 °C before adding filter sterilized carbon sources and antibiotics. After thorough mixing of the additives in the agar, the agar mixture was poured into culture plates. The agar plates were dried at room temperature for 2-3 days. To store the plates, they were sealed in plastic bags and kept at 4 °C. In case the agar medium contained light sensitive compounds such as antibiotics, plates were additionally wrapped in aluminum foil.

Standard media recipes are listed in the following (Table 8):

Table 8. Summary of growth media recipes for 1 L of medium each.

Luria Bertani broth (LB)		
Bacto-tryptone	10	g
Bacto-yeast extract	5	g
NaCl	5	g
ddH_2O	ad 1	L

Super optimal broth (SOC)		
Bacto-tryptone	10	g
Bacto-yeast extract	2.5	g
NaCl	0.3	g
KCl	0.1	g
ddH_2O	ad 500	mL
after autoclaving, add glucose (1M)	2 ml to 100	ml

YPD medium		
Bacto-yeast extract	10	g
Bacto-peptone	20	g
glucose	20	g
ddH_2O	ad 1000	mL

YPED medium		
adenine	120	mg
Bacto-yeast extract	10	g
Bacto-peptone	20	g
glucose	20	g
ddH_{2O}	ad 1000	mL

Synthetic Complete (SC) medium		
Yeast nitrogen base without amino acids and without ammonium sulfate[a]	1.7	g
L-glutamic acid monosodium salt[b]	1	g
Synthetic complete powder[c]	2	g
ddH_2O	ad 800	mL
after autoclaving, add carbon source (as specified below)		

Synthetic Complete (SC) medium lacking uracil		
Yeast nitrogen base without amino acids and without ammonium sulfate	1.7	g
L-glutamic acid monosodium salt	1	g
Yeast Synthetic Drop-out Medium Supplements without uracil[d]	1.92	g
ddH_2O	ad 800	mL
after autoclaving, add carbon source (as specified below)		

SD medium (supplemented with 2% glucose)		
SC medium	800	ml
after autoclaving, add		
20% glucose, autoclaved	100	ml
ddH_2O	ad 1000	mL

SC media supplemented with 2% raffinose and 2% galactose		
SC medium	800	ml
after autoclaving, add		
20% raffinose, sterile filtered	100	ml
20% galactose, sterile filtered	100	ml

SC media supplemented with 2% raffinose and 0.1% glucose)		
SC medium	800	ml
after autoclaving, add		
20% raffinose, sterile filtered	100	ml
20% glucose, autoclaved	5	ml
ddH_2O	ad 1000	mL

[a] Yeast nitrogen base without amino acids and without ammonium sulfate contains salts, vitamins, minerals and trace elements. [b] L-glutamic acid monosodium salt serves as nitrogen source. It is important to use this compound instead of ammonium sulfate when supplementing the media with aminoglycoside antibiotics such as G418 or nourseothricin.

[c] Synthetic complete powder is a mixture of all amino acids (as listed in Table 9) and all possible growth supplements (indicated by name "complete"). [d]Synthetic Drop Out (SC-) powder contains the supplements and listed amino acids except the ones that are deliberately left out as specified (indicated as "drop-out mix"). For example, if L-uracil were omitted, the resulting synthetic minimal media would be called SC-ura.

Table 9. Final concentration of amino acids and supplements in 1 L synthetic complete medium.[a]

Amino acid	**[mg L^{-1}]**	**Amino acid**	**[mg L^{-1}]**
adenine hemisulfate	21	L-leucine	173.4
L-alanine	85.6	L-lysine	85.6
L-arginine	85.6	L-methionine	85.6
L-asparagine	85.6	para-aminobenzoic acid	8.6
L-aspartic acid	85.6	L-phenylalanine	85.6
L-cysteine	85.6	L-proline	85.6
L-glutamine	85.6	L-serine	85.6
L-glutamic acid	85.6	L-threonine	85.6
L-glycine	85.6	L-tryptophan	85.6
L-histidine	85.6	L-tyrosine	85.6
myo-inositol	85.6	uracil	85.6
L-isoleucine	85.6	L-valine	85.6

[a] Amino acid and supplement concentrations according to recipe instructions using SC powder mix (Sunrise bioscience, 1300-030).

3.1.6.2 Buffers for yeast transformations, molecular biology and biochemistry

The following table lists the buffers used in this work as well as their compositions.

Table 10. Summary of buffer recipes.

1 x TAE buffer			**1 x TAE, 0.1 % SDS**		
Tris	242.0	g	Tris	24.2	g
Acetic acid	57.0	mL	Acetic acid	5.7	mL
0.5 mM EDTA, pH 7.5	100.0	mL	0.5 mM EDTA, pH 7.5	10.0	mL
ddH_2O	ad 10	L	20 % Sodium dodecyl sulfate	5.0	mL
			ddH_2O	ad 1000	mL

LiOAc buffer

1 M lithium acetate	1.0	mL
1 M Tris-HCl pH 8.0	0.1	mL
0.5 M EDTA	0.02	mL
ddH_2O	ad 10	mL

5x reducing SDS sample buffer

Sodium dodecyl sulfate	5	g
Glycerol	30.5	g
Tris (1M), pH 7.0	15	ml
Bromphenol blue	0.025	g
β-mercaptoethanol	2.5	ml
ddH_2O	up to 50	ml

Lysis buffer (simple lysate fractionation)

1 M HEPES pH 8.0	150	µl
5 M NaCl	150	µl
50 % glycerol	100	µl
0.3 M DTT	17	µl
0.1 M PMSF	50	µl
EZBlock IV protease inhibitor cocktail	10	µl
50 % Triton X-100	50.0	µl
ddH_2O	ad 5	mL

Lysis buffer for SDD-AGE

Tris pH 8.0	1.0	mL
50 % Triton X-100	0.2	mL
β-mercaptoethanol	35.0	µl
EZBlock IV protease inhibitor cocktail	0.1	mL
N-Ethylmaleimide	375.0	mg
Benzonase 250 U/µl	5.0	µl
0.1 M PMSF	0.1	mL
ddH_2O	ad 10	mL

Tris-buffered saline (TBS)

NaCl	8.8	g
Tris-HCl	2.4	g
Tris base	5.6	g
ddH_2O	ad 800	ml
adjust pH to 7.4 with HCl		
ddH_2O	ad 1000	ml

4x sample buffer for SDD-AGE

50 x TAE buffer	0.2	mL
50 % Glycerol	4.0	mL
20 % SDS	4.0	mL
Bromophenolblue 0.01 %	1.0	mL
ddH_2O	ad 10	mL

TES buffer

1 M Tris-HCl pH 7.5	0.1	mL
0.5 M EDTA	0.02	mL
20% SDS	0.25	mL
ddH_2O	ad 10	mL

1x SDS running buffer

Tris base	3.0	g
Glycine	14.4	g
Sodium dodecyl sulfate (SDS)	1.0	
ddH_2O	ad 800	mL
adjust pH to 8.3		
ddH_2O	ad 1000	mL

Protein solubilizing buffer

1 M HEPES-KOH pH 7.4	2	mL
1 M KCl	1.2	mL
0.5 M EDTA	0.04	mL
0.3 M DTT	6.7	µl
0.1 M PMSF	0.1	mL
EZBlock IV protease inhibitor cocktail	0.1	mL
ddH_2O	ad 10	mL

Phosphate-buffered saline (PBS)

NaCl	8	g
KCl	0.2	g
Na2HPO4	1.44	g
KH2PO4	0.24	g
ddH_2O	ad 800	ml
adjust pH to 7.4 with HCl		
ddH_2O	ad 1000	ml

Tris-buffered saline, 0.1% Tween (TBS)

NaCl	8.8	g
Tris-HCl	2.4	g
Tris base	5.6	g
ddH_2O	ad 800	ml
Tween 20	1	ml
adjust pH to 7.4 with HCl		
ddH_2O	ad 1000	ml

3.1.7 Oligonucleotides and plasmids

3.1.7.1 Oligonucleotide primers

Table 11. Primers used in this work.

Primer name	Sequence
PVS007	TTTGTAGCCTGCTTTTTTGTACA
PVS010	AACCCAGCTTTCTTGTACAAAGT
PVS045	CTGACCCGGGGCAGGGCATGCTCATG
PVS046	GTAGTGGTGGTAAGCCTATCCCTAACCCTCTCCTCG
PVS047	TCACCACTACCTGACCCGAAGAACTCGTCAAGAAGGCGATAGAAG
PVS048	CTACAAAGACGATGACGACAAATGAGTTTCTAGAGGGCCGCATCATG
PVS122	CAAAAAAGCAGGCTACAAAATGAAAAGAAATAAACCAGG
PVS123	GTACAAGAAAGCTGGGTTTTTACCTCTATGAATATCAATATGTC
PVS126	AGCGGATCCGGCTCGAGCGGTTCCGGGAGCAGGGAACT
PVS127	GAGCCAGAGCTCGAACCGC
PVS249	ATACCCGGGCGGCCGCCACCGCGGTGGAGCT
PVS250	TTAGTCGACGACATCCGCGCGTTGGCCGATTCAT
PVS327	AGCGGATCCGGCTCGAGCGGTTCCGGGAGCCTGGATGTATTCATGAAAGGACTTTCAAAGGCC
PVS328	CCAGAGCTCGAACCGGCTTCAGGTTCATAGTCTTGATACCC
PVS396	AGTCTCCAAATTTAAAAAATAGCATAAAATTCGTTATACAGCAAATCTATGTGTTGCAATTAAGAACTAAAAGATATAGAGTGC
PVS397	AGTATAAAAGTGTTACTACTCGTTATTATTGCGTATTTTGTGATGCTAAAGTTATGAGTAGAAAAAAATGAGAAGTTGTTCTG
PVS400	CAAATGTATTTGAAGACCCGCTGGGAGAAGTTCAAGATATATAAGTAACAAGCAGCCAATAGTATAAAAAAAAATCTGAGTTTATTAC CTTTCCTGGAATTTCAGTG
PVS401	CAGTTCTTATTCAATAACTAATATTTTATTCTCTTATTATATATTATTCTCGGAGTTTTTAAGTGACATCACCCGAAAAGAAGCTAAGTCT TTTCTCCTAATTCATATTTA
PVS411	ACTAGTGTATTCAATTCCTATTCTAAATGGCTTTTATTTCTATTACAACTATTAGCTCTAAATCCATATCCTCATAAGCAGCAATCAATTC TATCTATACTTTAAACGGATTAGAAGCCGCCGAG
PVS412	CAGCATTCTAGTTAAGAAAAAGTCTAAAAATGGTTTTTTTCATCCAAAATATTAAATTTTACTTTTATTACATACAACTTTTTAAACTAAT ATACACATTGACATGGAGGCCCAGAATACCC
PVS428	CATAAGCTTATGAGTGCTGATGCCTTGATCAAG
PVS429	CATGAATTCCTCGGCAATTTTAACAATTTTACCAATTGCTATTG
PVS413	CAAAGATCTGACATGGAGGCCCAGAATAC
PVS414	GATACTAGTCAGTATAGCGACCAGCATTCAC
HK15	GGGGGATCCGGCTCGAGCGGTTCCGGGAGCCTGGATACGGATAAGTTAATC
HK16	GGGGAGCTCGAACCGTAGCGGTTCTGGTTG
HK17	GGGGGATCCGGCTCGAGCGGTTCCGGGAGCCTGTCGGATTCAAACCA
HK18	GGGGAGCTCGAACCCTCGGCAATTTTAACAA
HK20	GGGGAGCTCGAACCATCGTTAACAACTTCGTCAT
HK22	GGGGGATCCGGCTCGAGCGGTTCCGGGAGCCTGCAAGGTCAGGGACAAG
HK24	GGGGGATCCGGCTCGAGCGGTTCCGGGAGCCTGGATGCAGAATTCCG
HK25	GGGGAGCTCGAACCCGCTATGACAACACCG
qPCR_APH_F	GTGGTGAATGGGCAGATAGAT
qPCR_APH_R	ACCGTCATGGTCTTTGTAGTC
qPCR_ACT_F	GGTTATTGATAACGGTTCTGGTATG
qPCR_ACT_R	ATGATACCTTGGTGTCTTGGTCTAC

3.1.7.2 Plasmids

Table 12. Features of representative plasmids used in this study.

Plasmid number	Plasmid name	C-terminal tag	Promoter	Yeast copy number	Selection marker *S. cerevisiae*	Selection marker *Escherichia coli*
Invitrogen V8251-20	pYES/CT-empty vector/ lacZ	V5-His6	pGal1	2 µ	URA3	Amp
Invitrogen V8255-20	pYC2/CT-empty vector/lacZ	V5-His6	pGal1	CEN/ARS	URA3	Amp
VS186	pYC2-APH Im7 WT-FLAG	3x FLAG	pGal1	CEN/ARS	URA3	Amp
VS466	pFA6-pGal1-yoAPH-Aβ42 wt-FLAG	3x FLAG	pGal1	N/A	CaURA	Amp
MJ5	pTrc99A-NAT78	V5-His6	LacI	N/A	none	Amp
VS180	pYES-APH Im7 WT-FLAG	3x FLAG	pGal1	2 µ	URA3	Amp
VS186	pYC2-APH Im7 WT-FLAG	3x FLAG	pGal1	CEN/ARS	URA3	Amp
VS197	pYC2-Gal1-APH-Im7-L53A/I54A-Flag	3x FLAG	pGal1	CEN/ARS	URA3	Amp
VS206	pAG424-E7 H162A nuclease fragment	3x FLAG	pTDH3	2 µ	Trp	Amp
VS222	pYC2-NAT-Im7 WTt-V5-His6	V5-His6	pGal1	CEN/ARS	URA3	Amp
VS466	pFA6-pGal1-yoAPH-Aβ42 wt-FLAG	3x FLAG	pGal1	N/A	CaURA	Amp
VS519	pGal1-NAT78- Aβ42 WT-V5His6	V5-His6	pGal1	N/A	HygMX	Amp
VS540	pYC2-Sup35CTD	V5-His6	pGal1	CEN/ARS	URA3	Amp
pRS416-Ubc6-HA	pRS416-Ubc6-HA (pJW4, kind gift of Mark Hochstrasser)	HA		CEN/ARS	URA3	Amp
BED205	pAG424-empty vector		pTDH3	2 µ	Trp	Amp

3.1.8 Strains

3.1.8.1 *Escherichia coli* strains

Table 13. E. coli strains used for the optimization of the NAT insertion site [a]**.**

Strain name	Plasmid
MJ-1	pTrc99a-NAT76-linker
MJ-5	pTrc99a-NAT78-linker
MJ-9	pTrc99a-NAT80-linker
MJ-17	pTrc99a (empty vector)
MJ-18	pTrc99a-NAT76-Im7 WT
MJ-20	pTrc99a-NAT76-Im7 L53A I54A
MJ-21	pTrc99a-NAT78-Im7 WT
MJ-23	pTrc99a-NAT78-Im7 L53A I54A
MJ-24	pTrc99a-NAT80-Im7 WT
MJ-26	pTrc99a-NAT80-Im7 L53A I54A

[a]Strain NEB 10-beta *E. coli* was used for all experiments. This strain is a derivative of the popular DH10B and has the genotype Δ*(ara-leu) 7697 araD139 fhuA* Δ*lacX74 galK16 galE15 e14-* φ*80*d*lacZ*Δ*M15 recA1 relA1 endA1 nupG rpsL* (Str^R) *rph spoT1* Δ*(mrr-hsdRMS-mcrBC).*

3.1.8.2 *Saccharomyces cerevisiae* strains

***Table 14. S. cerevisiae* strains used in this work**

Strain name	Genotype	Plasmid 1	Plasmid 2
InvSc1[a]	MATa his3Δ1 leu2 trp1-289 ura3-52 MAT alpha his3Δ1 leu2 trp1-289 ura3-52		
Y14537[b]	HAP1+ ura3Δ0 his3Δ1		
BY4741[c]	MATa his3Δ1 leu2Δ0 met15Δ0 ura3Δ0 lys2Δ0::Gal1-NAT80-Im7-S58R-V5-His6-Cyc1TT		
MDY669[d,47]	MATa ura3Δ0 leu2Δ0 his3Δ0 met15Δ0 SpHIS5::pACT1-GAL3 gal1Δ,gal10Δ::LEU2 (v.1.1), ho::pGal1-mKate2-CaURA3		
aYC-38	InvSc1	pYES-APH-Im7-I54A	Ajamaluddin Malik
aYC-4	InvSc1	pYES-APH	Ajamaluddin Malik
aYC-5	InvSc1	pYES-APH-Im7-WT	Ajamaluddin Malik
L1749	MATa ade1-14 leu2-3, 112 Δhis3-200 trp1-289 ura3-2 high [PIN+] [psi-]		
L1758	MATa ade1-14 leu2-3, 112 Δhis3-200 trp1-289 ura3-2 weak [PSI+] high [PIN+]		
L1762	MATa ade1-14 leu2-3, 112 Δhis3-200 trp1-289 ura3-2 strong [PSI+] high [PIN+]		
L2910	MATa ade1-14 ura3-52 leu2-3,112 trp1-289 his3-200 HSP104 [psi−] [pin−]		
VES1027	Y14537 hoΔ::pGal1-mKate2_ADH1TT_HygMX	pYC2-empty vector	
VES1029	Y14537 hoΔ::pGal1-mKate2_ADH1TT_HygMX	pYC2-Sup35C-V5His6	
VES1031	Y14537 hoΔ::pGal1-yoAPH-linker-6GS-3xFLAG_ADH1TT_HygMX	pYC2-empty vector	
VES1033	Y14537 hoΔ::pGal1-yoAPH-linker-6GS-3xFLAG_ADH1TT_HygMX	pYC2-Sup35C-V5His6	
VES1035	Y14537hoΔ::pGal1-yoAPH-Sup35 FL-6GS-3xFLAG_ADH1TT_HygMX	pYC2-empty vector	
VES1037	Y14537 hoΔ::pGal1-yoAPH-Sup35 FL-6GS-3xFLAG_ADH1TT_HygMX	pYC2-Sup35C-V5His6	
VES174	InvSc1	pYC2/LacZ (Invitrogen)	
VES252	InvSc1	pYES-LacZ	pAG424 empty vector
VES252	InvSc1	pYES-LacZ	pAG424-empty vector
VES255	InvSc1	pYC2-APH WT-FLAG	
VES256	InvSc1	pYC2-APH Im7 WT-FLAG	
VES257	InvSc1	pYC2-APH Im7 I54V-FLAG	
VES258	InvSc1	pYC2-APH Im7 S58R-FLAG	
VES262	InvSc1	pYC2-APH-Im7-L53A I54A-FLAG	
VES263	InvSc1	pYC2-Im7-I54A-FLAG	
VES267	InvSc1	pYC2-APH Im7 I22V-FLAG	
VES268	InvSc1	pYC2-APH-Im7-L34A-FLAG	
VES269	InvSc1	pYC2-APH-Im7-F15A-FLAG	
VES270	InvSc1	pYC2-APH WT-FLAG	pAG424 empty vector
VES271	InvSc1	pYC2-APH WT-FLAG	pAG424-E7 H162A (residues 63–193)
VES272	InvSc1	pYC2-APH WT-FLAG	pAG424-Spy
VES273	InvSc1	pYC2-APH Im7 WT-FLAG	pAG424 empty vector
VES274	InvSc1	pYC2-APH Im7 WT-FLAG	pAG424-E7 H162A (residues 63–193)

VES278	InvSc1	pYC2-APH-Im7-L53A I54A-FLAG	pAG424-empty vector
VES279	InvSc1	pYC2-APH-Im7-L53A I54A-FLAG	pAG424-E7 H162A (residues 63–193)
VES280	InvSc1	pYC2-APH-Im7-L53A I54A-FLAG	pAG424-Spy
VES288	InvSc1	pYC2-APH Im7 WT-FLAG	pAG424-Spy
VES286	InvSc1	pYC2-APH-Im7-V33E-FLAG	
VES287	InvSc1	pYC2-APH-Im7-L18A L19A L37A-FLAG	

VES430	BY4741 lys2Δ0::Gal1-NAT80-Im7-S58R-V5-His6-Cyc1TT
VES650	MDY669 ho::pGal1-mKate2-CaURA3
VES651	MDY669 ho::pGal1-yoAPH-linker 10GS-mKate2-CaURA3
VES652	MDY669 ho::pGal1-yoAPH-Im7 WT 10GS-mKate2-CaURA3
VES653	MDY669 ho::pGal1-yoAPH-Im7 L53A I54A 10GS-mKate2-CaURA3
VES654	MDY669 ho::pGal1-mKate2-10GS-yoAPH-linker-CaURA3
VES657	MDY669 ho::pGal1-yoAPH-linker 6GS-3xFLAG-CaURA3
VES668	MDY669 ho::pGal1-mKate2-10GS-yoAPH-Im7 WT-CaURA3
VES671	MDY669 ho::pGal1-mKate2-10GS-yoAPH-Im7 L53A I54A-CaURA3
VES683	MDY669 ho::pGal1- yoAPH-Asyn WT-6GS-3xFLAG_ADH1TT_CaURA3
VES685	MDY669 ho::pGal1-yoAPH-Asyn A53T-6GS-3xFLAG_ADH1TT_CaURA3
VES687	MDY669 ho::pGal1-yoAPH-Asyn E46K-6GS-3xFLAG_ADH1TT_CaURA3
VES700	MDY669 ho::pGal1-yoAPH-Abeta42 F19,20T, I31P-6GS-3xFLAG_CaURA3
VES702	MDY669 ho::pGal1-yoAPH-Abeta42 WT-6GS-3xFLAG_CaURA3
VES706	MDY669 ho::pGal1-yoAPH-Asyn A30P-6GS-3xFLAG_ADH1TT_CaURA3
VES715	BY4741 lys2Δ0::Gal1-LacZ-V5-His6-Cyc1TT
VES717	BY4741 lys2Δ0::Gal1-NAT80-linker-V5-His6-Cyc1TT
VES719	BY4741 lys2Δ0::Gal1-NAT80-Im7-WT-V5-His6-Cyc1TT
VES721	BY4741 lys2Δ0::Gal1-NAT80-Im7-I54V-V5-His6-Cyc1TT
VES724	BY4741 lys2Δ0::Gal1-NAT80-Im7-I22V-V5-His6-Cyc1TT
VES725	BY4741 lys2Δ0::Gal1-NAT80-Im7-L53A I54A-V5-His6-Cyc1TT
VES727	BY4741 lys2Δ0::Gal1-NAT80-Im7-L18AL19A-V5-His6-Cyc1TT
VES729	BY4741 lys2Δ0::Gal1-NAT80-Im7-L34A-V5-His6-Cyc1TT
VES731	BY4741 lys2Δ0::Gal1-NAT80-Im7-I54A-V5-His6-Cyc1TT
VES733	BY4741 lys2Δ0::Gal1-NAT80-Im7-V33E-V5-His6-Cyc1TT
VES735	MDY669 SpHIS5::pACT1-GAL3 gal1Δ,gal10Δ::pGal1-YFP-V5His6_Cyc1TT_HygMX
VES736	MDY669 SpHIS5::pACT1-GAL3 gal1Δ,gal10Δ::pGal1-NAT78-linker-V5His6_CYC1TT_HygMX
VES737	MDY669 SpHIS5::pACT1-GAL3 gal1Δ,gal10Δ::pGal1-NAT78-asyn wt-V5His6_CYC1TT_HygMX
VES738	MDY669 SpHIS5::pACT1-GAL3 gal1Δ,gal10Δ::pGal1-NAT78-asyn A30P-V5His6_Cyc1TT_HygMX
VES739	MDY669 SpHIS5::pACT1-GAL3 gal1Δ,gal10Δ::pGal1-NAT78-asyn E46K-V5His6_Cyc1TT_HygMX
VES740	MDY669 SpHIS5::pACT1-GAL3 gal1Δ,gal10Δ::pGal1-NAT78-asyn A53T-V5His6_Cyc1TT_HygMX
VES741	MDY669 SpHIS5::pACT1-GAL3 gal1Δ,gal10Δ::pGal1-NAT78-Abeta42 wt-V5His6_Cyc1TT_HygMX
VES742	MDY669 SpHIS5::pACT1-GAL3 gal1Δ,gal10Δ::pGal1-NAT78-Abeta42 F19,20P I31P-V5His6_Cyc1TT_HygMX
VES743	MDY669 SpHIS5::pACT1-GAL3 gal1Δ,gal10Δ::pGal1-NAT78-Sup35 full-V5His6_Cyc1TT_HygMX
VES744	MDY669 SpHIS5::pACT1-GAL3 gal1Δ,gal10Δ::pGal1-NAT78-Sup35 NM-V5His6_Cyc1TT_HygMX
VES745	MDY669 SpHIS5::pACT1-GAL3 gal1Δ,gal10Δ::pGal1-NAT78-Rnq1 full-V5His6_Cyc1TT_HygMX
VES746	MDY669 SpHIS5::pACT1-GAL3 gal1Δ,gal10Δ::pGal1-NAT78-Rnq1-C-V5His6_Cyc1TT_HygMX
yHH74	MDY669 ho::pGal1-yoAPH-Im7 WT -6GS-3xFLAG-CaURA3
yHH75	MDY669 ho::pGal1-yoAPH-Im7 L53A I54A-6GS-3xFLAG-CaURA3
yHH86	MDY669 ho::pGal1-yoAPH-Sup35full-6GS-3xFLAG-CaURA3
yHH88	MDY669 ho::pGal1-yoAPH-Sup35NM-6GS-3xFLAG-CaURA3

yHH90	MDY669 ho::pGal1-yoAPH-Rnq1full-6GS-3xFLAG-CaURA3	
yHH93	MDY669 ho::pGal1-yoAPH-Rnq1C-6GS-3xFLAG-CaURA3	
yXD622	MDY669 pdr5Δ ho::pGal1-yoAPH-Iinker 6GS-3xFLAG- HygMX	
yXD623	MDY669 pdr5Δ ho::pGal1-yoAPH-Abeta42 WT-6GS-3xFLAG-HygMX	
yXD624	MDY669 pdr5Δ ho::pGal1-yoAPH-Abeta42 F19,20T, I31P-6GS-3xFLAG-HygMX	
yXD625	MDY669 pdr5Δ ho::pGal1-yoAPH-Iinker 6GS-3xFLAG- HygMX	pRS416-Ubc6-HA[93]
yXD626	MDY669 pdr5Δ ho::pGal1-yoAPH-Abeta42 WT-6GS-3xFLAG-HygMX	pRS416-Ubc6-HA
yXD627	MDY669 pdr5Δ ho::pGal1-yoAPH-Abeta42 F19,20T, I31P-6GS-3xFLAG-HygMX	pRS416-Ubc6-HA
yXD628	MDY669 pdr5Δ ho::pGal1-yoAPH-Abeta40 WT-6GS-3xFLAG-HygMX	
yXD629	MDY669 pdr5Δ ho::pGal1-yoAPH-Abeta42 scrambled-6GS-3xFLAG-HygMX	

[a]InvSc1 is a *S. cerevisiae* strain from Invitrogen (InvSc1, Invitrogen, C81000) with the genotype MATa his3Δ1 leu2 trp1-289 ura3-52 MATalpha his3Δ1 leu2 trp1-289 ura3-52 and allows maintenance of plasmids encoding APH-Im7 variant fusions featuring a URA3 selection marker as well as a plasmid encoding the E7 variant fragment featuring a TRP selection marker. [b]Strain Y14537 (a kind gift from Dr. Charlie Boone) is a *S. cerevisiae* strain with the genotype HAP1+ ura3Δ0 his3Δ1. The strain was used for the co-expression of the APH-Sup35 full length fusion (integrated with a hygromycine selection marker) with plasmid pYC2-Sup35C-V5His6 (URA3 selection marker) for reasons of selection marker compatibility. [c]BY4741 is a *S. cerevisiae* strain with the genotype MATa his3Δ1 leu2Δ0 met15Δ0 ura3Δ0. [d]MDY669 (a kind gift of Dr. Allan Drummond) is a derivative of BY4741 with the genotype MATa ura3Δ0 leu2Δ0 his3Δ0 met15Δ0 SpHIS5::pACT1-GAL3 gal1Δ,gal10Δ::LEU2 (v.1.1), genetic modifications allow a galactose mediated, tunable induction of the GAL promoter.[47]

3.1.9 Im7 thermodynamic stabilities.

The thermodynamic stabilities of Im7 variants as obtained in *in vitro* equilibrium urea denaturation experiments are listed in the following table.[71,94–96]

Table 15. Im7 thermodynamic stabilities

Im7 variant	**ΔG°_{UN} (kJ mol^{-1})[a,b,c,d]**	**$\Delta\Delta G^\circ_{UN} = \Delta G^\circ_{UN}$ (mutant) – ΔG°_{UN} (WT) (kJ mol^{-1})**
WT	–24.9[b,c]	0
S58R	–26.3[c]	–1.4
V33E	–23.9[c]	1
L34A	–17.2[b]	7.7
I22V	–16[b]	8.9
I54V	–13.9[b]	11
F15A	–9.7[b]	15.2
I54A	–4.9[b]	20
L53AI54A	–11.1[d]	13.8
L18AL19A	0 (unfolded)[e]	24.9
L18AL19AL37A	0 (unfolded)[e]	24.9

[a]ΔG°_{UN}: free energy of unfolding. The parameter was measured by equilibrium urea denaturation. [b] Capaldi et al., 2002.[94] [c]Foit et al., 2009.[71] [d]Spence et al., 2004.[95] [e] Pashley et al., 2012.[96]

3.1.10 Databases and software

Software and databases used in this work are compiled in the following list (Table 16).

Table 16. Databases and software used in this work.

Databases	**Homepage**
RCSB Protein Data Bank	https://www.rcsb.org/
UniProt	https://www.uniprot.org/
ExPASy	https://www.expasy.org/
NCBI BLAST	https://blast.ncbi.nlm.nih.gov/Blast.cgi
Saccharomyces genome database	https://www.yeastgenome.org/

Softwares
Microsoft Powerpoint
Microsoft Excel
Snapgene
ImageJ
PyMOL

3.2 Methods

The description of methods used in this work is in part adopted from Sachsenhauser, V., Deng, X., Kim, H.-H., Jankovic, M., C.A. Bardwell, J., and Bardwell, J. C. A. (2020) Yeast tripartite biosensors sensitive to protein stability and aggregation propensity. *ACS Chem. Biol. XXXX*, XXX, XXX–XXX, https://doi.org/10.1021/acschembio.0c0008.[97]

3.2.1 Microbiology

3.2.1.1 Microbiology of *Escherichia coli*

3.2.1.1.1 Cultivation and storage

Growth of *E. coli* cells on agar plates involved streaking of *E. coli* cells on LB-agar plates supplemented with 200 µg ml^{-1} ampicillin followed by incubation at 37 °C over-night. To grow bacterial cells in liquid media single bacterial colonies were inoculated into liquid LB media supplemented with 200 µg ml^{-1} ampicillin. Cultures were incubated in a roller drum incubator at

37 °C over-night.[98] For the preparation of glycerol stocks for long term storage, 500 µl of bacterial over-night cultures were mixed with 1 ml of 10% (v v^{-1}) sterile glycerol and stored at -80 °C.

3.2.1.1.2 Preparation of chemically competent *E. coli* cells

Competent *E. coli* cells were prepared according to Inonue et al.[99] In brief, 5 mL LB medium supplemented with the appropriate antibiotic(s) if applicable were inoculated with the *E. coli* strain that was desired to make competent cells with. The culture was incubated overnight at 37°C in a roller drum. The following day the overnight culture was used to inoculate 500 mL LB medium and incubated at 25°C until the absorbance of the cells was between 0.4-0.6. Then, cells were chilled on ice for at least 10 min and kept on ice in between the following steps. The chilled cell suspension was spun down for 10 min at 2,000*g* and the pelleted cells gently resuspended in 100 ml ice-cold buffer (10 mM Hepes, 15 mM $CaCl_2$, 55 mM $MnCl_2.4H_2O$, 250 mM KCl). The resuspended cells were incubated on ice for at least 10 min and then pelleted by centrifugation for 10 min at 2,000*g* at 4°C. The cell pellet was gently resuspended in 18.6 mL ice-cold buffer and 1.4 ml of DMSO added. After another incubation step on ice for 10 min the cell suspension was distributed in 100 µl aliquots in 1.5-ml microfuge tubes and flash frozen in liquid nitrogen. The tubes were stored at -80 °C.

3.2.1.1.3 Transformation of chemically competent *E. coli* cells

Frozen stocks of chemically competent *E. coli* 10β cells were thawed on ice and 50 µl of cells mixed with 0.01-50 ng of DNA per transformation reaction. The cell-DNA mixtures were incubated on ice for 20-30 min following a heat shock by placing the tube in a 42 °C water bath for 30 seconds. Then, the cells were chilled on ice for 2 min. 950 µl of SOC media was added per transformation reaction and outgrowth enabled by incubation at 37 °C and shaking at 200 rpm for 1 h. 200 µl of the recovered cells were plated on LB agar media which was supplemented with the appropriate antibiotic for the selection of successfully transformed bacteria.

3.2.1.1.4 Testing antibiotic resistance of *E. coli* strains

To determine the level of antibiotic resistance of *E. coli* cells expressing the NAT tripartite biosensor fusions spotting assays were performed. *E. coli* 10β carrying pTrc99a-NAT plasmid variants were grown to mid-log phase to an OD_{600} of 0.4 in 5 mL LB media supplemented with 200 µg mL^{-1} ampicillin at 37 °C and with shaking at 200 rpm. Cells were induced for 1 h with 1 mM IPTG prior to collecting the cells by centrifugation at 2,000*g* for 5 min at room temperature and adjusting the OD_{600} to 1 in phosphate buffered saline (0.04 M K_2HPO_4, 0.01 M KH_2PO_4, 0.15 M NaCl, pH 7.4). Each strain was 10-fold serially diluted in phosphate-buffered saline and 3 µl of each dilution (10^0 through 10^{-7}) were spotted on LB agar supplemented with 1 mM IPTG, 200 ug/mL ampicillin and increasing concentrations of nourseothricin. Agar plates were incubated for 16-24 h at 37 °C and the growth documented by imaging.

3.2.1.2 Microbiology of *Saccharomyces cerevisiae*

3.2.1.2.1 Cultivation and storage

To grow cells on solid agar media yeast cells were streaked on YPD agar or respective selective SD agar media, wrapped in plastic foil to prevent evaporation and incubated at 30 °C for 2-3 days. To cultivate yeast cells 5 mL of liquid YPD or appropriate synthetic media supplemented with 2% glucose were inoculated with a single yeast colony and incubated at 30 °C for 16 h and shaking at 200 rpm. For long term storage of yeast cells, glycerol cell stocks were prepared by mixing 500 µl of saturated culture with 1 ml of 40% sterile glycerol (v v^{-1}) and frozen at -80 °C.

3.2.1.2.2 Preparation of competent *S. cerevisiae* cells

To prepare competent *S. cerevisiae* cells, liquid cultures were grown to saturation in 5 mL YPD media at 30 °C and agitating at 200 rpm as described in 3.2.1.2.1 Cultivation and storage. Cells were diluted in 50 mL fresh YPD media to an OD_{600} of 0.1 and grown to mid-log phase (OD_{600} = 0.6-0.8) at 30 °C and shaking at 200 rpm for 4-5 h. The cells were harvested by centrifugation at 2,000*g* for 5 min at room temperature and the cells washed by carefully resuspending the cell pellet in 50 ml sterile ddH_2O. The cells were collected again following another round of washing

in 50 ml sterile ddH_2O and centrifugation. The generated spheroplasted cells were resuspended in 250 µl of LiOAc buffer (0.1 M lithium acetate, 10 mM Tris, 1mM EDTA) and mixed with 150 ul of sterile 50% glycerol (v v^{-1}) following freezing the cells at -80 °C for later use.

3.2.1.2.3 Transformation of *S. cerevisiae*

Transformations of plasmids and linearized DNA into *S. cerevisiae* were performed according to the High efficiency transformation protocol published in the CSH yeast genetics and genomics handbook 2015.[100] In brief, to 50-100 µl of competent *S. cerevisiae* cells, 10 µl of plasmid DNA or >250 ng linearized DNA, 10 µl of 10 mg ml^{-1} single stranded salmon sperm carrier DNA solution and 280 µl of 50% PEG were added per reaction and mixed by vortexing for 1 min. Reactions were incubated at room temperature for 30 min before adding 45 µl of DMSO. The reactions were incubated for 10 min in a 42 °C water bath followed by incubation on ice for 2 min. 950 µl of YPD media was added per reaction.

To allow the expression of auxotrophy marker genes URA3 or LEU2 for subsequent selection, cells were incubated at 30 °C for at least 4 h. To allow expression of antibiotic selection markers, cells were incubated at 30 °C overnight. Recovered cells were washed and resuspended in sterile water before plating them on the respective selective minimal agar media lacking uracil or leucine to select for an auxotrophy marker or on YPD agar supplemented with the respective antibiotic.

In case hygromycin B resistant transformants or the deletion of the LYS2 gene was selected, a slightly different selection protocol was applied: Following transformation cells were plated on YPD agar media and incubated at 30 °C overnight to allow recovery. The grown cell lawns were replica plated on YPD agar plates supplemented with 300 ug ml^{-1} hygromycin or α-aminoadipate, respectively, and grown for 2-3 days at 30 °C to select for transformants.

Colonies growing on selective agar media were purified for clonality by streaking on selective agar for single colonies.

3.2.1.2.4 Spot titer assay and determination of the minimal inhibitory concentration in *S. cerevisiae*

Antibiotic resistance of *S. cerevisiae* cells was determined in spot titer assays by measuring the minimum inhibitory concentrations (MICs), i.e., the lowest concentration of an antibiotic that is sufficient to inhibit visible growth. For spot titer experiments, cultures were inoculated from a single colony into 5 mL of synthetic complete (SC) media (1.7 g L^{-1} of yeast nitrogen base without amino acids and without ammonium sulfate, 1 g L^{-1} L-glutamic acid monosodium salt, 2 g L^{-1} SC powder) or SC lacking uracil (1.7 g L^{-1} of yeast nitrogen base without amino acids and without ammonium sulfate, 1 g L^{-1} L-glutamic acid monosodium salt, 1.92 g L^{-1} yeast synthetic drop-out medium supplements without uracil) supplemented with 2% raffinose and 0.1% glucose as carbon source. Following inoculation, the cultures were incubated for 18 h at 30 °C while shaking at 200 rpm. Cultures were diluted to an OD_{600} of 0.1 into 5 mL of fresh SC media supplemented with 2% raffinose and 0.1% glucose and grown for 3 doublings (~6 h) at 30 °C while shaking at 200 rpm. Per culture 4 mL of cells were harvested by centrifugation at 2,000*g* at room temperature for 5 min, adjusted to an OD_{600} of 5 in phosphate-buffered saline, pH 7.4, and 5-fold serially diluted in phosphate-buffered saline. 3 µL of each dilution were spotted on pre-warmed SC agar media plates supplemented with 2% galactose and 2% raffinose and increasing concentrations of nourseothricin or G418, respectively. The agar plates were incubated at 30 °C for 72 h unless specified otherwise and cell growth was documented by imaging of the agar plates every 24 h. The strains' growth on agar plates over the range of tested antibiotic concentrations was evaluated. MICs were calculated according to standard protocols.[71] Five-fold cell dilutions were used to calculate the average MIC of each strain. To calculate relative MICs of the tripartite-Im7 variant fusions, they were compared to the reference strain, namely cells expressing Im7 WT in the tripartite fusion.

3.2.1.2.5 Yeast growth curves to determination antibiotic sensitivity

Single colonies were grown overnight in 5 mL SC medium supplemented with 2% raffinose and 0.1% glucose and grown at 30 °C while shaking at 200 rpm. The following day the cultures

were diluted to an OD_{600} of 0.1 in fresh SC medium supplemented with 2% raffinose and 0.1% glucose and grown for 3 doublings (~6 h) at 30 °C while shaking at 200 rpm until they reached an OD_{600} of ~0.8. Cells were spun down at 2,000*g* and room temperature for 5 min and then resuspended in SC medium supplemented with 2% raffinose and 2% galactose to adjust their OD_{600} to 1. The OD-adjusted cultures were diluted ten-fold to an OD_{600} of ~0.1 through pipetting 20 µL per sample into 180 µL of SC medium supplemented with 2% raffinose and 2% galactose and respective antibiotic concentrations in a Costar 96-well flat bottom transparent polystyrene plate. Specific wells were inoculated with medium only for background correction purposes. The wells on the edge of the plate were not used for growth curve experiments but filled with H_2O. After pipetting the cultures, buffers and H_2O into the wells, the plate was sealed with a Breath-Easy film (USA Scientific, 9123-6100). The plate was then shaken for 550 s in a thermostated microplate reader (TECAN M200 Infinite Pro) at 30 °C or as specified for followed by OD_{600} measurement for ~100 cycles (about 24 hours in total with OD_{600} measurement every 15 min). Using the plate reader software, the raw OD_{600} data were exported as table in EXCEL format with the addition of kinetic time stamps and growth curves plotted using the EXCEL Microsoft program.

3.2.2 Molecular biology and genetics

Standard methods for molecular biology were adapted from the laboratory manual books of Sambrook and Russell on molecular cloning.[101]

3.2.2.1 Isolation of plasmid DNA from *E. coli* cells

Plasmid DNA was prepared from 5 mL of saturated *E. coli* culture using the NucleoSpin plasmid kit (Macherey-Nagel). The plasmid DNA was isolated according to the manufacturer's instructions and eluted from the silica-membrane columns with either ddH_2O or elution buffer (EB buffer) provided in the kit.

DNA solutions were stored at 4 °C (short-term) or at -20 °C (long-term).

3.2.2.2 Isolation of genomic DNA from yeast cells

To isolate genomic DNA (gDNA) from yeast cells the Wizard® Genomic DNA Purification Kit (Promega) was used according to the manufacturer's instructions for yeast cells (*3.F. Isolating Genomic DNA from Yeast*). In brief, the multi-step purification involved the lysis of yeast cells by incubation of 5 OD_{600} cells in 300 µl of 50mM EDTA supplemented with 562 units of lyticase for 30-60 min at 37 °C followed by alkaline lysis of the cells and their nuclei. Then, cellular proteins were removed by salt-precipitation following desalting and concentrating of the gDNA by isopropanol and ethanol precipitation. The dried gDNA was rehydrated and subjected to a final RNase A digestion step. gDNA preparations were stored at -20 °C.

3.2.2.3 Determination of DNA concentration

To determine DNA concentrations DNA absorbance was measured at 260 nm using a NanoDrop™ 2000/2000c spectrophotometer (Thermo Scientific). By using Lambert-Beer Law the DNA concentration was calculated. The ratio of the absorbance at 260 nm compared to 280nm (A_{260nm}/A_{280nm}) were used to determine protein contamination in the sample.

3.2.2.4 DNA modifications

3.2.2.4.1 Restriction of DNA

For the site-specific restriction of plasmid DNA or PCR product, the DNA was incubated with the respective restriction enzymes using buffer conditions and temperatures according to the manufacturer's recommendations. Per µg of DNA 5-10 units of restriction enzyme were used. If possible, the enzyme was heat inactivated after incubation according to the manufacturer's instructions. In case the DNA was used in downstream applications the buffer was exchanged and small nucleotide fragments removed using the PCR clean-up kit (Macherey-Nagel) according to the manufacturer's instructions. Alternatively, the restriction enzymes, buffer components and unwanted nucleotide fragments were removed by separating the DNA fragments by agarose gel electrophoresis. The desired DNA fragments were excised and extracted from the gel as described in 3.2.2.5.

3.2.2.4.2 Ligation of DNA

To covalently ligate DNA fragments T4 DNA ligase (400 units per 20 µl ligation reaction) and the appropriate ATP-containing, reducing ligase buffer were added. To optimize the ligation reactions vector:insert ratios of 1:3, 1:5 or 1:7 and a total DNA amount between 50- 200 ng per 20 µl ligation reaction were used. The ligation reactions were incubated at 16 °C overnight. The enzyme was heat-inactivated by incubation at 65 °C for 10 min.

3.2.2.4.3 Phosphorylation and dephosphorylation of DNA

To prevent religation of a digested vector backbone in a ligation reaction, the cohesive ends of the vector were dephosphorylated with antarctic phosphatase. A standard 20 µl dephosphorylation reaction contained 1-5 µg of digested vector DNA, antarctic phosphatase buffer as recommended by the manufacturer and 5 units of antarctic phosphatase. The reaction was incubated at 37 °C for 1 - 3 h followed by heat inactivation of the enzyme at 80 °C for 5 min. For phosphorylation of PCR products prior to ligation, 100-200 ng of purified PCR product were incubated with 500 units of T4 polynucleotide kinase in the appropriate buffer and 1 mM ATP in a 50 µl reaction and incubated at 37 °C for 1 h.

3.2.2.4.4 Gibson assembly cloning

To assemble 2-3 DNA fragments into a vector Gibson Assembly (NEB) was used. First, desired fragments including the vector were linearized by amplification from a plasmid templates using Phusion polymerase and primers designed in SnapGene. The primers were complementary to the ends of the fragment and generated a 15-25 bp overlap at their ends. After the PCR reaction was finished a small aliquot per reaction was analyzed by agarose gel electrophoresis to check the PCR efficiency and PCR product integrity. PCR fragments were then digested with Dpn1 before using them for Gibson Assembly to avoid contamination with the PCR template DNA. 0.02-0.5 pmols of DNA fragments were used in Gibson Assembly. To calculate the number of pmols of each fragment for optimal assembly based on fragment length and weight the NEBBioCalculator online tool was utilized. Generally, 50-100ng of vector with a 2-5 fold molar excess of each insert was added to 10 µl of 2x Gibson Assembly Master Mix and the reaction volume adjusted to 20

µl. The assembly reaction was incubated at 50 °C for 60 min followed by storage at -20 °C or subsequent transformation into chemically competent *E. coli* cells.

A typical Gibson Assembly reaction was set up as follows:

Gibson Assembly reaction	
Total amount of fragment	0.02-0.5 pmols
Gibson Assembly Master Mix (2x)	4 µL
Nuclease-free water	Ad 20 µL

3.2.2.4.5 In-Fusion cloning

The In-Fusion HD Cloning Plus Kit (Takara) was used to assemble multiple PCR fragments into a vector. The reaction was set up according to the manufacturer's recommendations for the kit. PCR primers that generate a 15-25 bp overlap with the ends of each of the flanking fragments were designed in SnapGene. To amplify DNA fragments including a linearized vector the Kit's CloneAmp HiFi PCR Premix was used in a 25 µl PCR reaction with 10-50 ng of DNA template and 7.5 pmol of each of the respective primers.

Typical CloneAmp HiFi PCR reaction to amplify fragments:

CloneAmp HiFi PCR reaction	
CloneAmp HiFi PCR Premix	12.5 µL
Primer 1	7.5 pmol
Primer 2	7.5 pmol
Template DNA	10-50 ng
Nuclease-free water	Ad 25 µL

The prepared CloneAmp HiFi PCR reaction was incubated in a thermocycler using the following program:

Cycle step	**Temperature**	**Time**	**Number of cycles**
Initial denaturation	98 °C	10 s	1
Denaturation	98 °C	10 s	
Annealing	55 °C	5 s	30-35
Extension	72 °C	5-30 s/kb	
Final extension	72 °C	10 min	1

The efficiency of the PCR reaction and integrity of the PCR product was analyzed by separating a small sample of the PCR reaction by agarose gel electrophoresis (see 3.2.2.5). The PCR reaction was incubated with Dpn1 to digest the DNA template and avoid contamination by the original template DNA. Then the PCR products were spin-column purified using a PCR clean-up kit (Macherey-Nagel) according to the manufacturer's instructions and the eluted fragment concentration determined using a NanoDrop spectrophotometer (3.2.2.3). For the In-Fusion cloning procedure 50-100 ng of linearize vector and a maximum amount of 100 ng of purified fragments (molar ratio of vector:insert is 1:3 or 1:5) were mixed with In-Fusion HD Enzyme Premix in a 10 µl reaction and incubated at 50 °C for 15 min in a thermocycler. After completion of the incubation the sample was either stored at -20 °C or transformed into *E. coli* cells.

A typical In-Fusion cloning reaction was set up as follows:

In-Fusion cloning reaction with purified PCR fragments	
PCR fragments	10-100 ng
Linearized vector	50-100 ng
In-Fusion HD Enzyme Premix (5x)	2 µL
Nuclease-free water	Ad 20 µL

3.2.2.5 Agarose gel electrophoresis and DNA isolation

DNA fragments were separated by horizontal agarose-gel electrophoresis using 0.8-1.5% agarose gels depending on the size of the DNA fragments. Agarose gels were prepared by melting agarose in 1x TAE buffer in a microwave, the solution cooled at room temperature to 60 °C and SYBR Safe DNA gel stain added in a 1:10,000 dilution. The solution was poured into an agarose gel casting chamber, bubbles were removed and a comb added to generate wells and the gel left at room temperature for 20-30 min to solidify. Once the gel solidified, the comb was removed and the agarose gel submerged in 1x TAE running buffer in the agarose gel chamber. DNA was mixed with 6x loading dye, loaded into the wells of the gel and the DNA separated at 120 V for 1-2 h. For the visualization of the DNA, a gel imaging system (ChemiDoc MP Imaging System, BioRad) was used. DNA sizes were estimated by comparison to a DNA standard (1 kb DNA Plus ladder).

For the isolation of DNA from agarose gels the DNA fragment of choice was excised while visualizing with the gel imaging system using a razor blade. The DNA was extracted and purified from the gel using a polymerase chain reaction (PCR) and Gel clean-up kit (Macherey-Nagel) according to the manufacturer's instructions. The DNA was eluted from the spin-column with either ddH_2O or in elution buffer supplied with the kit.

5.2.2.6 Polymerase chain reaction (PCR) techniques

5.2.2.6.1 Standard PCR using Phusion polymerase

PCR was performed to selectively amplify DNA sequences in vitro. The method is based on the repeated duplication of a DNA sequence by a thermostable DNA polymerase in the presence of dNTPs and two specific oligonucleotide sequences that are complementary to the ends of the desired DNA fragment. PCR reactions with Phusion polymerase were set up according to the manufacturer's recommendations.

A typical 20 µl PCR reactions with Phusion polymerase contained following components:

Phusion PCR reaction	
Phusion polymerase	0.2-1 unit
5x Phusion high fidelity buffer	4 µL
Template DNA	1-50 ng
dNTPs	100 µM
Primer 1	0.1-0.5 µM
Primer 2	0.1-0.5 µM
Nuclease-free water	Ad 20 µL

20 µl PCR reactions were pipetted together on ice before they were transferred to a thermocycler.

A typical thermocycler program for PCR reactions with Phusion polymerase involved the following steps:

Cycle step	**Temperature**	**Time**	**Number of cycles**
Initial denaturation	98 °C	30 s	1
Denaturation	98 °C	10 s	
Annealing	Various (55-72 °C)	20 s	25-35
Extension	72 °C	15-30 s/kb	
Final extension	72 °C	10 min	1

The annealing temperature for the primers in the Phusion PCR reaction were determined by the NEB Tm Calculator online tool (https://tmcalculator.neb.com/#!/main) and depended on the length and GC-content of the oligonucleotide.

5.2.2.6.2 Site-directed mutagenesis

To site-specifically generate point mutations or replace amino acids in a double-stranded plasmid DNA the QuickChange II Site-Directed Mutagenesis Kit (Agilent) was used according to the manufacturer's instructions. The three-step procedure involved the synthesis of mutant DNA strands by PCR amplification of a miniprep plasmid DNA with appropriate mutagenesis primers, subsequent digestion of the parental, (hemi-)methylated template DNA by Dpn I, and lastly transformation of the mutated molecule into competent *E. coli* cells to repair the nicked strands. Oligonucleotide primers encoding the desired mutation(s) were designed using Agilent's web-based QuickChange Primer Design Program (https://www.agilent.com/store/primerDesignProgram.jsp).

For the synthesis of mutant DNA strands the following PCR reaction with PfuUltra HF polymerase was typically set up:

Mutant strand synthesis reaction using PfuUltra HF DNA polymerase	
PfuUltra HF DNA polymerase (2.5U/ul)	0.5 µL
10x reaction buffer	2.5 µL
Primer 1	0.5 µM
Primer 2	0.5 µM
Template DNA	2.5-25 ng
dNTPs	0.5 µL
Nuclease-free water	Ad 25 µL

The prepared PCR reaction was incubated in a thermocycler using the following cycling parameters:

Cycle step	**Temperature**	**Time**	**Number of cycles**
Initial denaturation	95 °C	30 s	1
Denaturation	95 °C	30 s	
Annealing	55 °C	60 s	18
Extension	68 °C	60 s/kb	

The amplification was checked by electrophoresis of a small aliquot (5 µL) of the product on an agarose gel. The PCR reaction was proceeded with a Dpn I (5 units 20 μL^{-1} reaction) digest at

37 °C for 1-4 h to digest the parental, nonmutated double stranded plasmid template DNA used in the PCR reaction. Then, 5 µL of the reaction was transformed into 50 µL chemically competent 10β cells (NEB) by heat-shock transformation.

5.2.2.6.3 Yeast genotyping using Taq polymerase

To screen yeast transformants for the presence of a gene insertion or deletion at a specific locus in the genome or to amplify a piece of DNA from the genome for sequencing PCR with GoTaq polymerase was performed. The PCR reactions were conducted according to instructions by the manufacturer. Primers were designed to upstream and downstream flank the genomic region of interest (upstream and downstream primers), to produce PCR products with a length between 500 - 2000 bp and to have identical melting temperatures around 60 °C as calculated by Promega's web-based biomath tool (https://www.promega.com/resources/tools/biomath/tm-calculator/).

Prior to setting up the PCR reaction gDNA was extracted and purified from yeast. The gDNA was used as DNA template in the PCR reaction.

A single 25 µL genotyping PCR reaction using GoTaq polymerase contained the following components:

Genotyping PCR using GoTaq polymerase	
2x GoTaq Green Master Mix	12.5 µL
Upstream primer	0.5-1 µM
Downstream primer	0.5-1 µM
Template gDNA	<250 ng
Nuclease-free water	Ad 25 µL

The PCR reaction was pipetted together on ice before it was transferred to a thermocycler. A typical thermocycler program for the GoTaq PCR reaction involved the following steps:

Cycle step	**Temperature**	**Time**	**Number of cycles**
Initial denaturation	95 °C	2 min	1
Denaturation	95 °C	45 s	
Annealing	Various (55-65 °C)	45 s	30-40
Extension	72 °C	60 s/kb	
Final extension	72 °C	5 min	1

Following amplification, the PCR products were directly analyzed by electrophoresis on an agarose gel. If desired the PCR products were purified by spin-column purification using the PCR and Gel clean-up kit (Macherey-Nagel) according to the manufacturer's instructions for PCR clean up, eluted in 25 µL of elution buffer supplied with the kit and sent for sequencing.

5.2.2.6.4 Direct PCR from yeast cells for genotyping

To analyze yeast transformants for the presence of a gene insertion or deletion at a specific locus in the genome directly from yeast cell without prior extraction of gDNA, the Phire Plant Direct PCR kit was used. PCR primers were designed that flank the genomic locus of interest upstream and downstream and the melting temperature and optimal annealing temperature calculated using the PCR web tool available from Thermo Scientific.

20 µL PCR reactions were typically set up as follows:

Genotyping PCR using Phire Plant Direct PCR master mix	
2x Phire Plant PCR master mix	10 µL
Upstream primer	0.5 µM
Downstream primer	0.5 µM
Yeast cells	0.5 µL
Nuclease-free water	Ad 20 µL

The following cycling program was typically used to incubate the PCR reaction in a thermocycler.

Cycle step	**Temperature**	**Time**	**Number of cycles**
Initial denaturation	98 °C	5 min	1
Denaturation	95 °C	5 s	
Annealing	Various (55-65 °C)	5 s	35-40
Extension	72 °C	20 s/kb	
Final extension	72 °C	1 min	1

After the PCR reaction was completed samples were directly loaded onto an agarose gel and analyzed by electrophoresis.

5.2.2.7 DNA Sequencing

To determine the DNA sequence or check the integrity of a DNA sequence of purified plasmid or PCR products, the DNA of interest was analyzed by Sanger sequencing. For this purpose, a

sequencing primer that is complementary to the DNA sequence around 100 bp upstream of the sequence of interest was prepared. 5 µL of sequencing primer with a concentration of 5 µM was added per sequencing reaction. The template DNA was diluted to 80 ng μL^{-1} in 10 µL nuclease-free, ddH_2O for plasmid DNA or 5 ng μL^{-1} in 10 µL nuclease-free, ddH_2O for purified PCR products. The premixed samples were submitted to sequencing services GENEWIZ or Genscript and the results analyzed using the software SnapGene.

5.2.2.8 Construction of tripartite fusion plasmids

5.2.2.8.1 Construction of APH tripartite fusion plasmids

The APH tripartite constructs were derived from the plasmids pYES-APH WT and pYES-APH55-Im7 WT which are both derived from the Bardwell lab collection. These plasmids contain the intact APH antibiotic resistance marker and that marker containing an insertion of the WT Im7 gene at residue position 55 of APH, respectively, as previously described.[3] pYES2/CT (Invitrogen, V825120) is a 2 µ yeast protein expression vector that features a galactose inducible promoter and the URA3 auxotrophic marker gene for selection in yeast. C-terminally to the multiple cloning site the vector carries a V5 epitope that allows for detection and a polyhistidine (6xHis) for purification purposes when they are in fusion with the 3' end of the inserted sequence. The untagged APH tripartite sequences of pYES-APH WT and pYES-APH55-Im7 WT were encoded on the pYES2/CT vector and modified by the addition of a C-terminal 3xFLAG tag using primers PVS047 and PVS048 which generated plasmids pVS178 and pVS180. The tagged APH-tripartite fusion sequences were cloned into the CEN/ARS plasmid pYC2/CT (Invitrogen, V825520), which has the same features as pYES2/CT by Gibson Assembly with primers PVS072-PVS075. This cloning step generated plasmids pYC2-APH wt-Flag (pVS008) and pYC2-APH Im7 wt-Flag (VS009). To insert various Im7 variant sequences into the tripartite fusion Im7 variant sequences were isolated from plasmids available in the Bardwell lab collection by PCR with primers PVS126 and PVS127. The PCR amplification step generated a BamHI restriction site on the 5' end and a SacI restriction site on the 3' end of the Im7 variant fragment. The PCR product as well as the APH

tripartite plasmid were digested with enzymes BamHI and SacI and subsequently ligated to generate APH-Im7 variant tripartite fusions.

To try to enable rapid microscopic distinction between misfolding, proteolysis or aggregation of the tripartite variants we fused a red fluorescent protein (mKate2) to the C- or N-terminus of APH-Im7 variant fusions. For this purpose, pFA6a-link-yomKate2-CaURA3 (addgene 44878) was modified by eliminating its SacI restriction site by site directed mutagenesis using primers PVS315 and PVS316 which generated plasmid pVS151. To add a galactose inducible promoter, a respective pGal1 promoter sequence was amplified with primers PVS307 and PVS308 from plasmid template pKG001. The PCR amplification step added a 5' PvuII and 3' HindIII restriction site to the pGal1 sequence. The PCR fragment and vector pVS151 were digested with PvuII and HindIII and ligated to generate plasmid pFA6a-pGal1-link-yomKate2-CaURA3 (pVS152). A yeast codon optimized sequence of the APH-Im7 WT tripartite fusion with a C-terminal 10 GS linker sequence (yoAPH-Im7 WT-10GS) was synthesized by Genscript and a 5' HindIII and a 3' PacI restriction site added to the sequence by PCR with PVS309 and PVS310. The PCR product and pVS152 were digested with HindII and PacI and the fragment and vector ligated to generate plasmid pFA6-pGal1-yoAPH-Im7wt-10GS-mKate2 -CaURA3 (pVS155). Alternatively, the yeast codon optimized APH sequence was inserted 3' to the plasmid encoded yomKate2 sequence and the two protein encoding sequences fused with a GGSGGSGGSG encoding linker sequence to generate pGal1-mKate2-APH (pVS400, pFA6a-pGal1-yomKate2-10xGS-yoAPH-CaURA). The mKate2 sequence of pVS155 was eliminated and a 6 amino acid glycine serine linker (GGSGGS) followed by a 3xFLAG tag added to the 3' terminus of the APH tripartite fusion by PCR with primers PVS348 and PVS349 and the product ligated to generate pFA6-pGal1-yoAPH-Im7 WT-GS-3xFlag (BHH66) and pGal1-yoAPH-3xFLAG (pFA6a-pGal1-yoAPH-3xFLAG-CaURA (BHH64), respectively. The earlier elimination of a SacI restriction site in the original pFA6a-link-yomKate2-CaURA3 vector backbone allowed restriction digestion cloning of test proteins using SacI and BamHI into the 40 amino acid glycine-serine rich linker (CLNGSGSGSGSGSGSSGSGSGSSSGSSGSGSGGGGSGLNT) fusing the APH marker halves. In order to allow simultaneous selection for another construct using URA3, the CaURA3 auxotrophy cassette of APH tripartite fusions was changed to a hygromicin B selection marker (HygMX) in some of the

constructs. This was accomplished by PCR amplification of the HygMX cassette from pVS141 (described below) with primers PVS413 and PVS414, which added flanking SpeI and BglII restriction sites to the HygMX. The HygMX cassette was cloned into the vector pFA6-pGal1-yoAPH-Im7 WT-GS-3xFlag (BHH66) as well as its derivatives fused with different test proteins by restriction digest with SpeI and BglII. This cloning procedure generated plasmid pFA6-pGal1-yoAPH-3xFLAG-HygMX (pVS498).

3.2.2.8.2 Construction of NAT tripartite fusion plasmids

The NAT80 tripartite fusion was derived from pYC-NAT80 Im7 F15A, a yeast CEN/ARS plasmid that contains the Im7 F15A variant cloned into pYC2/CT (Invitrogen, V825520) and was available from the lab collection. The V_5-His_6 epitope tag encoded on the pYC2/CT plasmid was fused 3' to the NAT tripartite coding sequence by PCR with primers PVS045 and PVS046 and ligation of the PCR product. The resulting plasmid pVS024 was used as a template to clone different Im7 variants into the NAT tripartite fusion with BamHI and SacI restriction digest. The NAT80-Im7 variant fusions were integrated into the LYS2 locus of the yeast strain BY4741.

To evaluate the role of the exact insertion site on tripartite fusion function, 4 different expression constructs of the NAT tripartite fusion were made by first inserting a 39-amino acid GS linker (AAAGSGSGSGSGSGSSGSGSGSSSGSSGSGSGGGGSAAA) at residues 76, 78, 80, or 82. All constructs were cloned into *E. coli* expression plasmid pTrc99a. This was followed by the insertion of either the WT Im7 or the double mutant sequence of Im7, Im7 L53A I54A, between BamHI and SacI restriction sites that were located in the middle of the GS linker. To further regulate the expression of the tripartite fusion, the NAT78 tripartite fusions were cloned into a backbone of pKG001 (pDAD1006-WT YFP, a kind gift from Prof. Allan Drummond) (REF). This plasmid contains a yellow fluorescent protein (YFP) under the control of a galactose inducible promoter (pGal1) as well as sequences homologous to Leu2 flanking sequences for genomic integration into the yeast genome. The kanamycin selection marker (KanMX) of this backbone was replaced with a hygromycin resistance marker (HygMX). To swap out the KanMX sequence, pKG001 was digested with XmaI and SalI, and the HygMX cassette was amplified from pCORE-UH (addgene, 72239) with primers PVS249 and PVS250 that generated flanking sequences encoding XmaI and SalI

restriction sites. XmaI and SalI digestion of the amplified product following ligation into the XmaI and SalI digested vector pKG001 generated plasmid pVS141. The NAT78 tripartite fusion sequences were inserted into pVS141 to replace the YFP sequence by Gibson Assembly. For this cloning step the NAT tripartite fusion was amplified with primer pair PVS287, PVS288 and the plasmid amplified with primer PVS289 and PVS290. To enable BamHI- and SacI-mediated restriction site cloning of test proteins into the antibiotic resistance marker as part of the tripartite fusion, the BamHI restriction site in the backbone and the SacI restriction site in the hygromycin resistance cassette were eliminated by site directed mutagenesis with primer PVS259 and PVS260 and PVS319 and PVS320, respectively. To avoid any unintended recombination events *in vivo* the FRT site encoded in the plasmid was removed by PCR with primer HK39 and HK40 and ligation of the product (pBHH62). To add a transcriptional terminator sequence to the plasmid the Cyc1 transcriptional terminator sequence was cloned 3' of the stop codon of the NAT tripartite fusion using Gibson Assembly. For this purpose, the Cyc1 transcriptional terminator sequence was amplified from plasmid pYC2/CT with primers HK28 and HK29 and cloned into the PCR amplified vector using primers HK30 and HK31.

The Leu2 homologous sequences encoded on the plasmid were replaced by sequences homologous to flanking sequence of the gal1/gal10 locus. To allow linearization of the plasmid for integration into the gal1/10 locus by convenient restriction digest a SpeI restriction site was engineered between the gal1/10 flanking sequences encoded on the plasmid. This cloning procedure resulted in the plasmids pGal1-NAT78-linker-V5His6 (pVS485), pGal1-NAT78-Im7 WT-V5His6 (pVS486), pGal1-NAT78-Im7 L53AI54A-V5His6 (pVS487) and pVS144-YFP-CYC1terminator, Gal1/10 overhang, SpeI (pBHH71) as control plasmid. The NAT78-Im7 WT fusion construct was used as a template for cloning various test proteins into the NAT78 tripartite fusion by BamHI and SacI restriction digest. The cloned constructs were used for genomic integration of the NAT78 tripartite expression constructs into strain MDY669 (REF Geiler Samerotte) to replace the gal1/gal10 locus or into yeast strain Y14537 in the HO locus.

3.2.2.8.3 Construction of test protein sequences into the tripartite fusion

BamHI and SacI restriction sites located in the glycine-serine-rich sequence (GS linker; 40 GS-linker sequence for APH-tripartite: CLNGSGSGSGSGSGSSGSGSGSSSGSSGSGSGGGGSGLNT; 39 GS linker for NAT-tripartite fusions: AAAGSGSGSGSGSGSSGSGSGSSSGSSGSGSGGGGSAAA) that fused the two antibiotic resistance marker halves enable the facile and convenient insertion of various test proteins into this GS linker using restriction site cloning. To add compatible restriction sites to the test protein gene sequence a 5' BamHI and a 3' SacI restriction site was added to the test protein gene sequences by overhang extension PCR with appropriate primers. The following primer sets were used to amplify the test protein encoding sequences: PVS126 and PVS127 for Im7 variants, PVS327 and PVS328 for a-synuclein variants, HK24 and HK25 for Aβ42 variants, HK15 and HK16 for the complete Rnq1 sequence, HK15 and HK22 for Rnq1C variants, HK17 and HK18 for the complete Sup35 sequence, and HK17 and HK20 for Sup35NM. To avoid any potential alternative translational start site within the tripartite fusions, the start codon for the fused variants of Aβ42, α-synuclein, Rnq1, and Sup35 was changed from the Met codon ATG to the Leu codon CTG. The respective sequences of each of the test proteins that were used as templates for cloning were derived from plasmids pDONR221-Abeta 1-42 and pDONR221-Abeta 1-42 m2[102] for Aβ42 WT and Aβ42 F19T F20T I31P, a scrambled Aβ42 DNA template sequence was designed according to Marshall et al.[103] with the amino acid sequence AIAEGDSHVLKEGAYMEIFDVQGHVFGGKIFRVVDLGSHNVA and the respective DNA sequence (gcaattgcagaaggagactcacatgtcctcaaagaaggagcgtatatggaaatattcgatgtccaaggtcatgtatttggtggtaaaat cttccgagtggtcgatttgggctcacataacgtcgca) was and synthesized by Genscript. Plasmids pRS426-α-SynWT, -α-SynA53T, -α-SynA30P and -α-SynE46K[81] served as templates for cloning of α-synuclein variants, plasmid pD08[104] served as cloning template for Sup35 variant sequences and plasmid pRS416 Gal-RNQ1[105] served as template for cloning of Rnq1 variants.

3.2.2.9 Genomic integration of the tripartite fusions

Tripartite fusions were integrated into the yeast genome by homologous recombination of PCR amplified sequences. The linearized sequences for genomic integration included the Gal1 promoter, the tripartite fusion encoding sequence, the transcriptional terminator, and the yeast

selection marker. PCR amplification using the primers listed below generated flanking sequences which were homologous to the respective integration locus on the genome. For integration into the *S. cerevisiae* HO locus of strain Y14537 with the genotype MAT alpha HAP1+ ura3Δ0 his3Δ1 (a kind gift from Prof. Charlie Boone), tripartite fusions were amplified using primers PVS411 and PVS412. Y14537 allows maintenance of the plasmid pYC2-Sup35C-V5His6 (see below) through URA3 autotrophy. For integration of the APH tripartite fusions into the gal1/gal10 locus of MDY669 (a kind gift from Prof. Allan Drummond) with genotype MATa ura3Δ0 leu2Δ0 his3Δ0 met15Δ0 SpHIS5::pACT1-GAL3 gal1Δ,gal10Δ::LEU2 (v.1.1) primers PVS396 and PVS397 were used. Strain MDY669 is derived from BY4741 and genetically modified such that the endogenous promoter of GAL3 is replaced with the constitutively active ACT1 promoter and the adjacent gal1 and gal10 genes are replaced by a LEU2 marker.[47] These modifications should allow a tunable induction of the Gal1 promoter with the inducer galactose instead of a switch-like induction. We thought this tunable features is especially important for the expression of the tripartite fusions with misfolding proteins which may exhibit a dose-dependent fitness cost on the cells.[47] Moreover, a tunable expression is also desirable for the expression of tripartite fusions with aggregation prone proteins since aggregation is also a concentration dependent process. To integrate NAT78 tripartite constructs into the gal1/gal10 locus of MDY669, the plasmids were linearized by digestion with SpeI as described above. For integration of the NAT80-Im7 tripartite fusions into the LYS2 locus of BY4741 (MATa his3Δ1 leu2Δ0 met15Δ0 ura3Δ0), primers PVS400 and PVS401 were used for amplification and linearization of the tripartite fusion sequence. Transformed yeast cells were selected for URA auxotrophy, hygromicin B resistance, or growth on alpha-aminoadipate, depending on the marker contained in the template sequence.

3.2.2.10 Cloning of colicin E7

The nuclease fragment of the binding partner of Im7, namely colicin E7 (GenBank: RDQ95010.1, residues 63–193), was synthesized by GenScript and cloned into pAG424 featuring a TDH3 promoter and a TRP auxotrophy cassette using Gibson Assembly with primers PVS007, PVS010, PVS122, and PVS123. The H162A mutation was incorporated into this construct to

inactivate its otherwise deleterious nuclease activity.[106] This cloning procedure yielded plasmid pAG424-E7 H162A nuclease fragment.

3.2.2.11 Generation of a pdr5Δ yeast strain background

To delete the endogenous multidrug transporter gene PDR5 of yeast strain MDY669 and to subsequently recycle the utilized selection marker, a linearized DNA fragment was designed according to Akada et al. [107] The DNA fragment encoded a URA3 cassette with flanking sequences homologous to flanking sequences of the PDR5 gene. After transformation of the PCR amplified fragment into yeast cells and selection on minimal agar media lacking uracil, cells were selected for loss of the URA3 marker cassette by growth in media supplemented with 5-FOA. Further details on this method can be found in Akada et al.[107]

3.2.2.12 Cloning of the C-terminal domain of Sup35

The C-terminal domain of Sup35 was amplified from the Sup35-containing template pDJ346 (a kind gift from Prof. Daniel Jarosz) using primers PVS428 and PVS429 and cloned into the backbone of pYC2 featuring a galactose inducible promoter and URA3 selection marker by restriction digestion with HindIII and EcoRI. This cloning procedure yielded plasmid pYC2-Sup35C-V5His6 (pVS540).

3.2.2.13 RNA extraction and reverse transcription PCR (RT-qPCR)

For quantification of mRNA levels of APH tripartite fusions, quantitative reverse transcription PCR (RT-qPCR) was performed. Cells were grown to early log-phase (OD_{600} ~0.3) at 30 °C and shaking at 200 rpm in SC medium with 2% raffinose and 0.1% glucose following induction with 2% galactose to express tripartite fusion proteins for 4 h. Cells were collected and washed with ice cold, sterile, double-distilled water and cell pellets stored at –80 °C. To extract RNA cells were incubated at 65 °C for 1 h in 400 µL of TES buffer (10 mM Tris pH 7.5, 10 mM EDTA, 0.5% SDS) and 400 µL of acid phenol:$CHCl_3$ (Calbiochem, 6800). RNA was extracted twice from cells with acid phenol:$CHCl_3$ and once with chloroform (Sigma, C2432), and finally isolated by ethanol precipitation. For removal of genomic DNA, 20 µg of RNA were treated with DNA removal kit

(DNA-free DNA Removal Kit, Invitrogen, AM1906) according to the manufacturer's instructions. To generate cDNA, 1 µg of DNA-free RNA was transcribed using PrimeScript 1st strand cDNA Synthesis Kit (Takara, 6110A) and then diluted 1:5,000 for subsequent quantitative PCR reactions. Reverse transcription-quantitative PCRs were performed and analyzed using Bullseye EvaGreen qPCR master Mix (Bullseye, BEQPCR-R) according to the manufacturer's instructions in an Eppendorf Mastercycler epgradient S realplex2 detection system. The average of two technical replicates were used to determine relative mRNA abundance using the 2−ΔΔCt method, by normalizing to ACT1. Experiments were performed in three biological replicates. The sequences of primers (qPCR_APH_F, qPCR_APH_R, qPCR_ACT_F, qPCR_ACT_R) used for qPCR are listed in 3.1.7.1 Oligonucleotide primers.

3.2.3 Protein biochemistry

3.2.3.1 SDS-Polyacrylamide gel electrophoresis (SDS-PAGE)

Polyacrylamide gel electrophoresis (PAGE) is a well-established method for the separation, detection, and analysis of proteins in a sample and also the first step of western blotting analyses (3.2.3.2 Western blotting and quantification of protein expression levels).

To run an SDS-PAGE, the comb as well as the green tape on the bottom of a Mini-PROTEAN TGX stain-free precast gel (Bio-Rad) was removed. The gel was clamped into the running module of the Mini-PROTEAN Tetra system. 1x SDS-running buffer was added to the inner and outer chambers. The protein samples were mixed with 5x reducing SDS sample buffer, boiled for 5 min at 95 °C, spun down briefly and loaded into the wells of the gel. 6-10 ul of a protein standard (Prestained protein MW marker, Pierce, 26612) was included in the gel as molecular weight reference. The gel was run at 120 V for 1-1.5 h on ice until the dye front reached the bottom of the gel. After completing the run, the gel was removed from the cassette and washed briefly in ddH_2O to remove the SDS-running buffer from the gel.

Using a Bio-Rad ChemiDoc imaging system, the proteins were visualized on the polyacrylamide gel to determine sample quality, level of separation, and protein load. For the

detection of proteins in the gel, the stain-free imaging technology of the gels was taken advantage of. The stain-free imaging technology utilizes a proprietary polyacrylamide gel chemistry to make proteins fluorescent directly in the gel with a short photoactivation. During the short UV-induced reaction a trihalo compound in the Bio-Rad Mini-PROTEAN TGX stain-free gels reacts with tryptophan residues in proteins to produce fluorescence. The to the protein molecules covalently bound fluorescent stain allowed the immediate visualization of proteins in the gel at any point during electrophoresis or later during Western blotting. To document the separation of the proteins in the gel, an image was taken after photoactivation of the compound.

3.2.3.2 Western blotting and quantification of protein expression levels

For quantitative western blotting, proteins of cell lysates were resolved by SDS-PAGE (3.2.3.1) using 10% acrylamide gels (Bio-Rad 10% Mini-PROTEAN stain-free TGX gels), and proteins were visualized using a Bio-Rad stain free gel imaging system as described above. Separated proteins were transferred onto a 0.2 mm PVDF membrane (Bio-Rad Trans-Blot Turbo Mini PVDF Transfer Packs) using semi-dry transfer (Bio-Rad Trans-Blot Turbo system). After the transfer the blot was soaked in ddH_2O to avoid drying of the membrane, and the quality of the protein transferred to the membrane was analyzed by the Bio-Rad stain-free blot imaging function provided in the Bio-Rad ChemiDoc imaging system. Then the membrane was blocked in Tris-buffered saline (137 mM NaCl, 2.7 mM KCl, 19 mM Tris base, pH 7.4) supplemented with 0.1% Tween 20 and with 5% non-fat dry milk for 1 h at room temperature with agitation at 60 rpm. Then the blot was incubated with the appropriate primary antibody which was diluted in Tris-buffered saline pH 7.4 supplemented with 0.1% Tween and 5% non-fat dry milk to an optimal concentration as recommended by the manufacturer or adjusted from experience: the anti-FLAG antibody (anti-FLAG, M2, Sigma F3165) and the anti-V5 antibody (anti-V5 antibody, Invitrogen, R96025) used for detection of the tripartite fusions were diluted 1:2000, the anti-Sup35 antibody (anti-Sup35, Abnova, PAB15578), or an anti-Rnq antibody (anti-Rnq, Abnova, PAB15579) were diluted 1:1000, and the antibodies used to detect a loading control protein, anti-G6PDH antibody or an anti-PGK1 antibody (anti-PGK1 antibody, Abcam, ab154613) were used at a dilution of 1:2000. The blot was incubated at 4 °C overnight on a horizontal platform with shaking at 60 rpm. After washing the

immunoblot 3 times with Tris-buffered saline pH7.4 supplemented with 0.1% Tween for 10 min, the blot was incubated with the appropriate secondary antibody (IRDye 800CW, Licor Biosciences, 926-32210; IRDye 680RD, Licor Biosciences, 926-68071) in Odyssey blocking buffer in Tris-buffered saline (Licor, 927-50000) for 1 h on a horizontal platform with shaking at 60 rpm at room temperature. Secondary antibodies were used in dilution 1:15,000. The membrane was washed 3 times in Tris-buffered saline supplemented with 0.1% Tween for 10 min at room temperature following fluorescence detection of the protein of interest using the Odyssey CLx detection system. Signal intensities were quantified using ImageJ software. For normalization of the V5 signal of NAT-Aβ42 tripartite fusions in the cycloheximide chase assays and for normalization of the FLAG signal in the analysis of aggregation propensities of APH tripartite fusions, signal intensities of the tripartite fusions were divided by the sample's PGK1 signal. To normalize the FLAG signal of tripartite fusions in all other assays the FLAG signal intensity was divided by the sample's G6PDH signal.

3.2.3.3 Preparation of cell extracts for tripartite-Im7 solubility assay

Yeast cells carrying APH- or NAT-Im7 tripartite fusion plasmids were grown in 5 mL SC media lacking uracil and supplemented with 2% raffinose and 0.1% glucose at 30 °C and shaking at 200 rpm. The saturated cultures were diluted to an OD600 of 0.1 in 30 ml fresh SC media lacking uracil and supplemented with 2% raffinose and 0.1% glucose and grown at 30 °C and shaking at 200 rpm until they reached an OD600 of 0.5 (~5 h). Then the expression of the tripartite fusions was induced by the addition of 2% galactose (final concentration) and the cultures incubated further for 4 h. In the case of the NAT-tripartite fusion cultures the cells were shifted to an incubation temperature of 34 °C after induction, as this temperature provided better antibiotic distinctions between strains for the NAT-Im7 constructs. A cell volume equaling a total OD600 of 22.5 was harvested by centrifugation at 2,500g for 30 s at room temperature. The following cell lysis was performed according to a published standard protocol.[50] In brief, the harvested cells were washed with ice cold, sterile, double-distilled water followed by centrifugation at 5,000g at 4 °C for 30 s. The cell pellet was resuspended in 150 mL 1x native yeast lysis buffer (30 mM HEPES pH 8.0, 150 mM NaCl, 1% glycerol, 0.5% Triton X-100, 1 mM DTT, 1 mM phenylmethylsulfonyl

fluoride (PMSF) and 1:500 EZBlock IV protease inhibitor cocktail) and flash frozen in liquid nitrogen. Lysates were prepared by beating with 100 mL acid washed glass beads (bead diameter 500 mm) at 4 °C using 10 cycles of 1 min vortexing followed by 1 min on ice. Lysates were clarified by centrifugation at 3,000g for 30 s at 4 °C. 50 mL of this supernatant was set aside as the total protein fraction. Another 50 µL of clarified lysate was centrifuged at 16,000g at 4 °C for 30 min. The supernatant was removed and designated the soluble fraction. The residual supernatant was removed from the pellet. To make sure all supernatant was removed, the pellet was washed by resuspending it in 200 mL lysis buffer by pipetting up and down followed by vortexing for 1 min at 4 °C to ensure resuspension of the pellet. The sample was centrifuged at 16,000g for 30 s at 4 °C and the supernatant removed following another centrifugation step at 16,000g for 5 s at 4 °C, after which residual supernatant was removed with a small volume pipette. The pellet was resolubilized by resuspending it in 10 mL 1x reducing SDS sample buffer, which concentrated the insoluble protein content five-fold compared to the soluble protein fraction. 12.5 mL of 5x reducing SDS sample buffer was added to the total protein and soluble protein fractions. All samples mixed with reducing sample buffer including the total, soluble and insoluble fractions were boiled at 95 °C for 5 min before running equal volumes of each lysate fraction on SDS–PAGE. The SDS-PAGE gels were processed for immunoblot analysis of the tripartite expression level using anti-FLAG (anti-FLAG, M2, Sigma F3165) or anti-V5 (anti-V5 antibody, Invitrogen, R96025), or anti-APH (Anti-Neomycin Phosphotransferase II Antibody, Sigma, AC113) together with an anti-glyceraldehyde 3-phosphate dehydrogenase (G6PDH) antibody (anti-G6PDH antibody, Sigma, A9521) that was used as a protein loading control and for normalization of the FLAG signal.

3.2.3.4 Preparation of cell extracts for lysate fractionation

To analyze the aggregation propensities of tripartite fusions, yeast cells were lysed and separated into supernatant (soluble) and pellet (insoluble) fractions following the protocol published by Wallace et al.[108] In brief, cells were grown in SC media supplemented with 2% raffinose and 0.1% glucose at 30 °C with shaking at 200 rpm to an OD_{600} of 0.3. Tripartite expression was induced by the addition of 2% galactose followed by 12 h of further shaking at 30 °C. Cell amounts equivalent to an OD_{600} of 5 were collected and resuspended in 100 mL of protein

solubilizing buffer (20 mM HEPES-KOH pH 7.4, 120 mM KCl, 2 mM EDTA, 0.2 mM DTT, 1:100 PMSF, 1:100 EZBlock IV protease inhibitor cocktail). Cells were dripped onto a mortar that was filled with liquid nitrogen. Frozen cells were ground with a pestle until they turned into a fine powder. This powder was then thawed on ice, and 400 mL of protein solubilizing buffer was added followed by centrifugation at 3,000*g* for 30 s at 4 °C. 50 mL of the supernatant was taken as the total lysate fraction. The remaining supernatant was processed by ultracentrifugation at 100,000*g* for 20 min. The supernatant from this step was taken as the soluble protein fraction. The pellet was washed with 500 mL protein solubilizing buffer and centrifuged again at 100,000*g* for 20 min. 100 mL of protein solubilizing buffer was added to the pellet before sonicating it for 3 s. 100 mL of 2x reducing SDS sample buffer was added following boiling of the pellet fraction for 5 min at 95 °C. Samples were processed for quantitative western blotting and probed with anti-FLAG (anti-FLAG, M2, Sigma F3165) and anti-PGK1 antibodies (anti-PGK1, Abcam, ab154613).

3.2.3.5 Cycloheximide chase assay to determine proteolytic stability

To assay the stability of tripartite fusions, cycloheximide chase experiments were performed as described by Tran et al[109]. Briefly, yeast cells were grown in SC media supplemented with 2% raffinose and 0.1% glucose at 30 °C with shaking at 200 rpm to mid-log phase (OD_{600} of 0.4), and tripartite protein expression was induced through the addition of 2% galactose. After 6 h of expression, the cells were adjusted to OD600 = 1 in fresh SC media supplemented with 2% raffinose and 0.1% glucose, treated with either 100 mM of the proteasome inhibitor MG132 or dimethyl sulfoxide (DMSO), and incubated for 1 h at 30 °C with shaking at 200 rpm. For yeast cells with *pdr5*Δ, 75 µM of the proteasome inhibitor MG132 were used. Before and after addition of 200 mg mL^{-1} cycloheximide to the cultures, 1 mL samples were taken and added to 30 mL of 0.5 M sodium azide (final concentration of sodium azide 20 mM). The samples were pelleted at 15,000*g* for 1 min at 4 °C, and the supernatant was aspirated. The pellet was snap frozen in liquid nitrogen and stored at –80 °C. The cultures were further incubated at 30 °C with shaking at 200 rpm, and chase samples were taken every 20 min. Protein lysates were prepared by thawing the pellets on ice and resuspending them in 2x reducing SDS sample buffer. They were then heated

for 5 min at 95 °C followed by beating with 100 mL acid washed glass beads (bead diameter 500 mm) for 5 min on a vortexer. Lysates were processed for quantitative western blotting using anti-FLAG (anti-FLAG, M2, Sigma F3165) for detection of the FLAG tag on the C-terminus of the APH tripartite fusions or anti-V5 (anti-V5 antibody, Invitrogen, R96025) antibodies for detection of the V5 epitope on the C-terminus of NAT tripartite fusion. These primary antibodies were used in combination with anti-G6PDH (anti-G6PDH antibody, Sigma, A9521) or anti-PGK1 (anti-PGK1 antibody, Abcam, ab154613) or antibodies (all at dilutions of 1:2000) for normalization of the tripartite signal intensities. To test for the efficiency of proteasome inhibition lysates expressing the proteasome substrate protein Ubc6 (pJW4 (pRS416-Ubc6-HA, URA3)[93], kindly provided by Dr. Mark Hochstrasser) were probed with an anti-HA antibody (anti-HA, Roche, 12CA5, stock concentration 0.5 mg mL^{-1}) in a 1:1000 dilution.

3.2.3.6 Immunohistochemical detection of the cellular localization of tripartite fusions

To reveal the cellular localization of tripartite fusions in yeast cells, the biosensors were detected immunohistochemically using the protocol "Indirect Immunofluorescence for Budding Yeast," as published by the Meluh lab and in the CSH Yeast Genetics Handbook[110]. Yeast cells were grown in SC media supplemented with 2% raffinose and 0.1% glucose at 30 °C with shaking at 200 rpm to early-log phase (OD_{600} of 0.3), and tripartite expression was induced through addition of 2% galactose for 8 h or as otherwise specified. To fix the cells, 5 mL of cells were mixed with 37% formaldehyde to a final concentration of 4% (v v^{-1}) formaldehyde. Then the cells were incubated on a tube rotator at 10 rpm at room temperature for 1 h. Following the incubation step the fixed cells were pelleted by centrifugation at 1,000*g* for 3 min, the supernatant was aspirated, and the pellet was resuspended with 5 mL of 0.1 M $KHPO_4$, pH 6.5 followed by another centrifugation step at 1,000*g* for 3 min. This washing step was repeated 3 times before the cells were resuspended in 5 mL of 1.2 M sorbitol in 0.1 M $KHPO_4$, pH 6.5. Cells were centrifuged at 1,000*g* for 3 min and then resuspended in 1.0 mL of 1.2 M sorbitol in 0.1 M $KHPO_4$, pH 6.5. To spheroblast the cells, 0.5 mL of 1.2 M sorbitol in 0.1 M $KHPO_4$, pH 6.5 supplemented with 5 mL β-mercaptoethanol was added to 0.5 mL of cells, incubated for 5 min, followed by addition of lyticase at a final concentration of 50 units mL^{-1}. Cells were incubated on a tube rotator at 20 rpm

at room temperature for 20–40 min until at least 50% of cells were phase dark and appeared medium to dark gray in color by microscopic analysis. Spheroblasts were harvested by gentle centrifugation at 1,000 *g* for 2 min, and the cell pellet was gently resuspended in 1.5 mL 1.2 M sorbitol in 0.1 M $KHPO_4$, pH 6.5. Cells were centrifuged again at 1,000*g* for 2 min followed by gentle resuspension in 0.5 mL 1.2 M sorbitol in 0.1 M $KHPO_4$, pH 6.5. 20 mL of spheroplast suspension was added to each well of a poly-Lys-coated microscope slide (Microscope Slides, Immunofluorescence, Polysciences Inc., 18357-1), and the slide was placed in a humidity chamber and incubated for 15 min to allow cells to settle. After the cells had settled, the supernatants were aspirated and the slide was put into –20 °C methanol for 6 min followed by 30 s incubation in –20 °C acetone. Slides were air-dried for 2 min, and 20 mL of phosphate-buffered saline supplemented with 1% bovine serum albumin (BSA) and 0.1% sodium azide was added to each well for blocking. The slides were incubated in a humidity chamber for 1 h before removing the blocking solution. 20 mL of the primary antibody anti-FLAG (anti-FLAG, M2, Sigma F3165), which was diluted 1:1000 in phosphate-buffered saline supplemented with 1% BSA and 0.1% sodium azide, was added to each well. The slides were incubated overnight at 4 °C then washed 4–5 times with phosphate-buffered saline supplemented with 1% BSA and 0.1% sodium azide. The wash buffer was removed, and 20 mL of the secondary antibody Alexa488 plus (Thermo Fisher Scientific, A32723), which was diluted 1:200 in phosphate-buffered saline supplemented with 1% BSA and 0.1% sodium azide, was applied to each well. The slides were incubated in the dark at room temperature for 2 h, then washed 4–5 times with phosphate-buffered saline supplemented with 1% BSA and 0.1% sodium azide, followed by two washes with plain phosphate-buffered saline. The buffer was aspirated, and the slide was air-dried in the dark. One drop of SlowFade Diamond mounting medium (ThermoFisher, S36968) was added to each well, a cover slip was put on each slide, and after sealing with nail polish, imaging was performed with a Nikon Eclipse E800 microscope.

3.2.3.7 Semi-denaturing detergent agarose gel electrophoresis (SDD-AGE)

To visualize amyloid-like aggregates, semi-denaturing detergent agarose gel electrophoresis (SDD-AGE) was performed as described previously.[111,112] Briefly, cells were grown in SC media

supplemented with 2% raffinose and 0.1% glucose at 30 °C with shaking at 200 rpm to mid-log phase (OD_{600} of 0.5), and expression of tripartite fusion proteins was induced for 12 h by the addition of 2% galactose. Cell amounts equivalent to OD_{600} of 15 were centrifuged at 2,000*g* at room temperature for 5 min. The cell pellets were resuspended in sterile double-distilled water and centrifuged at 800*g* at room temperature for 5 min. 240 mL of lysis buffer (100 mM Tris pH 8.0, 1% Triton X-100, 50 mM β-mercaptoethanol, 1% EZBlock IV protease inhibitor cocktail, 30 mM N-ethylmaleimide, 12.5 units mL^{-1} benzonase nuclease, 1 mM PMSF) was added to each sample, and cells were flash frozen in liquid nitrogen. Cells were lysed by bead beating using 100 mL acid washed glass beads (bead diameter 500 mm) at 4 °C for 10 cycles of 1 min vortexing followed by 1 min on ice. Cell debris was removed by centrifugation at 3,000*g* for 1 min at 4 °C. The supernatant fraction was mixed with 4x sample buffer (2 x TAE consisting of 80 mM Tris, 40 mM acetic acid, and 2 mM EDTA, 20% glycerol, 8% sodium dodecyl sulfate, 0.01% bromophenol blue), vortexed briefly at room temperature to ensure proper mixing, and incubated 3–5 min at room temperature. Electrophoresis and capillary blotting to a nitrocellulose membrane were performed as previously described.[2] 30 ml of each sample was loaded on a 1.5% agarose gel containing 0.1% SDS and run in running buffer (1x TAE consisting of 40 mM Tris, 20 mM acetic acid, 1 mM EDTA) supplemented with 0.1% sodium dodecyl sulfate at low voltage (<3 V / cm gel length) at 4 °C until the dye front reached 1 cm from the end of the gel (6–8 h). A high molecular weight marker (HiMark Pre-Stained Protein Standard, Thermo Scientific, LC5699) was used. Blotting paper and nitrocellulose were cut to the same dimensions as the gel. The transfer stack was assembled from bottom up as follows: 20 pieces of dry GB004 blotting paper, 4 pieces of dry GB002 blotting paper, 1 piece of wet GB002 blotting paper, wet nitrocellulose membrane, gel, 3 wet GB002, and a wet wick of GB004. The wick was weighted down with a 1 L water-filled bottle, and each end of the wick was submerged in Tris-buffered saline, pH 7.4. The transfer proceeded overnight at 4 °C, and the nitrocellulose membrane was subsequently processed using standard western blotting procedures. The membranes were then probed using anti-FLAG (anti-FLAG, M2, Sigma F3165, dilution 1:2000), anti-Sup35 (anti-Sup35, Abnova, PAB15578, dilution 1:1000), or anti-Rnq antibodies (anti-Rnq, Abnova, PAB15579, dilution 1:1000) in Odyssey blocking buffer in Tris-buffered saline (Licor, 927-50000) overnight at 4 °C. To analyze the quality of cell lysates and

the levels of tripartite protein expressed relative to a G6PDH loading control, the remaining cell lysates were heated at 95 °C for 5 min and processed for SDS-PAGE and western blotting using anti-FLAG and anti-G6PDH antibodies.

3.2.3.8 Guanidinium prion curing

To chemically eliminate prions, multiple colonies of each strains were picked and passaged four times on rich agar medium (YPD agar consisting of 10 g L^{-1} yeast extract, 20 g L^{-1} bacto peptone, 20 g L^{-1} glucose and 20 g L^{-1} agar) containing low doses (3 mM) of the Hsp104 inhibitor guanidine hydrochloride (GdnHCl; Sigma, sterile filtered). Since GdnHCl is known to increase the frequencies of mitochondrial mutants (petites), single colonies of the GdnHCl-treated strains were tested for respiration competence on rich agar containing 3% of the non-fermentable carbon source glycerol (YPglycerol consisting of 10 g L^{-1} yeast extract, 20 g L^{-1} bacto peptone, 30 ml L^{-1} glycerol and 20 g L^{-1} agar). As control for respiration deficiency, we generated respiration-deficient petites of investigated strains through addition of 10 µg mL^{-1} ethidium bromide to mid-log phase cells and incubation for 2.5 h at 30 °C with shaking at 200 rpm. As control for effective prion curing we took advantage of the *ade1-14* system available in strains with defined Sup35 and Rnq1 prion states (L1762, L1758, L1749, L2910).[113–116] The system allows to infer the prion status by colony color. Control strains were GdnHCl-treated in parallel to the tripartite stains and assayed for the presence of Sup35 prion proteins [*PSI+*] by spotting 5 fold serial dilutions of log-phase cells on SC agar supplemented with 2% galactose and 2% raffinose and scoring for red (Sup35 prion protein negative, [*psi-*]) or white (Sup35 prion protein positive, [*PSI+*]) color.

4 Results and Discussion

The wording and figures of this section are largely based on my accepted paper (Sachsenhauser, V., Deng, X., Kim, H.-H., Jankovic, M., C.A. Bardwell, J., and Bardwell, J. C. A. (2020) Yeast tripartite biosensors sensitive to protein stability and aggregation propensity. *ACS Chem. Biol. XXXX*, XXX, XXX–XXX, https://doi.org/10.1021/acschembio.0c0008).[97] The results of this research project were acquired in collaboration with my colleagues Xiexiong Deng, Hyun-hee Kim, and Maja Jankovic. If not stated otherwise in the figure legends, the data were acquired by myself.

4.1 Development of tripartite folding biosensors in *S. cerevisiae*

To directly assess the *in vivo* stability of a protein of interest, the Bardwell lab previously developed a tripartite fusion system that links *in vivo* protein stability to antibiotic resistance.[117] In this approach, a protein of interest is inserted between the split halves of an antibiotic resistance protein and fused through long, flexible linkers to generate a tripartite fusion (Figure 1a). We hypothesize that if the inserted protein folds well and is soluble, the split marker halves of the tripartite fusion should be able to efficiently fold up and complement each other to confer its antibiotic resistance function (Figure 1b). However, if the inserted protein misfolds or is poorly soluble, the entire tripartite fusion will consequently be susceptible to degradation or aggregation and rendered non- or only partially functional. The latter scenario should result in low levels of antibiotic resistance. Therefore, the antibiotic resistance conferred by the tripartite fusion should provide a direct measure of the *in vivo* protein stability or aggregation susceptibility of the inserted protein of interest.

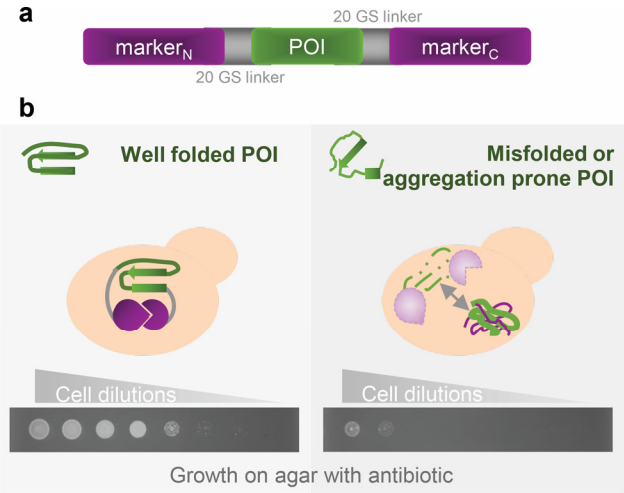

Figure 1. Design of a tripartite biosensor to study protein stability in yeast. a) Schematic diagram of the tripartite fusion system. The protein of interest (green) is inserted into an antibiotic resistance marker protein (purple) with flexible linkers (gray) as part of a tripartite fusion. marker$_N$ and marker$_C$: N- and C-terminal half, respectively, of a split antibiotic resistance marker protein; POI: protein of interest; 20 GS linker: Gly-Ser-rich, flexible linker with a total length of 40 amino acids; the POI is inserted in the middle of the linker such that a 20 GS linker portion fuses each end of the POI to a split marker half. b) How the tripartite biosensor works. If the POI is folded properly or has low aggregation propensity, the tripartite fusion should remain intact and confer high levels of antibiotic resistance. However, poor proteolytic stability or solubility of the test protein should result in increased susceptibility to proteolysis or aggregation in the yeast cytosol, which will in turn lead to lower antibiotic resistance. Therefore, the level of antibiotic resistance of yeast cells may be directly correlated to the folding or solubility of the inserted protein. Antibiotic resistance levels of yeast cells expressing the tripartite fusion can be quantified by a serial dilution spotting assay on agar media supplemented with antibiotic. The figure is reprinted with permission from Sachsenhauser, V., Deng, X., Kim, H.-H., Jankovic, M., C.A. Bardwell, J., and Bardwell, J. C. A. (2020) Yeast tripartite biosensors sensitive to protein stability and aggregation propensity. ACS Chem. Biol. *XXXX*, XXX, XXX–XXX, https://doi.org/10.1021/acschembio.0c0008. Copyright 2020 American Chemical Society.[97]

Previously, we developed a split β-lactamase system in the bacterial periplasm that confers a stability-dependent readout for a fused protein of interest in the presence of the antibiotic penicillin.[117,118] We extended the approach to the cytosolic compartment by developing tripartite biosensors that are based on two different antibiotic resistance markers.[119] One was based on the marker protein aminoglycoside-3'-phosphotransferase (APH), which confers resistance to the antibiotic G418. The second genetic marker protein was nourseothricin N-acetyl transferase (NAT), which is effective against the antibiotic nourseothricin (NTC). G418 and NTC are

aminoglycoside antibiotics that function in the cytosol by disturbing peptide elongation at the ribosome, giving rise to inaccurate mRNA translation and therefore biosynthesis of non-functional proteins.[120] These antibiotics are effective in various bacteria and eukaryotic species.[120,121]

Test proteins were fused between the split marker halves via flexible Gly-Ser (GS) linkers. The GS linker should span the distance between the N and C termini of the inserted test protein.[71,119] Previous experimental work in our lab demonstrated the importance of linker length in obtaining a good relationship between antibiotic resistance and the thermodynamic stability of the test protein fused in the tripartite system.[71] We used a 40 GS-rich linker for APH fusions and a 39 GS-rich linker for NAT fusions, respectively, which should span an effective range of ~ 30 Å. This distance is equivalent to that of a globular protein of up to 100 kDa in size when approximating the globular protein as a sphere and assuming the N and C termini of the inserted protein are at the opposite poles of the sphere.[122,123]

The APH- and NAT-based tripartite biosensors proved to be effective in the *E. coli* cytosol, but when used in yeast, they showed a comparatively low sensitivity.[119]

4.1.1 Optimization of the tripartite biosensor expression

To improve the tripartite biosensor readout for *S. cerevisiae*, we comprehensively re-engineered the APH and NAT biosensors to increase their sensitivity and extend their dynamic range. Since aminoglycoside-induced translation errors were shown to increase protein aggregation, oxidative damage, and upregulation of the unfolded protein response in *E. coli* (effects that could alter the tripartite biosensor's readout for protein stability or aggregation), we attempted to obtain a sensitive readout at relatively low starting antibiotic concentrations.[124–126]

To realize these goals, we focused on adjusting the expression level of the APH and NAT tripartite fusions by changing gene dosage (Figure 2a) and optimizing the APH fusion codon for use in yeast. To test the revised tripartite designs and determine their level of sensitivity and dynamic range in yeast, we fused the tripartite sensors with stability variants of the well-studied model folding protein immunity protein 7 (Im7). The thermodynamic stability of Im7 test proteins

was shown to be the key factor determining the antibiotic resistance level of Im7 tripartite fusions.[71,119] We inserted wild-type (WT) Im7 and a fairly thermodynamically destabilized Im7 variant, Im7 I54A, into the GS linker that fuses the two marker halves. Expression of the APH or NAT tripartite fusion that just contained the 40-residue GS-rich linker (for the APH fusion) or the 39-residue GS-rich linker (for the NAT fusion) was expected to confer high levels of antibiotic resistance and served as a positive control.[119] The tripartite fusions were expressed from a galactose inducible promoter and the resulting antibiotic resistance levels were determined by spot titer assays.

When we substantially lowered the gene copy number of APH and NAT tripartite fusions in yeast cells, we observed an antibiotic resistance readout that was sensitive to the stability of the inserted Im7 variant (Figure 2a). In order to maintain the good relationship between the antibiotic resistance readout and the stability of the inserted protein and to ensure uniform gene expression levels of the tripartite fusion across cells, in the case of the APH tripartite fusions, we settled on the use of genome integrated tripartite constructs that were additionally codon optimized.

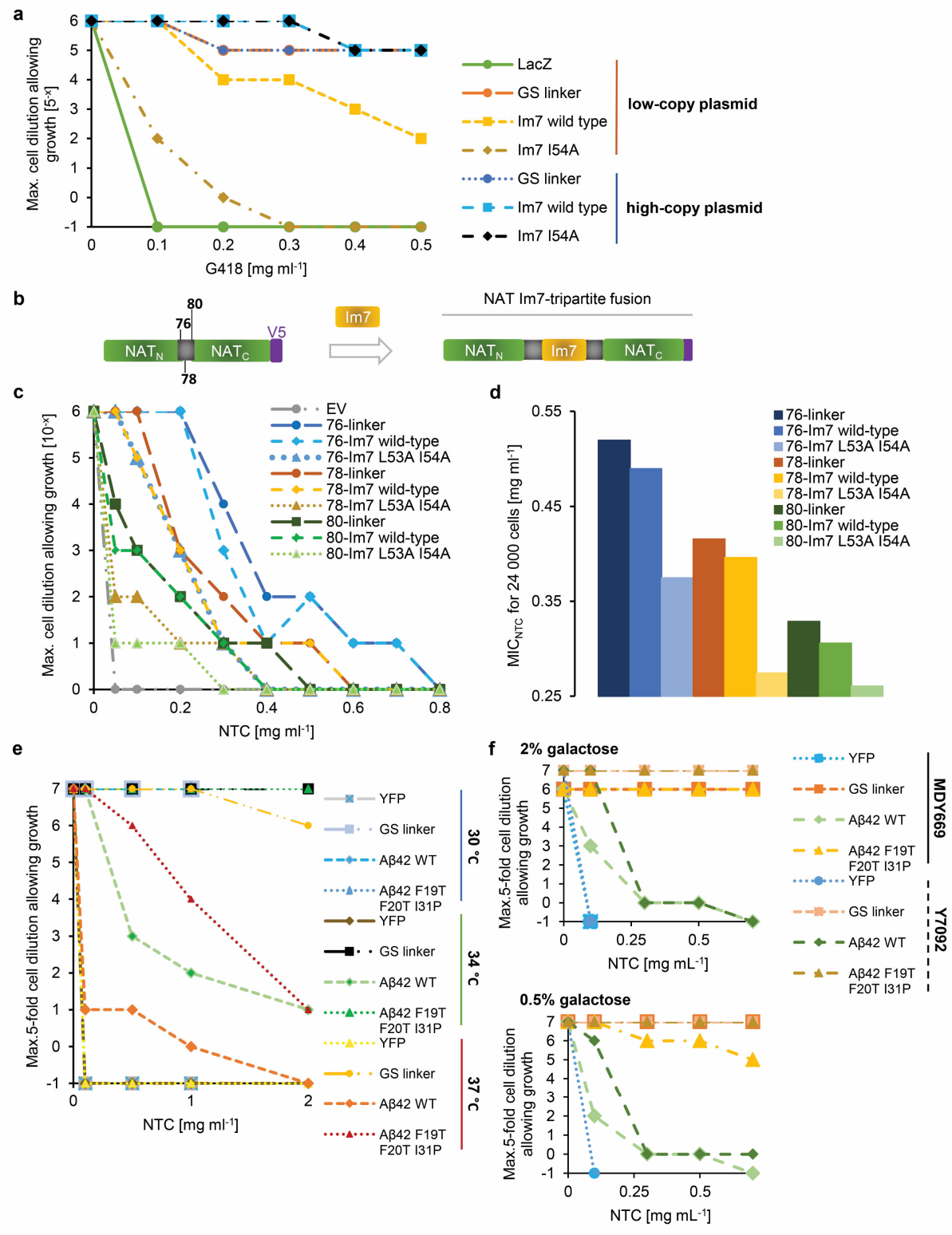

Figure 2. Antibiotic resistance observed for tripartite Im7 fusions in yeast depends on multiple variables. a) Comparison of conferred antibiotic resistance levels of yeast cells expressing APH tripartite fusions with WT Im7,

with destabilized Im7 I54A, or just a GS linker inserted from high copy number plasmids (strains aYC-5, aYC-38, and aYC-4, respectively, lab collection) and low copy number plasmids (strains VES255, VES256, VES263). A strain expressing LacZ from a low copy number plasmid (pYC2-LacZ, Invitrogen, strain VES174) served as a control for antibiotic sensitivity. The graph shows the maximal cell dilution that allows for yeast growth on SC agar media lacking uracil and containing 2% galactose and 2% raffinose supplemented with increasing concentrations of G418. b) Schematic showing construction of insertions of the test protein Im7 into the NAT marker protein at NAT residues 76, 78, or 80 for evaluation as alternative insertion positions. c) Maximum cell dilution that allows for growth of *E. coli* cells expressing NAT tripartite fusions containing just a GS linker insertion (strains MJ-1, MJ-5, MJ-9), additional insertion of WT Im7 (strains MJ-18, MJ-21, MJ-24) or the destabilized variant Im7 L53A I54A (strains MJ-20, MJ-23, MJ-26) within the GS linker, or an empty vector (MJ-17) on Luria-Bertani agar media supplemented with 1 mM IPTG to induce expression of the tripartite and increasing concentrations of NTC. d) Minimal inhibitory concentrations (MICs) of NTC for *E. coli* cells expressing the NAT tripartite fused with WT Im7, Im7 L53A I54A, or just the GS linker at NAT positions 76, 78, or 80. e) Comparison of antibiotic resistance levels observed at incubation temperatures of 30 °C, 34 °C, and 37 °C of yeast cells expressing a YFP (strain VES735) or NAT tripartite fusions with only a GS linker inserted (strain VES736) or additional insertion of proteolytically unstable WT Aβ42 (strain VES741), or an aggregation deficient variant, Aβ42 F19T F20T I31P (strain VES742). NAT residue 78 was used for GS linker and test protein insertion. YFP expression alone served as a control for antibiotic sensitivity. The graph shows the maximal cell dilution that allows for yeast growth on SC agar media containing 0.5% galactose and 2% raffinose supplemented with increasing concentrations of NTC. f) Comparison of the antibiotic resistance levels conferred by NAT tripartite fusions expressed either in a galactose titratable yeast strain MDY669 or a standard yeast strain (strain Y7092) depending on the galactose concentration added. YFP or NAT tripartite fusions with only a GS linker or additional insertion of WT Aβ42 or Aβ42 F19T F20T I31P were expressed in galactose titratable MDY669 yeast cells (strains VES735, VES736, VES741, and VES742) or non-galactose titratable Y7092 yeast cells (strains VES751, VES753, VES755, and VES757) through induction with either 2% or 0.5% galactose. The graph shows the maximal cell dilution in spot titer assays that allows cell growth at 37 °C on SC agar media supplemented with 2% raffinose, increasing concentrations of NTC and either 2% galactose (upper panel) or 0.5% galactose (lower panel). The data of figure panels c and d were acquired by my student Maja Jankovic. The figure is adapted with permission from Sachsenhauser, V., Deng, X., Kim, H.-H., Jankovic, M., C.A. Bardwell, J., and Bardwell, J. C. A. (2020) Yeast tripartite biosensors sensitive to protein stability and aggregation propensity. ACS Chem. Biol. *XXXX*, XXX, XXX–XXX, https://doi.org/10.1021/acschembio.0c0008. Copyright 2020 American Chemical Society.[97]

To optimize the dynamic range of the NAT tripartite biosensor in yeast, we additionally fine-tuned the insertion positions within the NAT marker. In a previous, comprehensive transposon screening approach NAT residue 80 was identified as suitable split that showed a good

relationship between the thermodynamic stability of the inserted protein and the conferred antibiotic resistance.[119] To further optimize the dynamic range of the NAT tripartite system, we reinvestigated the experimentally identified split sites within the NAT protein and took a closer look at three adjacent sites to NAT80 (NAT76, NAT78, and NAT82). Through a recently published crystal structure (PDB ID 5c82)[127], we found that NAT76 and NAT78 were positioned within an exposed loop in the 3D structure, whereas NAT80 and NAT82 were positioned within a β-sheet structure. Hence, we constructed NAT tripartite fusions that were split at residue 76, 78, or 80 and each fused with either a GS linker sequence, Im7 WT, or a partially folded variant, Im7 L53A I54A (Figure 2b). Plasmids encoding these constructs were expressed in the *E. coli* cytosol and spotted in serial dilution on agar supplemented with NTC to assess their conferred antibiotic resistance levels (Figure 2c,d). Im7 fusions based on the NAT78 tripartite design provided the greatest range of differential antibiotic resistance readout. These results indicate that the exposed loop in NAT is indeed a better site for the tripartite fusion design. Thus, for further NAT biosensor constructs designed for yeast, NAT residue 78 was used as the split site to insert the protein of interest.

Depending on the test protein fused, the yeast NAT tripartite fusions provided an antibiotic resistance readout that was only moderately sensitive to the stability of the test protein (further discussed below). In another approach to optimize the readout of the NAT tripartite fusions, we incubated cells expressing these NAT fusions at elevated temperatures (Figure 2e). As shown for NAT tripartite fusions with only a GS linker or additional insertion of an unstable peptide Aβ42 or the oligomerization deficient mutant Aβ42 F19T F20T I31P (Aβ variant biosensors described in detail below), challenging the proteostasis capacity of the cells by heat resulted in increased antibiotic sensitivity and was thus used as one strategy to optimize the readout of other tripartite biosensor constructs if necessary.

Incubation of yeast cells at temperatures over 36 °C has been shown to induce the heat shock response that leads to the upregulation of a number of chaperones and proteolytic systems.[128] Therefore, depending on the application purpose of the biosensor, elevating the incubation temperature may not be a desirable approach for optimizing the tripartite sensor readout. To

provide the possibility of optimizing the tripartite biosensor readout by tuning the tripartite expression level rather than by applying heat, we expressed the biosensor constructs in a yeast strain with a galactose titratable expression system. We thought that tunability of the expression level may be especially important for the expression of tripartite fusions with misfolding proteins since overexpression of misfolded proteins has been shown to have a dose-dependent fitness cost on cells.[47,129] Moreover, a tunable expression may also be desirable for the expression of tripartite fusions with proteins susceptible to aggregation since aggregation is a concentration-dependent process.[130–132] Specific genetic modifications (SpHIS5::pACT1-GAL3 gal1Δ,gal10Δ::LEU2) in the yeast strain MDY669 should enable a galactose inducible, tunable expression from the relatively strong GAL1 promoter instead of an otherwise switch-like induction.[47] MDY669 cells expressing variants of the NAT-Aβ42 biosensor or GS linker-only fusions displayed differential antibiotic resistance readouts depending on the galactose inducer concentration used (Figure 2f). Such titratable sensor expression was not observed using standard yeast strains (Figure 2f). This result indicated that a more sensitive antibiotic resistance readout could be obtained by modulating the expression level which is consistent with our previous findings. To further optimize this tunability if desired, a carbon source-independent, synthetic expression system with a broader linear titration range could conceivably be employed.[133–135] Regardless, the galactose titratable strain seemed useful to establish tripartite biosensors fused with dose-sensitive proteins as described below.

To assess the antibiotic resistance readout of the tripartite fusions with a different technique, we implemented growth curve assays. Compared to spot titers, growth curve assays are cheaper, faster, and more amenable to high-throughput procedures. These characteristics can be advantageous if the antibiotic resistance of many different biosensor expressing strains must be determined simultaneously. Using this assay, we found that cells expressing NAT-Im7 variant fusions showed an Im7 stability-dependent growth rate in the presence of a range of NTC concentrations (Figure 3). These results indicated that growth curve assays may be a viable alternative to spot titer assays to assess the antibiotic resistance readout of tripartite biosensors. However, growth curve experiments with both NAT and APH tripartite fusions revealed that distinctly lower and very precisely adjusted antibiotic concentrations are required to obtain a

sensitive readout compared to spot titer assays. In our hands, spot titer assays appear to provide a more robust and reliable antibiotic resistance readout. We therefore preferred to use spot titer assays to assess the antibiotic sensitivity readout of our tripartite fusions in yeast.

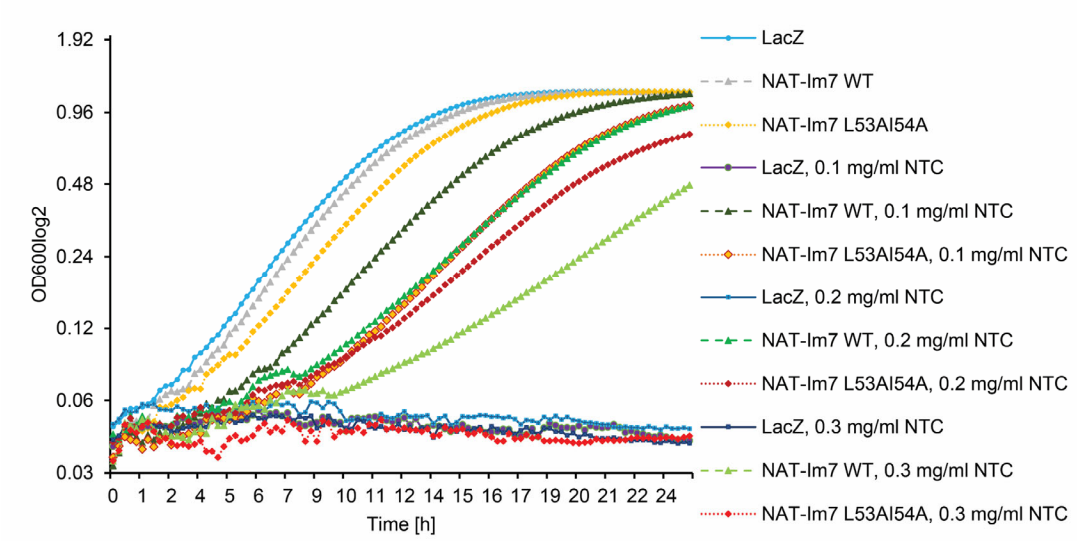

Figure 3. NAT-Im7 variant fusions display an Im7 stability-dependent antibiotic resistance readout in growth curve assays. Yeast cells expressing NAT tripartite fusions with insertion of WT Im7 (VES719) or the destabilized Im7 variant L53A I54A (VES725) were grown at 30 °C to mid-log phase in SC media supplemented with 2% raffinose and 0.1% glucose followed by adjustment of their OD_{600} to 0.1 in fresh SC media supplemented with 2% raffinose and 2% galactose to induce the tripartite fusions. The media was supplemented with no antibiotic or 0.1, 0.2, or 0.3 mg mL^{-1} of the antibiotic NTC. The cells were incubated at 34 °C in a microplate reader and their optical densities (OD600) recorded over time. Plotted are the log2-transformed absorbance values detected over 26 hours. Yeast cells expressing only LacZ (VES715) served as control for NTC sensitivity. The NAT proteins were fused at NAT residue 80.

4.1.2 Antibiotic resistance conferred by fluorescently tagged APH-tripartite fusions is insensitive to the stability of tripartite inserted Im7 variants

To try to enable rapid and simple microscopic distinction between misfolding, proteolysis, and aggregation of biosensor fusions, we fused the APH tripartite system with a red fluorescent protein, mKate2. The fluorescent protein was fused to either the C or N terminus of the APH biosensor via a 10 amino acid long GS-rich linker (Figure 4a). To validate the fluorescently tagged tripartite design, Im7 stability variants were inserted into the fusions. Using spot titer assays, we

assessed the relationship between the thermodynamic stability of the Im7 variants and the displayed antibiotic resistance level (Figure 4b, c).

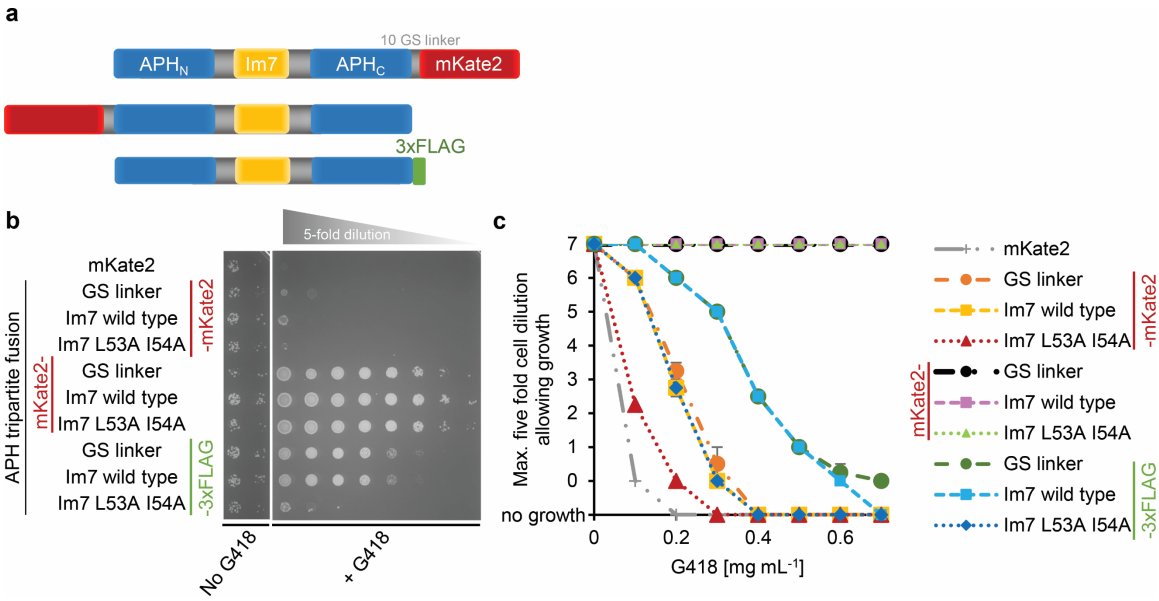

Figure 4. Antibiotic resistance conferred by fluorescently tagged APH tripartite fusions is insensitive to the stability of the inserted Im7 variant. a) Schematic diagram of the different APH-Im7 tripartite constructs fused with either a C-terminal (designated -mKate2) or an N-terminal fusion (designated mKate2-) with the red fluorescent protein, mKate2, via a 10 times GS linker sequence (10 GS linker). Non-fluorescently tagged APH-Im7 tripartite constructs were fused with a C-terminal 3xFLAG tag epitope through a 6 GS linker (designated -3xFLAG). b) Spot titer assay showing antibiotic resistance of yeast cells expressing either the non-G418 resistant fluorescent mKate2 protein only (VES650), or various G418 resistant APH constructs that are fused either C- or N-terminally with mKate2 or only with a C-terminal 3xFLAG tag. Each version of the APH construct contains either just a GS linker (VES651, VES654, VES657) or an additional insertion of WT Im7 (VES652, VES668, yHH74) or the destabilized Im7 variant, Im7 L53A I54A (VES653, VES671, yHH75). The spot titers without antibiotic (No G418) correspond to the cell dilutions 7th and 8th from the left of the spot titers in the presence of the antibiotic (+ G418). c) Five-fold serial dilution spotting assays of cells were used to score cell growth on SC agar supplemented with G418 concentrations ranging from 0 to 0.7 mg mL^{-1}. The experiment was performed in duplicate, and error bars indicate ± 1 SD. The figure is reprinted with permission from Sachsenhauser, V., Deng, X., Kim, H.-H., Jankovic, M., C.A. Bardwell, J., and Bardwell, J. C. A. (2020) Yeast tripartite biosensors sensitive to protein stability and aggregation propensity. ACS Chem. Biol. *XXXX*, XXX, XXX–XXX, https://doi.org/10.1021/acschembio.0c0008. Copyright 2020 American Chemical Society.[97]

Compared to C-terminally 3xFLAG tagged APH-Im7 variant fusions, the resulting range for the C-terminal fusions of mKate2 with the APH-Im7 variants was relatively low and narrow. In

contrast, cells expressing N-terminally mKate2 tagged tripartite fusions displayed a relatively high resistance readout that was insensitive to the thermodynamic stability of the inserted protein over the tested range of G418 concentrations. Hence, we conclude that C-terminal fusions with the fluorescent protein likely renders the chimeras less soluble and N-terminal fusions likely render the fusions more soluble. In both cases, the fused fluorescent protein appears to substantially interfere with the relationship between the thermodynamic stability of the inserted protein and the antibiotic resistance readout, which we were able to observe in the absence of the fluorescence fusion partner. Despite the great convenience fluorescent protein tags offer to microscopically track a protein of interest in live cells, they are well known to impact the stability of the fusion partner.[21,22,136] In our experience, this experimental approach seems to unfavorably shift and obscure the antibiotic resistance readout of the tripartite system. Therefore, we did not further pursue these designs.

4.1.3 Thermodynamic stability of Im7 variants fused in the tripartite system correlates with antibiotic resistance in *S. cerevisiae*

Previous studies in *E. coli* identified the thermodynamic stability of Im7 and other test proteins as a key determinant for the degree of antibiotic resistance conferred by the respective tripartite fusions.[71,119] Therefore, we anticipated that we would observe comparable relationships with our revised designs in yeast. To evaluate our new designs for this specific feature, we fused the yeast tripartite sensors with several different variants of Im7 that showed varying levels of thermodynamic stability in *in vitro* equilibrium urea denaturation experiments.[71,94–96] Using spot titer assays (Figure 5a-d), we estimated the average minimum inhibitory concentration (MIC) of the antibiotic that prevented cell growth for each tripartite variant as compared to the MIC of tripartite fusions with Im7 WT.[71] Both the APH- and the NAT-based tripartite biosensors showed a strong linear correlation between the *in vitro* thermodynamic stabilities and their relative MICs (Figure 5e, f). These observations were in keeping with our previous findings for the Im7 tripartite system in *E. coli*[71,119] and initial versions of the tripartite sensors in yeast.[119] The thermodynamic stabilities of the Im7 variants used range

from 24.9 to −1.4 kJ mol^{-1}, which shows that our revised yeast folding biosensors are sensitive at least over this range.

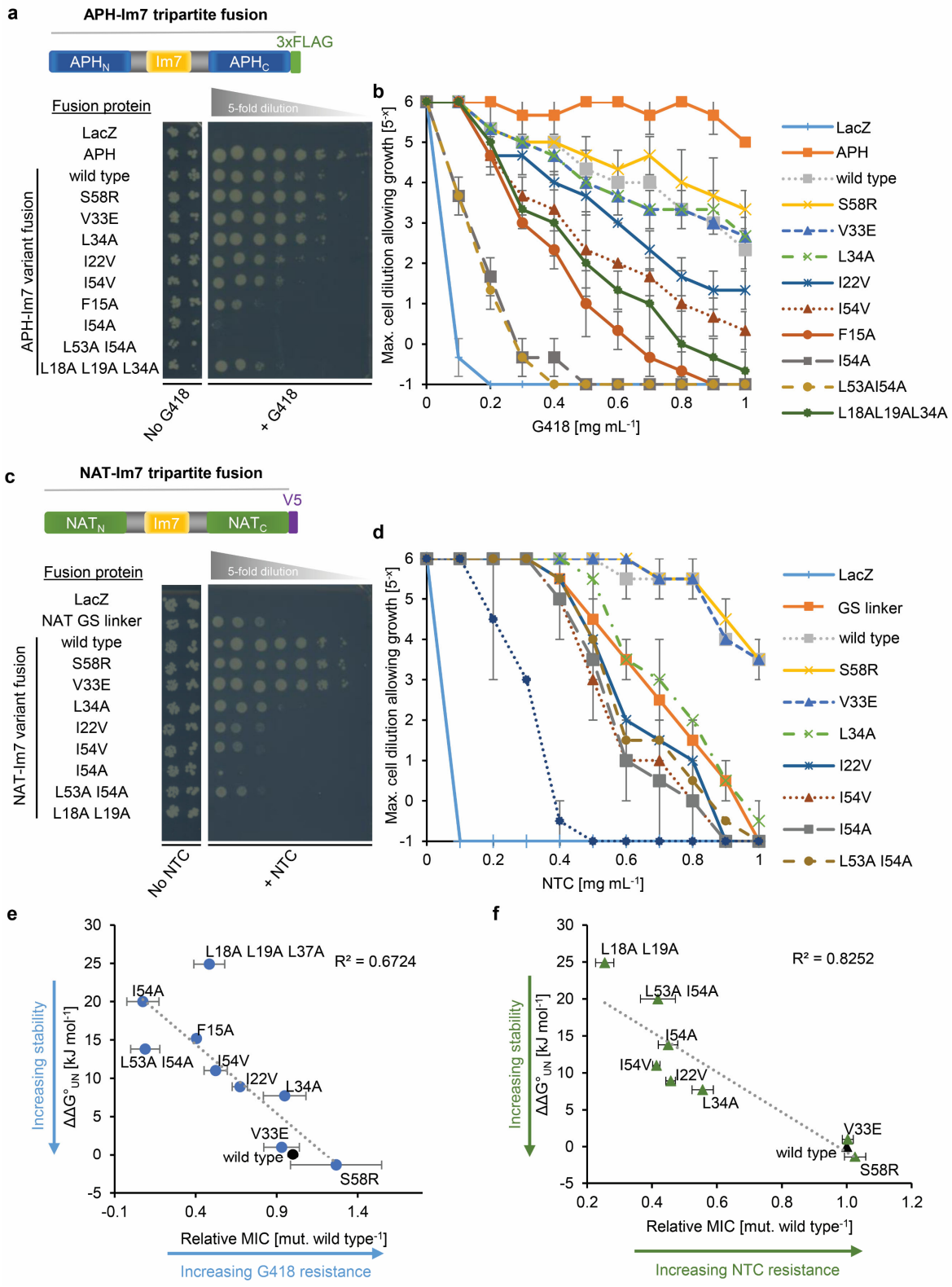

Figure 5. Stability of Im7 variants correlates with antibiotic resistance in spot titer assays. a) Thermodynamically destabilized Im7 variants (V33E, L34A, I22V, I54V, F15A, I54A, L53A I54A, L18A L19A, L18A L19A L34A) or a stabilized

variant of Im7 (S58R) were inserted into the APH marker via flexible, GS-rich linkers. Antibiotic resistance levels of yeast cells expressing the various APH-Im7 variant fusions was determined in spot titer assays. For this assay, yeast cells expressing APH tripartite fusions with WT Im7 (VES256), the Im7 variants indicated (VES258, VES286, VES268, VES267, VES257, VES269, VES263, VES262, VES287), or without any insertion in APH (VES255) were grown on SC agar media lacking uracil, supplemented with 2% galactose and 2% raffinose, and supplemented without or with 0.5 mg mL^{-1} of the antibiotic G418 at 30 °C. Yeast cells expressing only LacZ (VES174) served as a control for G418 sensitivity. The spot titers without antibiotic (No G418) correspond to the cell dilutions 7th and 8th from the left of the spot titers in the presence of the antibiotic (+ G418). b) Graph showing the maximal cell dilution that allows for growth of yeast cells expressing APH-Im7 tripartite fusions on the same SC agar media described in (a), except using increasing concentrations of G418. c) Antibiotic resistance of NAT-Im7 variant fusions as determined in spot titer assays. Yeast cells expressing NAT80 tripartite fusions with WT Im7 (VES719), with the stabilized Im7 variant S58R (VES430), with the destabilized Im7 variants indicated (VES733, VES729, VES724, VES721, VES731, VES725, VES727), or with just the GS linker (VES717) were grown on SC agar supplemented with 2% galactose and 2% raffinose without the antibiotic NTC (No NTC) and with 0.7 mg mL^{-1} NTC (+ NTC) at 34 °C. The NAT proteins were fused at NAT residue 80. Yeast cells expressing LacZ (VES715) served as control for NTC sensitivity. d) Graph showing the maximal cell dilution that allows for growth of yeast cells expressing NAT-Im7 tripartite fusions on SC agar supplemented with 2% galactose and 2% raffinose and increasing concentrations of NTC at 34 °C. The spot titers without antibiotic (No NTC) correspond to the cell dilutions 7th and 8th from the left of the spot titers in the presence of the antibiotic (+ NTC). e) The level of G418 resistance for cells expressing the corresponding fusion constructs was quantified as the MIC from serial dilution spot assays as described in (a, b). The average MIC for G418 relative to WT Im7 is plotted against the change in the free energy of unfolding, $\Delta\Delta G^\circ_{UN}$, with $\Delta\Delta G^\circ_{UN} = \Delta G^\circ_{UN}$ (mutant) $- \Delta G^\circ_{UN}$ (WT). The ΔG°_{UN} values for Im7 variants were taken from the literature.[71,94,96,137] f) The level of NTC resistance for cells expressing the corresponding fusion constructs was determined as the MIC in serial dilution spot assays as shown (c, d) and described in detail in (e). The average MIC for NTC relative to WT Im7 is plotted against $\Delta\Delta G^\circ$ values for Im7 variants. Experiments shown in panel e were performed in triplicate, and those shown in panel f were performed in duplicate; error bars indicate ± 1 SD. The figure is adapted with permission from Sachsenhauser, V., Deng, X., Kim, H.-H., Jankovic, M., C.A. Bardwell, J., and Bardwell, J. C. A. (2020) Yeast tripartite biosensors sensitive to protein stability and aggregation propensity. ACS Chem. Biol. *XXXX*, XXX, XXX–XXX, https://doi.org/10.1021/acschembio.0c0008. Copyright 2020 American Chemical Society.[97]

We asked whether the differences in Im7 thermodynamic stabilities are reflected in the steady state protein levels of the Im7 biosensor variants. To address this question, we conducted quantitative western blotting. The APH-Im7 fusion protein levels detected in the total protein and soluble lysate fractions showed a comparably linear relationship with Im7 thermodynamic

stabilities (Figure 6a, b). This observation led us to conclude that the changes in APH-Im7 steady state levels are most likely due to *in vivo* proteolysis, which is consistent with the well-characterized close relationship between *in vivo* and *in vitro* stability.[71,138–140]

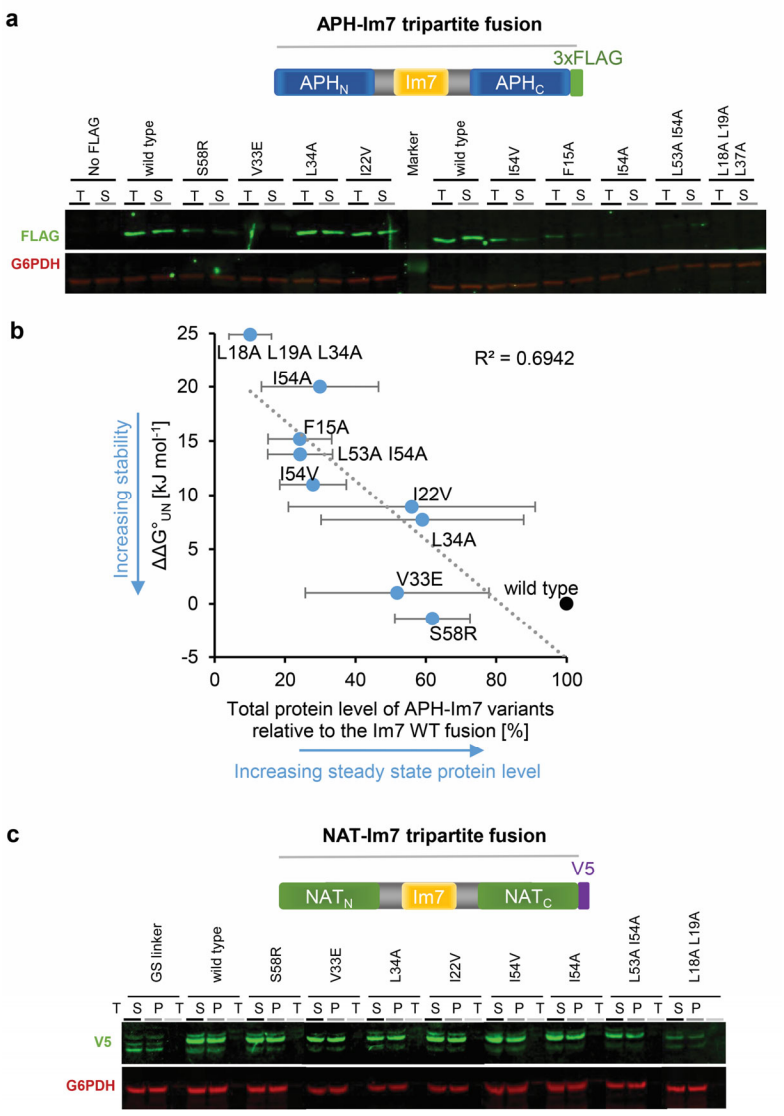

Figure 6. Protein levels of APH-Im7 variant fusions but not of NAT-Im7 variant fusions correlate with thermodynamic stability of the Im7 variants. a) Immunoblotting against the FLAG epitope on the C terminus of the APH tripartite fusions and against G6PDH as a loading control in yeast cell lysates. Shown are total protein (T) and soluble lysate (S) fractions. Prior to cell lysis, the yeast cells were grown at 30 °C to mid-log phase in SC media lacking uracil and supplemented with 2% raffinose and 0.1% glucose and then induced with 2% galactose to express APH-Im7 variant fusions for 4 h. b) Thermodynamic stabilities of Im7 variants were plotted against the total protein level of APH-Im7 fusions in *S. cerevisiae* as determined from immunoblotting against the FLAG epitope. The experiments were

performed in triplicate, and error bars indicate ± 1 SD. c) Immunoblotting against the V5 epitope on the C terminus of NAT tripartite fusions and against G6PDH as a loading control in yeast cell lysates. Shown are total protein (T), soluble lysate (S), and pellet fractions (P). The yeast cells were grown at 30 °C to mid-log phase in SC media supplemented with 2% raffinose and 0.1% glucose and then induced with 2% galactose to express NAT-Im7 variant fusions for 4 h at 34 °C before processing the cells for lysate fractionations. The experiment (c) was performed by Hyun-hee Kim. The figure is adapted with permission from Sachsenhauser, V., Deng, X., Kim, H.-H., Jankovic, M., C.A. Bardwell, J., and Bardwell, J. C. A. (2020) Yeast tripartite biosensors sensitive to protein stability and aggregation propensity. ACS Chem. Biol. *XXXX*, XXX, XXX–XXX, https://doi.org/10.1021/acschembio.0c0008. Copyright 2020 American Chemical Society.[97]

Conversely, we did not detect a linear relationship between the NAT-Im7 protein levels and Im7 thermodynamic stabilities (Figure 6c), despite the strong correlation observed between the MIC values and stabilities. This finding could be explained by the assumption that the NAT tripartite context affects the solubility of the fused Im7. Increased protein solubility has been frequently seen with other fusion partners such as green fluorescent protein or mKate2, as discussed earlier.[21] Yet, we think that the split antibiotic resistance markers act as a more neutral fusion partner compared to a fluorescent protein. Our reasoning is based on the fact that a linear relationship between the thermodynamic stability of the inserted protein and the antibiotic resistance readout was the main selection criteria in the transposon screen for an optimal antibiotic marker insertion site.[119] Since the Im7 thermodynamic stabilities correlate with the antibiotic resistance readouts conferred by the NAT-Im7 fusion variants, we conclude that the folding status of fused Im7 variants nevertheless defines the complementation efficiency of the split NAT protein. For this reason, the antibiotic resistance readouts observed with the APH- and NAT-based fusions appear to provide a more sensitive assessment for *in vivo* protein stability than analysis of protein levels by immunoblotting.

Since the two generated tripartite fusion designs are based on unrelated antibiotic resistance genes, it seems possible to combine the APH and NAT tripartite biosensors within one cell. This strategy could link *in vivo* protein stability to two independent antibiotic resistance readouts.

From these results, it can be concluded that the optimized, tripartite fusion system is a convenient tool that is sensitive to protein stability in the yeast cytosol.

4.2 Ligand binding enhances stability readout

Ligand binding thermodynamically stabilizes the binding partner, with the extent of stabilization depending on the binding affinity and concentrations of the two binding partners.[141] We wondered whether ligand binding-induced stabilization could be detected in yeast using the tripartite system. To explore this question, we expressed APH tripartite fusions with Im7 WT together with Im7's natural binding partner protein, colicin E7, using the colicin E7 nuclease deficient variant (H162A).[106] We expressed only the colicin E7 endonuclease domain (residues 63–193), which is sufficient for Im7-E7 complex formation.[106] The colicin E7-Im7 protein complex features an extraordinarily high binding affinity (K_d of ~ 10^{-14} M *in vitro*)[96,142] that approaches the affinity of a covalent bond. Indeed, when we co-expressed the colicin E7 H162A fragment, we observed a distinct increase in antibiotic resistance (Figure 7a) and a minor increase in APH-Im7 WT protein levels compared to co-expression of just an empty vector control (Figure 7b). These findings indicated that we might be able to use the tripartite fusion system to detect changes in a test protein's *in vivo* stability induced by intermolecular interactions.

To investigate whether our tripartite system could serve to detect stabilization through binding partners with weaker affinities, we expressed the APH biosensor fused with Im7 WT or with a partially-folded Im7 variant, Im7 L53A I54A, together with the chaperone Spy. Im7 is a natural client of this chaperone, and Spy binding has been shown to stabilize and prevent the degradation of unstable Im7 L53A I54A in the *E. coli* periplasm.[143] Spy has a modest binding affinity for Im7 (*in vitro* K_ds for Spy binding to Im7 L53A I54A and Im7 WT are 3.5 μM and 20.5 μM, respectively—8 orders of magnitude lower than E7's binding affinity for Im7 *in vitro*).[144–146] When expressing the APH-Im7 variant fusions together with Spy, we could not detect differences in antibiotic resistance levels compared to those conferred by cells that co-expressed only an empty vector control (Figure 7c). Spy expression was confirmed by qualitative western blotting (data not shown). These data indicate that the yeast tripartite system may not be sensitive enough to display stability changes induced by weaker binding partners, assuming the K_d values determined *in vitro* are similar in the yeast cytosol. Given the modest K_d for Spy, a relatively high chaperone concentration may be necessary for effective chaperone function *in vivo*. Under

stress, the concentration of Spy has been shown to increase from roughly 0 to ~2 mM in the *E. coli* periplasm, which has been suggested to allow tight association with proteins that are at least partially or transiently unfolded by the stressors.[143,145,146] Hence, the lack of measurable stabilization may be explained by ineffective Spy concentrations due to insufficient expression of Spy in the yeast cytosol.[52] Further experiments would be needed to explore this possible explanation and to determine the limits of sensitivity of the tripartite fusions.

In conclusion, we find that the yeast tripartite fusion system may enable the detection of changes in the *in vivo* stability of a test protein resulting from intermolecular interactions with high-affinity binding partners.

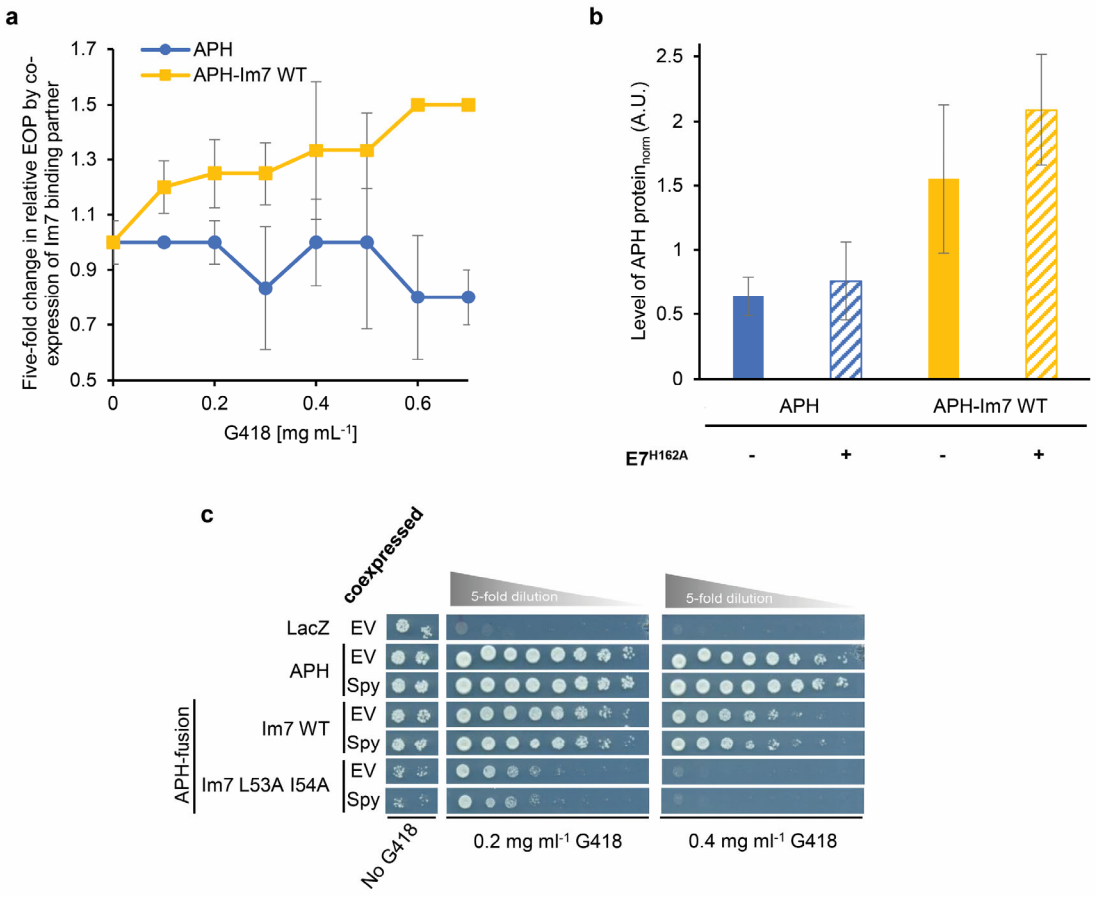

Figure 7. Expression of the APH-Im7 WT tripartite fusion together with a high-affinity Im7 binding partner. a) Antibiotic resistance levels of yeast cells expressing APH-Im7 tripartite fusions together with the endonuclease fragment of the high-affinity Im7 binding partner colicin E7 (residues 63–193) or just an empty vector control (EV) was determined in spot titers assays. The colicin E7 variant H162A ($E7^{H162A}$) was used to reduce the otherwise lethal

nuclease activity of this colicin.[106] The plot shows the 5-fold change in the efficiency of plating (EOP) of *S. cerevisiae* strains expressing only the APH protein or the APH-Im7 WT tripartite fusion together with the nuclease domain $E7^{H162A}$ relative to the EOP of cells expressing the APH protein or the APH-Im7 WT tripartite fusion with an empty vector. To score cell growth, yeast cells expressing the $E7^{H162A}$ fragment or the empty vector together with either APH tripartite fusions with WT Im7 (strains VES274, VES273) or without any insertion in APH (strains VES271, VES270) were grown to mid-log phase, OD normalized, and spotted in 5-fold serial dilutions on SC agar media lacking uracil and tryptophan, supplemented with 2% galactose and 2% raffinose, and supplemented without or with increasing concentrations of the antibiotic G418 and incubated at 30 °C. Yeast cells expressing only LacZ together with the empty vector (strain VES252) served as a control for G418 sensitivity. The experiment was performed in quadruplicate, and error bars indicate ± 1 SD. b) Expression of an Im7 binding partner together with the APH-Im7 WT tripartite fusion increases the APH-Im7 WT protein level. To assay the stability of the APH protein, *S. cerevisiae* cells were grown to log phase in SC media lacking uracil and tryptophan, supplemented with 0.1% glucose and 2% raffinose and induced with 2% galactose to express either the APH protein or the APH-Im7 WT tripartite fusion in the presence of either an empty vector or the nuclease fragment $E7^{H162A}$ for 4 h at 30 °C. Total protein cell lysates were immunoblotted against the APH protein and against G6PDH for normalization. Plotted is the normalized APH protein level in the absence (empty vector only) or presence of $E7^{H162A}$ (indicated by a "–" or "+", respectively, in the $E7^{H162A}$ row). The experiment was performed in triplicate, and error bars indicate ± 1 SD. c) Antibiotic resistance levels of yeast cells expressing APH tripartite fusions with WT Im7, with the destabilized Im7 variant L53A I54A or without any insertion in APH together with the chaperone Spy or just an empty vector control (EV). Im7 is a natural client of Spy in *E. coli* and Spy has a moderate affinity for the Im7 variants. For this assay, yeast cells expressing Spy or the empty vector together with either APH tripartite fusions with WT Im7 (strains VES288, VES273), with the destabilized Im7 variant L53A I54A (strains VES280, VES278) or without any insertion in APH (strains VES270, VES272) were grown to mid-log phase, OD normalized, and spotted in 5-fold serial dilutions on SC agar media lacking uracil and tryptophan, supplemented with 2% galactose and 2% raffinose, and supplemented without (No G418) or with 0.2 or 0.4 mg mL^{-1} of the antibiotic G418 at 30 °C. Yeast cells expressing only LacZ together with the empty vector (strain VES252) served as a control for G418 sensitivity. The spot titers without antibiotic (No G418) correspond to the cell dilutions 7th and 8th from the left of the spot titers in the presence of the antibiotic (0.2 mg mL^{-1} G418 and 0.4 mg mL^{-1} G418). The figure is adapted with permission from Sachsenhauser, V., Deng, X., Kim, H.-H., Jankovic, M., C.A. Bardwell, J., and Bardwell, J. C. A. (2020) Yeast tripartite biosensors sensitive to protein stability and aggregation propensity. ACS Chem. Biol. *XXXX*, XXX, XXX–XXX, https://doi.org/10.1021/acschembio.0c0008. Copyright 2020 American Chemical Society.[97]

4.3 Tripartite biosensors allow study of neuropathological proteins and yeast prions

We wondered whether our optimized yeast tripartite fusions could also serve to detect changes in protein solubility using the antibiotic resistance readout. If true, the fusions could be valuable in the *in vivo* investigation of pathologically misfolded and/or aggregation-prone proteins. To address this question, we fused the tripartite sensors with bona fide representatives of neuropathological protein misfolding and determined the antibiotic sensitivity readout. Specifically, we investigated the behavior of the neurodegenerative disease-relevant proteins Aβ42 and α-synuclein as well as the prion forming proteins Rnq1 and Sup35 in the tripartite fusion context.[13,147]

4.3.1 Aβ42

Alzheimer's disease is the most prevalent neurodegenerative disease.[148] Accumulation of abnormally folded Aβ42 peptide in the brains of Alzheimer's patients has been closely linked to this neurodegenerative disease.[42] Different misfolding or aggregation states of Aβ42 are reproduced in humanized yeast models for Alzheimer's disease. The nature of the Aβ42 misfolding depends largely on the reporter system used. Approaches involving cytotoxic overexpression of Aβ42 in the yeast endoplasmic reticulum, fusion of Aβ42 with fluorescent reporter proteins to microscopically determine Aβ42 solubility levels, or fusion with enzymes that can be linked to growth such as dihydrofolate reductase can mimic different misfolding, oligomerization, and aggregation states of Aβ42.[83,85–87,149,150] To provide a complementary yeast model for Alzheimer's disease that is based on a different reporter concept than these aforementioned approaches, we fused Aβ42 into our APH and NAT biosensors (Figure 8a).

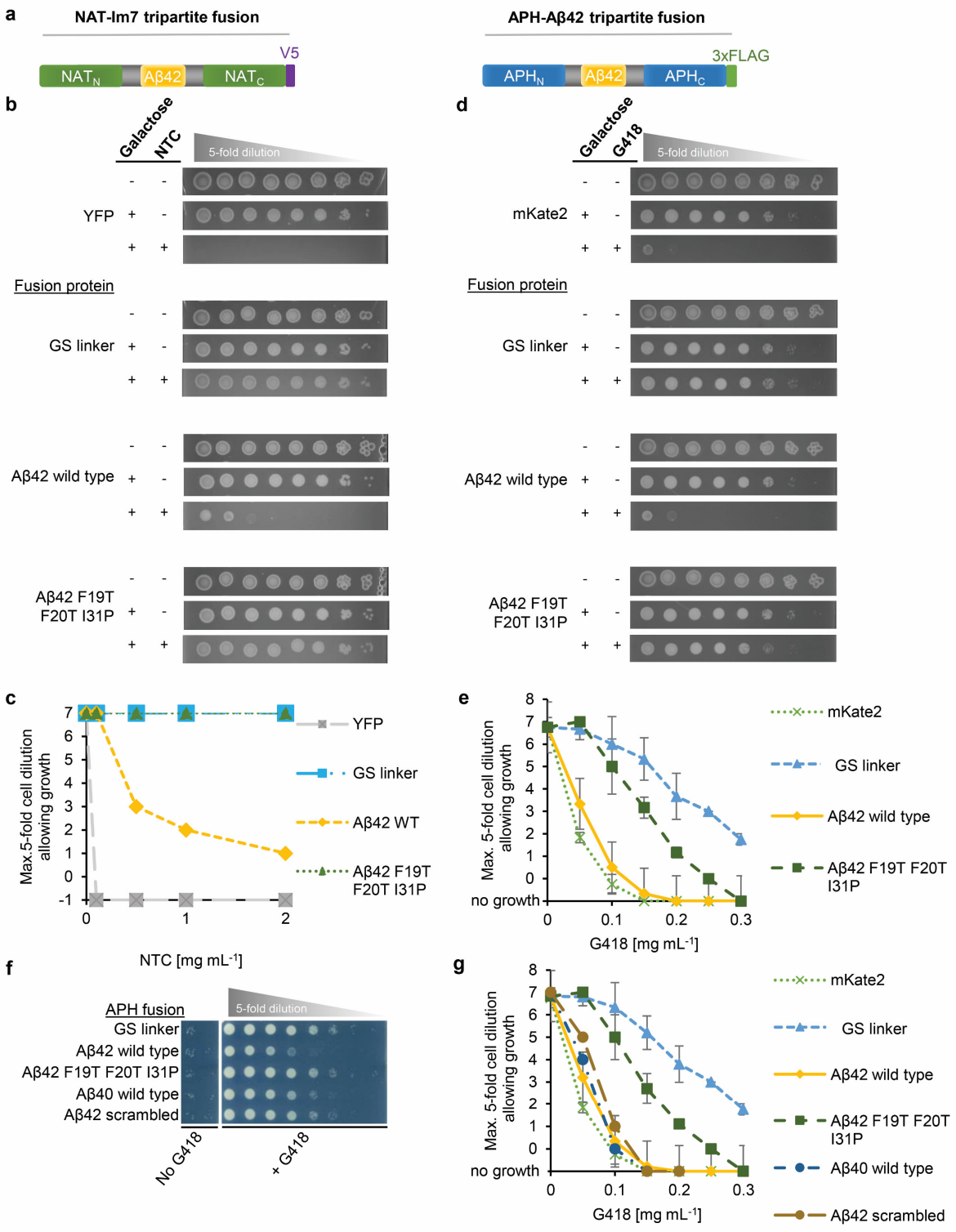

Figure 8. Antibiotic resistance conferred by tripartite fusions with Aβ variant peptides is Aβ sequence dependent. a) Schematic diagrams of the NAT-Aβ42 and APH-Aβ42 tripartite fusions. In the NAT-Aβ42 fusions, the test proteins were fused at NAT residue 78. b) Spot titers showing antibiotic resistance of yeast cells expressing either a non-NTC

resistant control protein, YFP (VES735), or various NTC resistant NAT constructs fused with just a GS linker (VES736) or the additional insertion of WT Aβ42 (VES741) or an oligomerization deficient Aβ42 variant, Aβ42 F19T F20T I31P (VES742). Five-fold serial dilution spotting assays were used to score cell growth at 34 °C on SC agar media supplemented without or with 2.0 mg mL^{-1} NTC (indicated by a "–" or "+", respectively, in the NTC column) and with either 2% glucose or 0.5% galactose (indicated by a "–" or "+", respectively, in the galactose column) to induce expression of the tripartite fusion. Prior to spotting, cells were grown to early or mid-log phase in SC media supplemented with 2% raffinose and 0.1% glucose at 30 °C, OD-normalized, and 5-fold serially diluted. c) Quantification of the antibiotic resistance phenotypes of the Aβ42 tripartite fusions over the range of 0 to 2.0 mg mL^{-1} NTC as observed in spotting assays as described in (b). d) Antibiotic resistance of yeast cells expressing either a non-G418 resistant control protein, mKate2 (VES650), or various G418 resistant APH constructs containing just a GS linker insert (VES657), or the additional insertion of WT Aβ42 (VES702) or the aggregation deficient Aβ42 variant, Aβ42 F19T F20T I31P (VES700). Five-fold serial dilution spotting assays were used to score cell growth on SC agar media supplemented without or with 0.1 mg mL^{-1} G418 (indicated by a "–" or "+", respectively, in the G418 column); media was also supplemented with either 2% glucose or 2% galactose (indicated by a "–" or "+", respectively, in the galactose column) to induce the expression of the tripartite fusion. e) Quantification of the antibiotic resistance phenotypes of the Aβ42 tripartite fusions over the range of 0 to 0.3 mg mL^{-1} G418 as observed in spotting assays. The data plotted are from four experiments; error bars indicate ± 1 SD. f) Spot titers showing antibiotic resistance of yeast cells expressing various G418 resistant constructs containing just a GS linker (yXD622) or the additional insertion of WT Aβ42 (yXD623), Aβ42 F19T F20T I31P (yXD624), Aβ40 (yXD628), or Aβ42 with a scrambled amino acid sequence (indicated as "Aβ42 scrambled") (yXD629) grown at 30 °C on SC agar media supplemented without or with 0.05 mg mL^{-1} G418. The spot titers without antibiotic (No G418) correspond to the cell dilutions 7th and 8th from the left of the spot titers in the presence of the antibiotic (+ G418). g) Five-fold serial dilution spotting assays of cells were used to score cell growth on SC agar supplemented with G418 concentrations ranging from 0 to 0.3 mg mL^{-1}. The spot titer data of panels f and g were acquired by Xiexiong Deng. The figure is adapted with permission from Sachsenhauser, V., Deng, X., Kim, H.-H., Jankovic, M., C.A. Bardwell, J., and Bardwell, J. C. A. (2020) Yeast tripartite biosensors sensitive to protein stability and aggregation propensity. ACS Chem. Biol. *XXXX*, XXX, XXX–XXX, https://doi.org/10.1021/acschembio.0c0008. Copyright 2020 American Chemical Society.[97]

In the absence of antibiotics, cells expressing the tripartite fusions all grew to comparable titers, indicating that no Aβ42-mediated cytotoxicity was induced; this result is in contrast to findings in some of the previously developed Aβ42 yeast models, which did show cytotoxic effects.[83,150,151] With the exception of fusions with full-length Sup35 (for details please see below), no toxic effect was observed with the expression of any of the tripartite biosensors described in this paper. The absence of toxicity can possibly be explained by the moderate

expression level that was deliberately obtained for the tripartite fusions. Another advantage of this moderate expression level is that it makes our biosensor results more physiologically relevant than, for example, the extreme overexpression of neuropathological and prion proteins used in yeast models that involve cytotoxicity readouts.[80–83]

Compared to cells expressing the biosensor fused with only a GS linker, we observed substantially lower antibiotic resistance levels for cells expressing tripartite fusions with WT Aβ42 (Figure 8). Tripartite fusions with an oligomerization deficient variant, Aβ42 F19T F20T I31P, conferred higher levels of antibiotic resistance that were close to those displayed by the GS linker-only controls (Figure 8). To examine whether the antibiotic resistant phenotype we observed was merely due to the hydrophobic nature of the inserted WT Aβ42 peptide, we expressed the tripartite biosensor fused with a shorter Aβ variant (Aβ40) and with Aβ42 that had a scrambled amino acid sequence.[103] We reasoned that if the hydrophobicity of the inserted peptide was the main determinant of the low antibiotic resistance levels, then the growth phenotypes conferred by the Aβ40 and scrambled Aβ42 fusions should be comparable to those conferred by the WT Aβ42 fusion. They were not; antibiotic resistance levels were up to ~5 fold and ~10-fold higher for tripartite fusions with Aβ40 and the scrambled Aβ42 variant, respectively, compared to fusions with WT Aβ42 (Figure 8f, g), leading us to conclude that Aβ42's sequence characteristic is the main determinant of its low antibiotic resistance phenotype.

To test if differences in transcription levels or mRNA stability of the tripartite fusions could simply explain the differential antibiotic resistance readouts, we performed quantitative reverse transcription PCR (RT-qPCR). The mRNA levels of the tripartite fusions with Aβ42 and with the test proteins described below were all very similar, leading us to exclude this possibility (Figure 9).

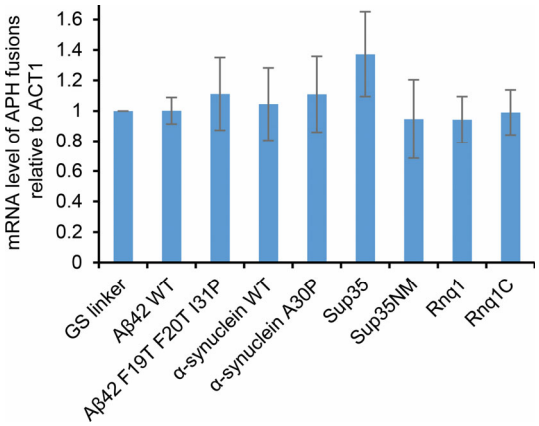

Figure 9. mRNA transcript levels of APH tripartite fusions are comparable. The graph shows mRNA transcript levels of cells expressing the APH fusions with WT Aβ42 (VES702), Aβ42 F19T F20T I31P (VES700), WT α-synuclein (VES683), α-synuclein A30P (VES706), full length Sup35 (yHH86), Sup35NM (yHH88), full length Rnq1 (yHH90), or Rnq1C (yHH93) relative to mRNA transcript levels of cells expressing the APH-GS linker tripartite fusion (VES657). Cells were grown at 30 °C in SC medium supplemented with 2% raffinose and 0.1% glucose to early log phase before inducing the expression of tripartite fusions through addition of 2% galactose. After 4 h of tripartite expression, cellular RNA was isolated, transcribed to cDNA, and mRNA transcript levels of APH tripartite fusions quantified relative to ACT1. The experiment was performed by Hyun-hee Kim. The figure is reprinted with permission from Sachsenhauser, V., Deng, X., Kim, H.-H., Jankovic, M., C.A. Bardwell, J., and Bardwell, J. C. A. (2020) Yeast tripartite biosensors sensitive to protein stability and aggregation propensity. ACS Chem. Biol. *XXXX*, XXX, XXX–XXX, https://doi.org/10.1021/acschembio.0c0008. Copyright 2020 American Chemical Society.[97]

To further characterize the *in vivo* behavior of the Aβ42 tripartite fusions, we analyzed their proteolytic sensitivity using cycloheximide chase experiments (Figure 10a–e) and their cellular localization by immunohistochemical detection (Figure 10f). Unlike Aβ42 F19T F20T I31P and GS linker-only fusions, which appeared dispersed in the cytosol, WT Aβ42 fusions were not detectable (Figure 10f). Consistently, WT Aβ42 tripartite fusions seemed to degrade at a much higher rate compared to Aβ42 F19T F20T I31P and GS linker-only fusions (Figure 10f). When the proteasome inhibitor MG132 was added, the protein levels of WT Aβ42 tripartite fusions remained fairly constant during the chase (Figure 10b, d). These results suggested that the proteolytic susceptibility of WT Aβ42 tripartite fusions is likely the reason for the observed antibiotic resistance phenotype.

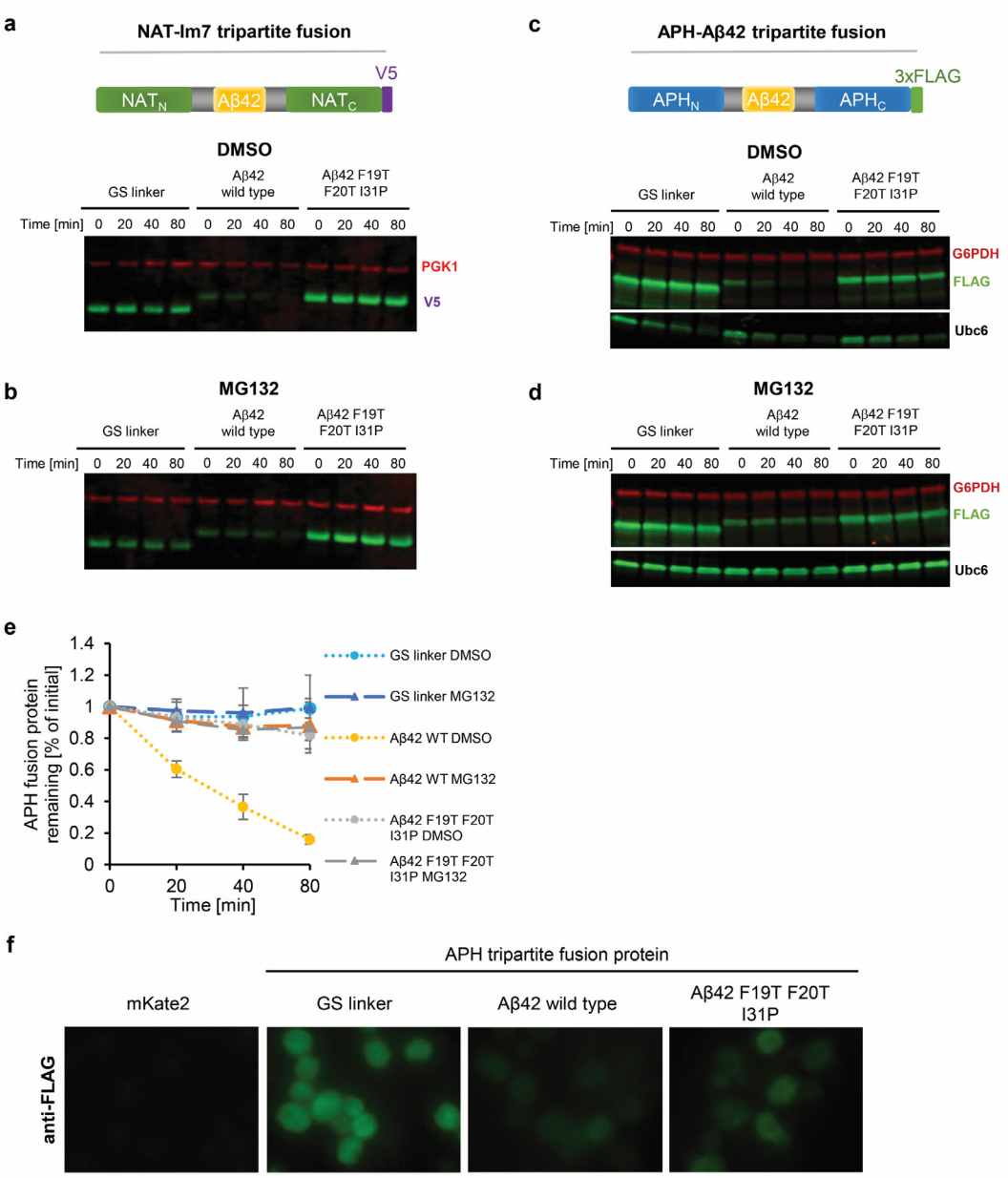

Figure 10. Antibiotic resistance conferred by the APH-Aβ42 tripartite biosensor varies depending on the in vitro stability of the Aβ insert. a) To assess the stability of the NAT-Aβ42 fusions, cycloheximide chase experiments were performed for the indicated times followed by immunoblotting against the V5 epitope on the C terminus of the fusions and against phosphoglycerate kinase 1 (PGK1) as a loading control. Prior to the chase experiments, cells were grown at 30 °C, induced with 2% galactose to express NAT constructs containing just a GS linker (VES736) or the additional insertion of WT Aβ42 (VES741) or Aβ42 F19T F20T I31P (VES742) for 6 h, followed by treatment with either DMSO or b) the proteasome inhibitor MG132, which was dissolved in DMSO. Note that the cells used in these chase experiments (panels a and b) do not have the gene for the drug efflux pump PDR5 deleted, in which case

treatment with MG132 leads to incomplete inhibition of the proteasome. c and d) To assess the stability of the APH-Aβ42 fusions, cycloheximide chase experiments with proteasome inhibitors were performed as described in (a) and (b) followed by immunoblotting against the FLAG epitope on the C terminus of the fusions, against G6PDH as a loading control, and against the proteasome substrate Ubc6 to get an indication of the efficiency of proteasome inhibition. Cycloheximide chase experiments of cells expressing APH constructs containing just a GS linker insert (yXD622), or the additional insertion of WT Aβ42 (yXD623) or Aβ42 F19T F20T I31P (yXD624) were performed in *pdr5*Δ strain backgrounds. e) Quantification of APH fusion levels relative to their initial cellular amounts in cycloheximide chase assays. These experiments were performed in triplicate; error bars indicate ± 1 SD. f) Immunohistochemical detection using anti-FLAG antibodies to determine the cellular localization of the APH-Aβ42 tripartite fusions. Prior to the detection, expression of tripartite fusions was induced with 2% galactose for 4 h and cells grown at 30 °C. Exposure time was 50 ms. The chase experiments and immunohistochemical detection of the Aβ42 tripartite fusions were performed by Xiexiong Deng. The figure is adapted with permission from Sachsenhauser, V., Deng, X., Kim, H.-H., Jankovic, M., C.A. Bardwell, J., and Bardwell, J. C. A. (2020) Yeast tripartite biosensors sensitive to protein stability and aggregation propensity. ACS Chem. Biol. *XXXX*, XXX, XXX–XXX, https://doi.org/10.1021/acschembio.0c0008. Copyright 2020 American Chemical Society.[97]

When soluble Aβ42 is present in low concentrations, it is efficiently eliminated by the quality control machinery.[44,56] In this clearance process, the ubiquitin-proteasome system seems to play an important role since its malfunctioning has been associated with Alzheimer's disease.[152] It has been shown that elevated Aβ42 steady state levels enhance primary nucleation events, which are a prerequisite for its pathological oligomerization and aggregation.[153] Increasing the degradation of the soluble Aβ peptide to mitigate its misfolding and self-association may be an effective strategy to treat Alzheimer's disease.[44,58,154] Since the antibiotic resistance readout of our Aβ42 tripartite biosensors seems to be based on the proteolytic processing of fused Aβ42, our approach could be useful in the exploration of factors that affect the intracellular stability of soluble Aβ42. Given the distinct antibiotic resistance phenotype of NAT- and APH-Aβ42 WT fusions, the biosensors should be amenable to screens for Aβ42 stabilizing factors (indicated by increased antibiotic resistance) or factors that increase the clearance of Aβ42 (indicated by decreased antibiotic resistance).

In summary, the Aβ42 tripartite fusions may provide the opportunity to extend our understanding of Aβ42 stability in Alzheimer's disease.

4.3.2 α-synuclein

To further validate the usefulness of the yeast tripartite fusion system for the investigation of neuropathogenic proteins, we fused it to α-synuclein. Multiplication of and missense mutations in the α-synuclein gene have been closely associated with the second most common neuropathogenic disease, Parkinson's disease.[155] Previously published yeast models of α-synuclein biology utilize fluorescent reporter fusions to monitor the localization of the protein *in vivo*.[81,92] Cytotoxicity resulting from its cytosolic overexpression was utilized as a readout to identify cellular factors and chemical compounds modifying α-synuclein aggregation.[77,156–158] Similar to cytotoxic Aβ42 reporter systems discussed earlier, the massive α-synuclein expression levels underlying the cytotoxicity phenotype likely lead to substantial side effects unrelated to α-synuclein and may only be marginally physiologically relevant for human α-synuclein pathology.

To establish an alternative yeast model to study α-synuclein*,* we evaluated the behavior of α-synuclein in our tripartite system. For this purpose, we inserted cDNA from WT α-synuclein and the disease-associated α-synuclein mutants A53T, E46K, and A30P into the APH biosensor (Figure 11a). In several *in vitro* studies, the α-synuclein A53T and E46K variants showed an increased aggregation rate compared to WT α-synuclein.[159,160] There is less agreement on the effects of the A30P mutation on α-synuclein aggregation behavior due to somewhat contradictory *in vitro* results: α-synuclein A30P has been found to aggregate at slower,[159,161] faster,[162,163] and comparable rates relative to other α-synuclein variants.[164]

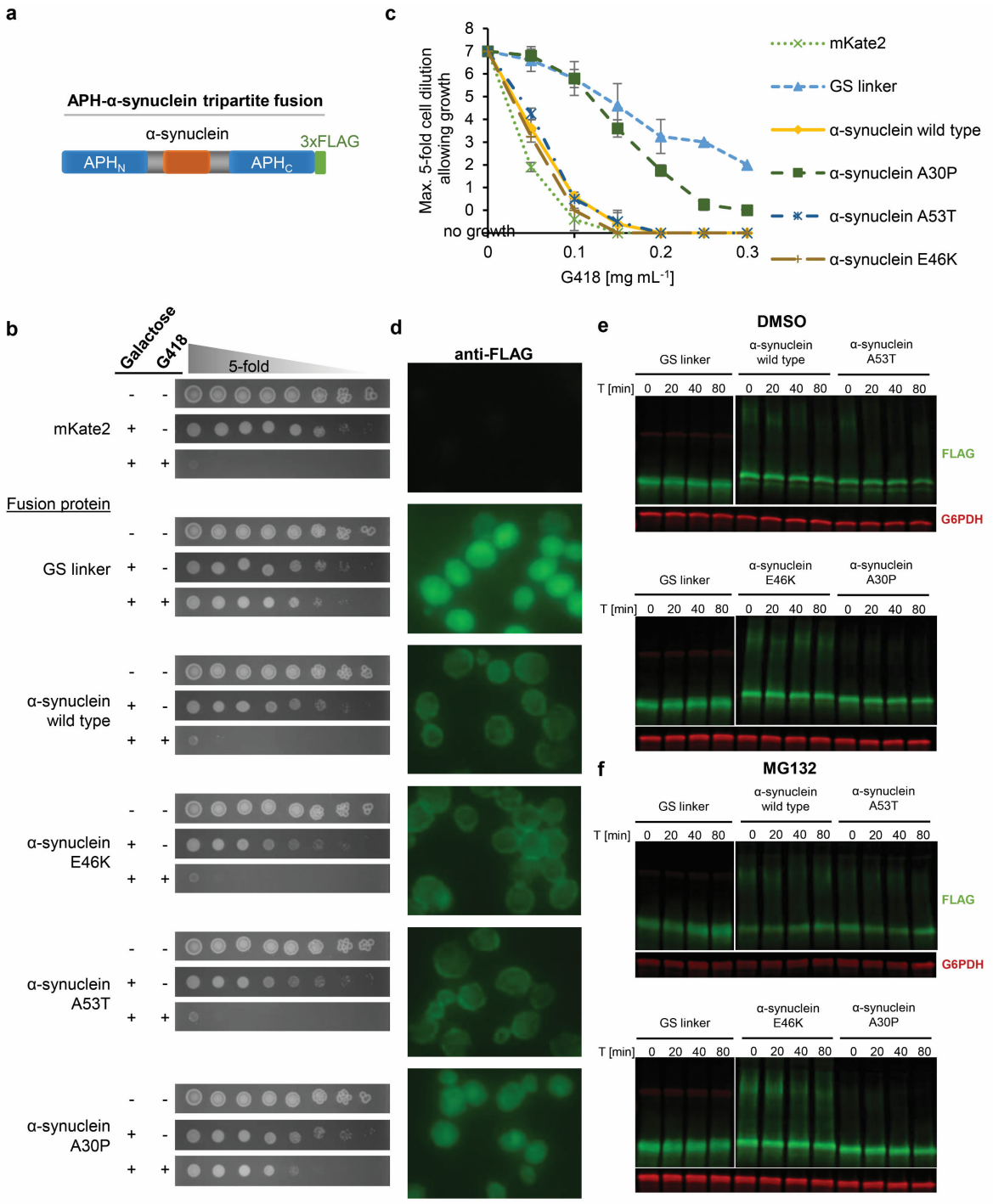

Figure 11. Antibiotic resistance conferred by the APH-α-synuclein tripartite biosensors varies depending on the ability of the α-synuclein inserts to interact with the membrane. a) Schematic diagram of the APH-α-synuclein tripartite fusion. b) Antibiotic resistance of yeast cells expressing either a non-G418 resistant control protein, mKate2 (VES650), or various G418 resistant APH constructs containing just a GS linker insert (VES657), or the additional insertion of: WT α-synuclein (VES683), α-synuclein E46K (VES687), α-synuclein A53T (VES685), or α-synuclein A30P

(VES706). Cells were grown to early or mid-log phase in SC media supplemented with 2% raffinose and 0.1% glucose prior to spotting of OD-normalized, five-fold serial diluted cells on SC agar media supplemented without or with 0.15 mg mL^{-1} G418 (indicated by a "–" or "+", respectively, in the G418 column) to score cell growth. c) Quantification of antibiotic resistance phenotypes of the α-synuclein tripartite fusions over the range of 0 to 0.3 mg mL^{-1} G418 as obtained from spotting assays. The reported data is from five experiments; error bars indicate ± 1 SD. d) Immunohistochemical detection using anti-FLAG antibodies to determine the cellular localization of the APH-α-synuclein fusions. Prior to the detection, expression of tripartite fusions was induced for 8 h with 2% galactose. Strain order from top to bottom was the same as in (b). Exposure time 50 ms. e and f) To assess the stability of the APH-α-synuclein fusions, cycloheximide chase experiments were performed for the indicated times followed by immunoblotting against the FLAG epitope on the C terminus of the fusions and against G6PDH as loading control. Prior to the chase experiments, tripartite expression was induced for 6 h with 2% galactose, and cells were treated with either DMSO (e) or the proteasome inhibitor MG132 dissolved in DMSO (f). Of note, cells did not have a deletion in PDR5. Immunohistochemical detection (d) and chase experiments (e, f) of the tripartite fusions were performed by Xiexiong Deng. The figure is adapted with permission from Sachsenhauser, V., Deng, X., Kim, H.-H., Jankovic, M., C.A. Bardwell, J., and Bardwell, J. C. A. (2020) Yeast tripartite biosensors sensitive to protein stability and aggregation propensity. ACS Chem. Biol. *XXXX*, XXX, XXX–XXX, https://doi.org/10.1021/acschembio.0c0008. Copyright 2020 American Chemical Society.[97]

When we expressed α-synuclein A30P in the APH tripartite fusion in yeast, it conferred distinctly higher antibiotic resistance levels compared to fusions with WT α-synuclein or with the variants A53T and E46K (Figure 11b, c). Unlike the tripartite fusions with WT Aβ42, α-synuclein variant fusions did not seem susceptible to degradation (Figure 11e, f). Instead, the variation in antibiotic sensitivity levels strikingly correlated with the localization pattern of α-synuclein fusions in the cell. We could detect fusions with WT α-synuclein, A53T or E46K at the cell membranes where they seemed to be partly present in foci. Fusions with α-synuclein A30P, however, were found dispersed throughout the cytosol (Figure 11d). These differential localization patterns are in agreement with previously developed yeast models of α-synuclein biology.[81,165] α-synuclein A30P has a relatively low membrane binding capacity *in vitro* compared to α-synuclein WT, which might explain the dispersed distribution pattern of the α-synuclein A30P tripartite fusion.[166] In contrast to the α-synuclein A30P fusion, a portion of the WT α-synuclein, E46K, and A53T tripartite fusions formed SDS-resistant oligomers as detected in standard western blotting on cell lysates (Figure 11e,f) and weakly indicated in semi-denaturing

detergent agarose gel electrophoresis (SDD-AGE) (Figure 12a, b). The differential presence of SDS-stable oligomers is consistent with the observed phenotypic readouts and localization patterns of the α-synuclein variant fusions. The proportion of bona fide insoluble aggregates formed by the α-synuclein tripartite fusions seemed only minor (~6–8%) and indifferent for the four α-synuclein variant fusions (Figure 12c).

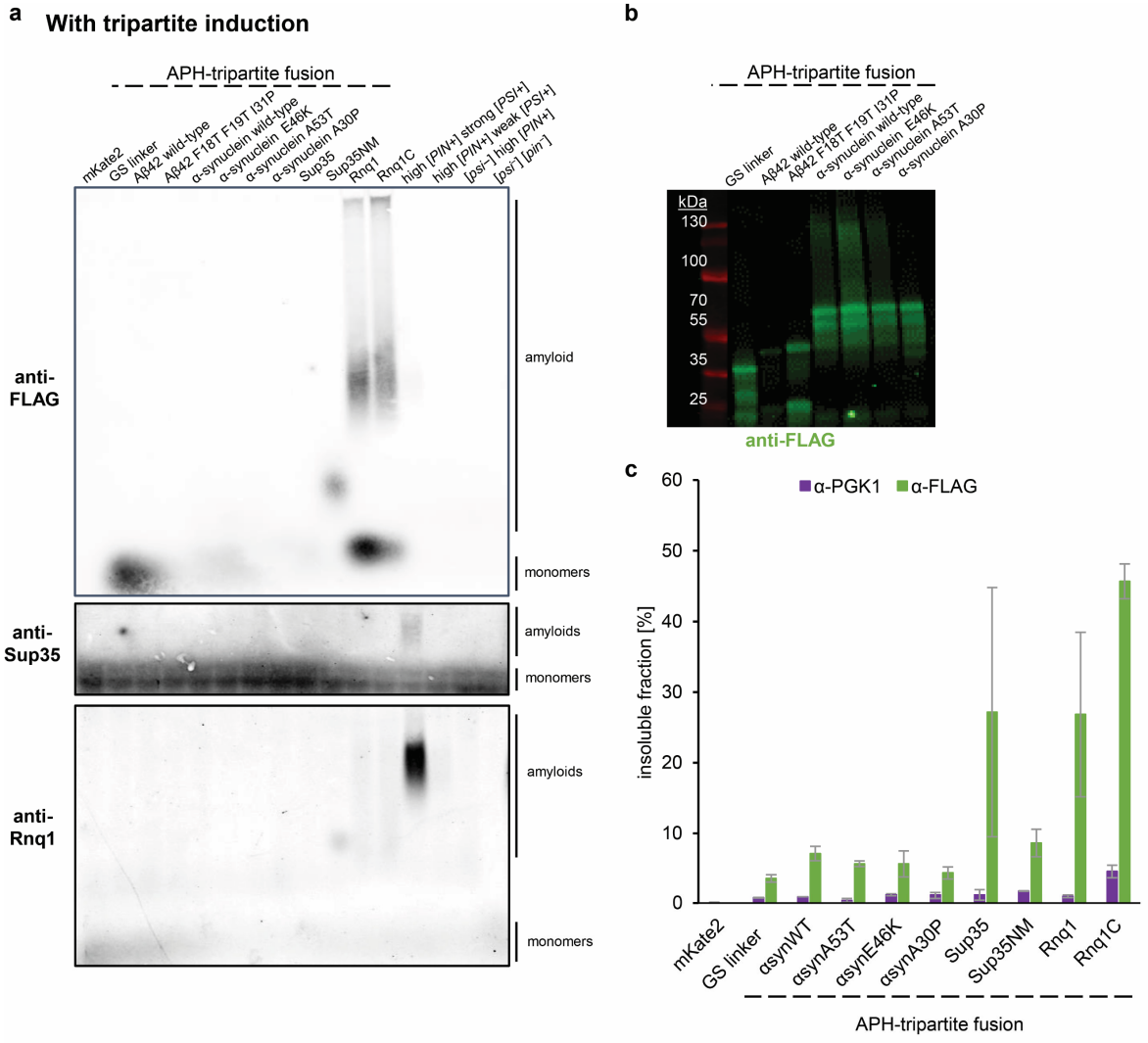

Figure 12. Tripartite fusions with prion proteins form insoluble aggregates that partially have amyloid-like structures. a) Cells expressing APH tripartite fusions were analyzed for the presence of tripartite aggregates with amyloid like structures and the presence of the amyloid form of Sup35 [PSI+] and Rnq1 [PIN+] as determined by semi-denaturing detergent agarose gel electrophoresis (SDD-AGE). Cells encoding APH tripartite fusion variants were grown at 30 °C in SC media supplemented with 2% raffinose and 0.1% glucose to mid-log phase and induced with 2% galactose to express tripartite fusions for 8 h. Amyloid-like species formed by the tripartite fusion were determined by SDD-AGE

followed by immunoblotting using antisera against a FLAG tag at the C terminus of the tripartite fusions. SDS-insoluble polymers formed by Sup35, prion [*PSI+*], or Rnq1, prion [*PIN+*], were detected by immunoblotting using anti-Rnq1 and anti-Sup35 antibodies. Analyzed strains encode only a fluorescent protein (mKate2) as a negative control or APH fusions with either a GS linker (VES657) or additional insertion of WT Aβ42 (VES702), Aβ42 F19T F20T I31P (VES700), WT α-synuclein (VES683), α-synuclein E46K (VES687), α-synuclein A53T (VES685), α-synuclein A30P (VES706), full length Sup35 (yHH86), Sup35NM (yHH88), full length Rnq1 (yHH90), or Rnq1C (yHH93). Yeast cells with known Sup35 and Rnq1 prion status served as controls for amyloid detection: high [*PIN*+] strong [*PSI*+] (L1762), high [*PIN*+] weak [*PSI*+] (L1758), [*psi*–] high [*PIN*+] (L1749), and [*psi*-] [*pin*-] (L2910)[113–116] Please note that although strains L1762, L1758, and L1749 are reported[113–115] as high [*PIN*+] strong [*PSI*+], high [*PIN*+] weak [*PSI*+], or high [*PIN*+] [*psi*-], respectively, for unknown reasons, we could only distinctly detect the presence of [*PIN*+] or [*PSI*+] in L1762. b) In parallel to SDD-AGE, the prepared cell lysates were analyzed by standard SDS-PAGE following immunoblotting against FLAG to determine tripartite steady state levels. c) Lysates of yeast cells that had been expressing APH fusions for 12 h were separated into soluble and insoluble protein fractions to determine the aggregation propensities for APH fusions containing α-synuclein (αsyn) WT and variants A53T, E46K, and A30P (yeast strains VES683, VES685, VES687, and VES706, respectively), full length Sup35 (yHH86), Sup35NM (yHH88), full length Rnq1 (yHH90), Rnq1C (yHH93), or just the GS linker (VES657). The amount of insoluble APH tripartite fusion relative to the total amount of APH tripartite protein in the cell lysates was determined by quantitative western blotting using antibodies against the FLAG epitope at the C terminus of the fusions (α-FLAG) and against phosphoglycerate kinase (α-PGK1) for normalization. Cells expressing only the fluorescent protein mKate2 (VES650) were used as a control. The experiment was performed in triplicate by Xiexiong Deng, and error bars indicate ± 1 SD. The figure is adapted with permission from Sachsenhauser, V., Deng, X., Kim, H.-H., Jankovic, M., C.A. Bardwell, J., and Bardwell, J. C. A. (2020) Yeast tripartite biosensors sensitive to protein stability and aggregation propensity. ACS Chem. Biol. *XXXX*, XXX, XXX–XXX, https://doi.org/10.1021/acschembio.0c0008. Copyright 2020 American Chemical Society.[97]

Unstable oligomers of α-synuclein fusions have been reported in recent studies.[36,167,168] It has been hypothesized that the initial stages of synuclein aggregation involve disordered oligomeric species and the accumulation of monomeric synuclein in lipid-like droplets.[167,169] These oligomeric and lipid-bound α-synuclein species could then serve as precursors for amyloid formation.[167,169]

It is hence conceivable that α-synuclein WT and α-synuclein variants A53T and E46K tripartite fusions, which show decreased antibiotic resistance levels, seem to localize at the membrane, and form SDS-stable species, mimic the initial α-synuclein misfolding events associated with lipid

binding and oligomer formation. Further, experiments focusing on the lipid binding capacity of the tripartite fusions *in vivo* could help to support this hypothesis.[81]

Our APH α-synuclein biosensors may be useful in screening host factors or chemical compounds that can modify the stability or lipid-association capacity of α-synuclein in the cellular environment.

Cells expressing α-synuclein variants inserted into the NAT tripartite fusion displayed indifferently high antibiotic resistance levels, comparable to those conferred by the GS linker-only fusions (Figure 13). Similarly, NTC-insensitive growth was observed for NAT fusions that had aggregation-prone Rnq1 or Sup35 proteins inserted (described in greater detail below; see 4.3.3 Rnq1 and Sup35).

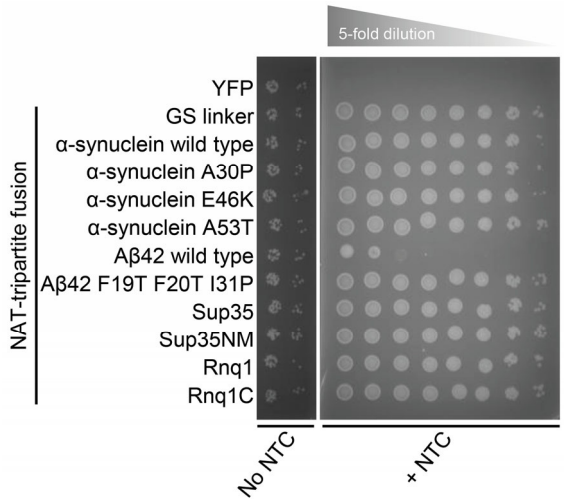

Figure 13. Antibiotic resistance levels conferred by NAT tripartite fusions with α-synuclein variants or prions Rnq1 or Sup35 are indifferent to the tripartite inserted protein. OD-normalized yeast cells expressing NAT tripartite fusions with WT α-synuclein (VES737), α-synuclein A30P (VES738), α-synuclein E46K (VES685), or α-synuclein A53T (VES706), Aβ42 WT (VES741), oligomerization deficient Aβ42 F19T F20T I31P, full length Sup35 (VES743), Sup35NM (VES744), full length Rnq1 (VES745), Rnq1's C-terminal prion domain, Rnq1C, (VES746), or with just the GS linker (VES736) were spotted in five-fold serial dilutions onto SC agar media supplemented with 2% galactose and 2% raffinose without (indicated as "No NTC") and with 0.1 mg mL^{-1} of the antibiotic NTC (indicated as "+ NTC") and grown at 37 °C. The spot titers without antibiotic (No NTC) correspond to the cell dilutions 7th and 8th from the left of the spot titers in the presence of the antibiotic (+ NTC). The GS linker alone and with the specified test proteins inserted were fused at NAT residue 78. Yeast cells expressing YFP (VES715) served as control for NTC sensitivity.

As discussed earlier, in some cases, the tripartite NAT context and possibly also the APH fusion context could increase the overall solubility of the fused test protein. In these circumstances, the tripartite sensor is of limited use for assessing the aggregation tendency of the respective protein of interest. The tripartite context could also interfere with the folding of the protein or sterically influence the formation of disease-associated amyloid structures, which has also been observed in other chimera-based approaches.[21,22] When the tripartite biosensor is aggregated in orderly stacked amyloid structures, the tripartite marker halves could interact intermolecularly and complement each other.[91] Fortunately, these potential limitations of the tripartite biosensor system can be identified through follow-up characterizations of the sensor constructs.

Overall, we conclude that the antibiotic resistance readout conferred by the APH reporter may be more useful than that of the NAT reporter, depending on the specific test protein fused.

4.3.3 Rnq1 and Sup35

Prions are misfolded proteins that are able to transmit their misfolded conformation onto normally folded variants of the same protein and propagate this misfolded status vertically and horizontally from cell to cell.[170] Prion structures have been found in several deadly and transmissible neurodegenerative disease in humans and several other kingdoms, including yeast.[147,171] In the unicellular organism, *de novo* prion formation seems to arise stochastically with a frequency of $\sim 10^{-5}$–10^{-7} and is thought to represent a protein-encoded, epigenetic switch.[147,171,172] The frequency of prion appearance is generally elevated by the overexpression of the prion protein and through the presence of existing prion structures of the same or different protein molecules in the cell.[113,114,173–176] The aggregation of amyloid and non-amyloid prion proteins is mediated by the protein's respective prion domain (PrD), which generally is composed of Gln (Q)- and/or Asn (N)-rich sequence stretches and is intrinsically disordered.[171,177] Two of the longest studied representatives of yeast prion proteins are the essential translation termination factor Sup35, which aggregates into the prion [*PSI*+], and the prion protein Rnq1, the function of

which has not yet been clarified, but which aggregates into the prion [*PIN*+]. The prion formed by Rnq1 is also known as prion [*RNQ*+].[114,176,178]

Yeast models to study prion formation commonly involve fusion with a fluorescent reporter or overexpression-induced cytotoxicity.[88,91,116,179] These approaches suffer from the same limitations as other yeast models that rely on similar sensor principles, as described earlier.

To test whether our tripartite fusion system can provide a complementary method to assess prion aggregation propensity, we inserted prion proteins Rnq1 and Sup35 into our APH tripartite system (Figure 13a). We generated sensor variants by inserting the complete Rnq1 protein, the complete Sup35 protein, or just their respective prion domains. For Rnq1 prion domain fusions, we inserted its Q/N-rich C-terminal half (Rnq1C) comprising residues 153–405.[174] For Sup35 prion domain fusions, we inserted the Sup35 NM-domain (Sup35NM), which spans Sup35's prion forming region (N, residues 1–123) and its highly charged prion stabilizing middle domain (M, residues 124–253).[178,180]

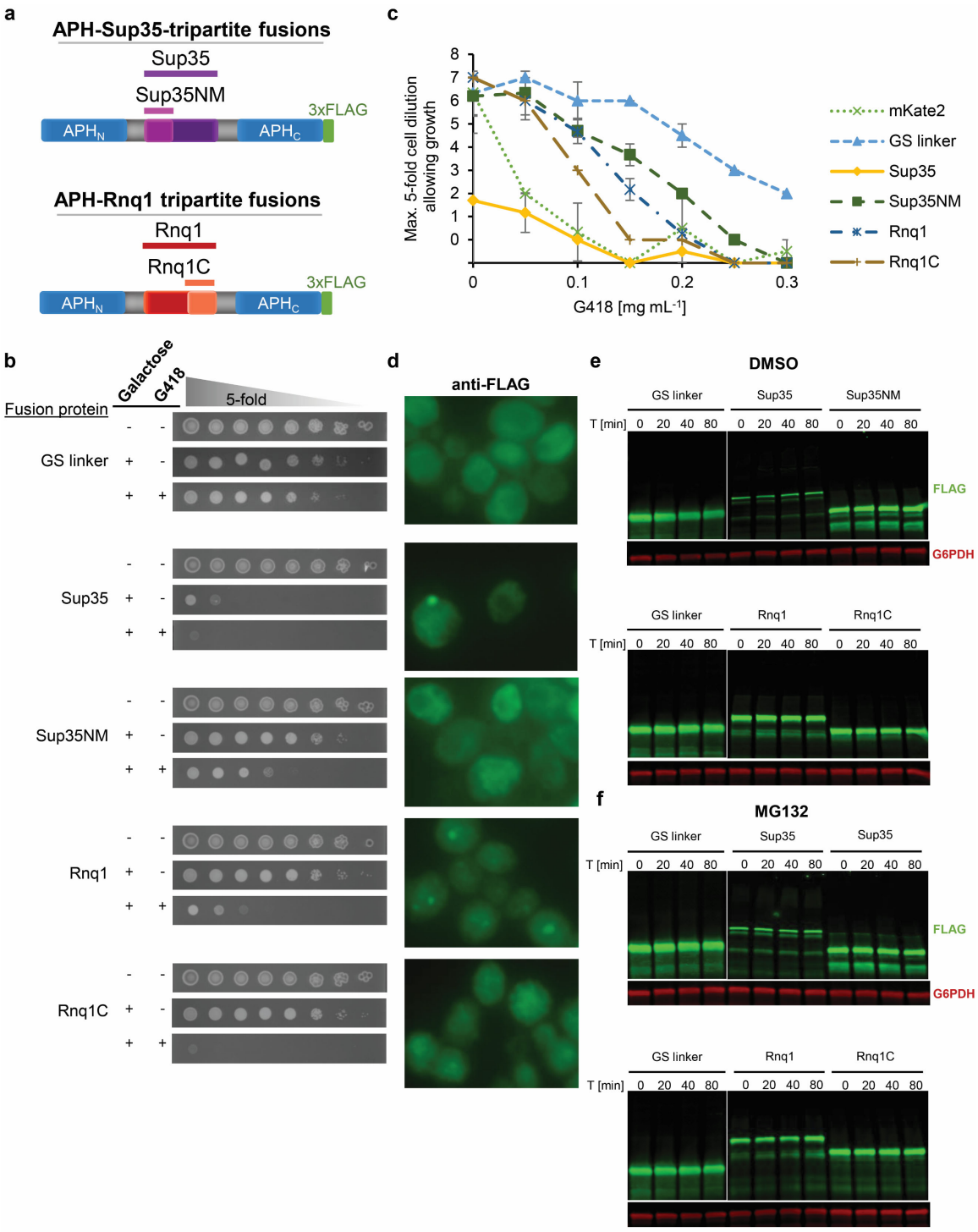

Figure 14. Antibiotic resistance of APH tripartite biosensors fused with variants of the yeast prion proteins Rnq1 and Sup35 correlates with the aggregation propensities of the inserts. a) Schematic diagram of the APH-Sup35 and APH-Rnq1 tripartite fusions. The complete Sup35 protein sequence or just its N-terminally located prion and middle domain (Sup35NM, residues 1–253) were inserted into the split APH marker. For the APH-Rnq1 tripartite fusion

variants, the complete Rnq1 sequence or only its C-terminal prion domain (Rnq1C, residues 153–405) was inserted. b) Antibiotic resistance of cells expressing various G418 resistant APH constructs containing just a GS linker (VES657), or the additional insertion of: the full length Sup35 sequence (yHH86), Sup35NM (yHH88), full length Rnq1 (yHH90), or Rnq1C (yHH93). Five-fold serial dilution spotting assays were used to score cell growth on SC agar media supplemented without or with 0.15 mg mL^{-1} G418 (indicated by a "–" or "+", respectively, in the G418 column); media was also supplemented with either 2% glucose or 2% galactose (indicated by a "–" or "+", respectively, in the galactose column) to induce expression of the tripartite fusions. c) Quantification of antibiotic resistance phenotypes of the Sup35 and Rnq1 tripartite fusions over the range of 0 to 0.3 mg mL^{-1} G418 observed in spotting assays. Plotted are the data from five experiments; error bars indicate ± 1 SD. d) Immunohistochemical detection using anti-FLAG antibodies to determine the cellular localization of the APH tripartite fusions. Prior to the detection, expression of tripartite fusions was induced for 8 h with 2% galactose. Strain order from top to bottom was the same as in (b). Exposure time was 100 ms. e and f) To assess the stability of the APH-prion fusions, cycloheximide chase experiments were performed for the indicated times followed by immunoblotting against the FLAG epitope on the C terminus of the fusions and against G6PDH as a loading control. Prior to the chase experiments, expression of the tripartite fusions was induced for 8 h, and cells were treated with either DMSO (e) or the proteasome inhibitor MG132 (f). Immunohistochemical detection (d) and chase experiments (e, f) of the tripartite fusions were performed by Xiexiong Deng. The figure is adapted with permission from Sachsenhauser, V., Deng, X., Kim, H.-H., Jankovic, M., C.A. Bardwell, J., and Bardwell, J. C. A. (2020) Yeast tripartite biosensors sensitive to protein stability and aggregation propensity. ACS Chem. Biol. *XXXX*, XXX, XXX–XXX, https://doi.org/10.1021/acschembio.0c0008. Copyright 2020 American Chemical Society.[97]

Cells expressing APH tripartite fusions with full length Rnq1 and especially Rnq1C conferred considerably lower antibiotic resistance levels than tripartite fusions with only the GS linker inserted (Figure 14b, c). Consistent with the antibiotic resistance phenotypes, tripartite fusions with full length Rnq1 and particularly those with Rnq1C collected into insoluble aggregates (Figure 12c). The Rnq1 fusions appeared to form proteolytically stable aggregates (Figure 14e, f) with amyloid-like structures (Figure 12 a, c), which is in keeping with the aggregation characteristic observed for Rnq1 reporter fusions in previous studies.[88,178] Contrary to the observed antibiotic resistance phenotypes, Rnq1C fusions were observed to a lesser extent in cellular foci than full length Rnq1 fusions (Figure 14d). From these data, we conclude that the antibiotic sensitivity observed for cells expressing the Rnq1 tripartite fusions is likely due to aggregation of the Rnq1 biosensors into prion-like aggregates.

Endogenous [*PSI+*] or [*PIN+*] structures, which could conceivably affect the aggregation propensity of the prion tripartite fusions,[88,91,178,181,182] were not detected prior to tripartite induction (Figure 15a), nor did we find any indication of their existence when we compared the observed antibiotic resistance readouts of untreated and prion cured cells (Figure 15b–d).

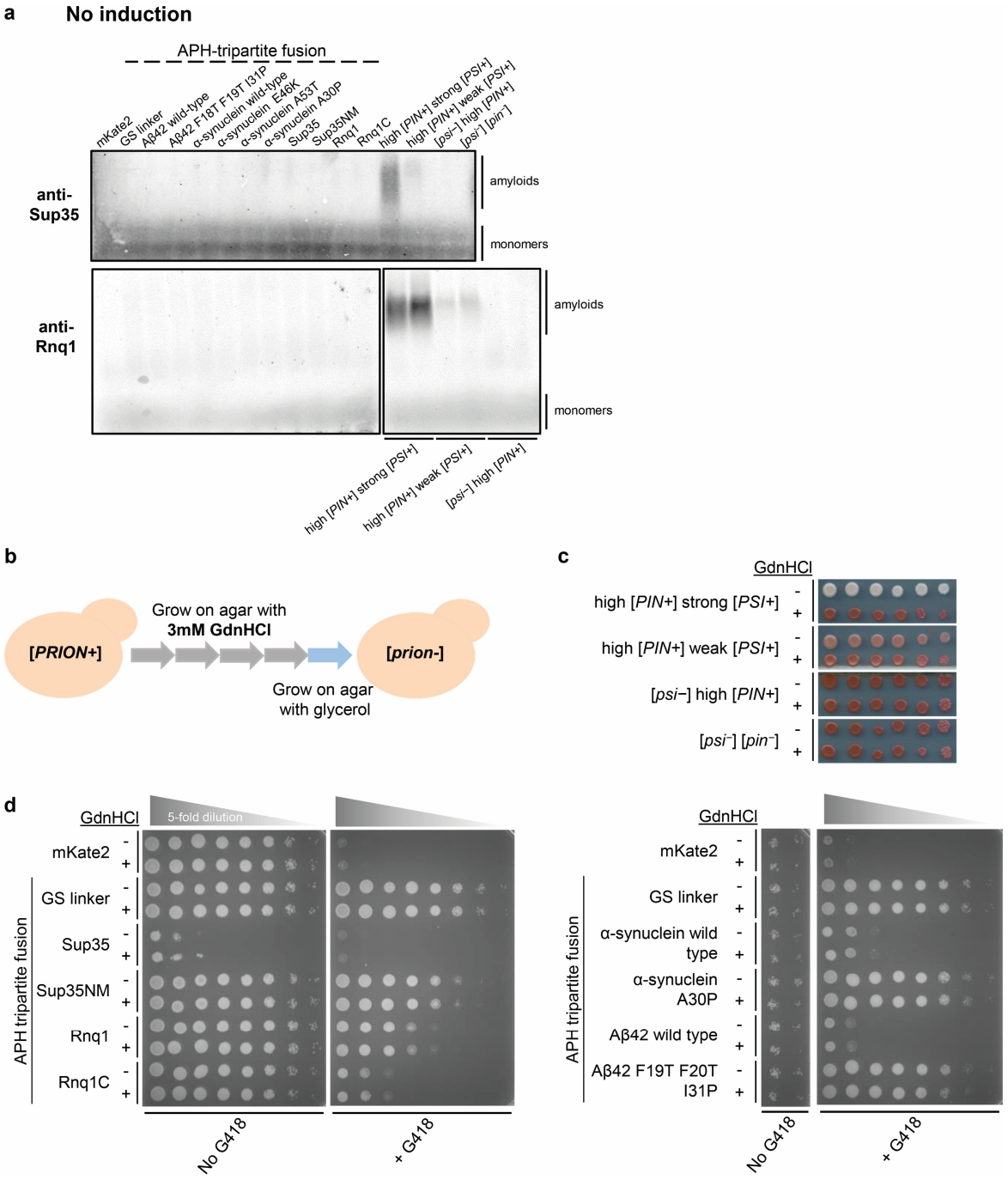

Figure 15. Preexisting prion structures were not indicated in yeast cells expressing the tripartite fusions. a) Uninduced cells encoding tripartite fusions were tested for the presence of [*PSI+*] and [*PIN+*] prions. Cells were grown at 30 °C in SC media supplemented with 2% glucose to repress expression of the tripartite fusion to mid-log phase, 2% glucose was added, and cells were incubated for 8 h. After cell harvest, lysates were prepared and the presence of amyloid-like species tested by SDD-AGE followed by immunoblotting. To probe for the presence of [*PSI+*] or [*PIN+*] polymers, immunoblots were probed with an anti-Sup35 or anti-Rnq1 antibody, respectively. Analyzed strains

encode either a fluorescent protein (mKate2) as a negative control or APH fusions with either a GS linker (VES657) or additional insertion of WT Aβ42 (VES702), Aβ42 F19T F20T I31P (VES700), WT α-synuclein (VES683), α-synuclein E46K (VES687), α-synuclein A53T (VES685), α-synuclein A30P (VES706), full length Sup35 (yHH86), Sup35NM (yHH88), full length Rnq1 (yHH90), or Rnq1C (yHH93). Yeast cells with known Sup35 and Rnq1 prion status served as controls for amyloid detection: high [*PIN*+] strong [*PSI*+] (L1762), high [*PIN*+] weak [*PSI*+] (L1758), [*psi*–] high [*PIN*+] (L1749), and [*psi*-] [*pin*-] (L2910)[113–116] Please note that although strains L1762, L1758, and L1749 are reported[113–115] as high [*PIN*+] strong [*PSI*+], high [*PIN*+] weak [*PSI*+], or high [*PIN*+] [*psi*-], respectively, for unknown reasons, we could only distinctly detect the presence of [*PIN*+] or [*PSI*+] in L1762. b) Schematic description of the prion curing procedure. To cure yeast cells from prion structures (indicated as [*PRION*+]), they are passaged 4 times on YPD agar media supplemented with 3 mM guanidine hydrochloride (GdnHCl) and grown at 30 °C. To exclude cells that have obtained mitochondrial mutations caused by the GdnHCl treatment and are therefore respiration deficient, cells were finally streaked on agar media supplemented with the non-fermentable carbon source glycerol. Cells that are able to grow on glycerol agar are considered prion cured (indicated as [*prion*-]). c) To control for efficient prion curing, strains with a defined prion status (from top to bottom: high [*PIN*+] strong [*PSI*+] (L1762), high [*PIN*+] weak [*PSI*+] (L1758), [*psi*–] high [*PIN*+] (L1749), and [*psi*-] [*pin*-] (L2910))[113–116] were treated with GdnHCl in parallel with the tripartite sensor strains. The genetic *ade1-14* modification present in the control strains allows one to infer the cells' Sup35 prion status based on cell color (white color indicates [*PSI*+] prions, whereas red color indicates soluble Sup35, [*psi*-]). Treatment of cells with 3 mM GdnHCl is indicated by a "+" or no treatment by a "–", respectively, in the GdnHCl column. d) Comparison of the antibiotic resistance readout of untreated cells expressing tripartite fusions (indicated by a "–" in the GdnHCl column) and corresponding strains that had been prion cured with GdnHCl (indicated by a "+" in the GdnHCl column) as described in (b) in spot titer assays. Strains expressing just the protein mKate2 (VES650) or the APH fusions with either just a GS linker inserted (VES657) or additional insertion of full length Sup35 (yHH86), Sup35NM (yHH88), full length Rnq1 (yHH90), Rnq1C (yHH93), WT α-synuclein (VES683), α-synuclein A30P (VES706), WT Aβ42 (VES702), or Aβ42 F19T F20T I31P (VES700) were grown to mid-log phase at 30 °C in SC medium supplemented with 2% raffinose and 0.1% glucose, normalized to an OD of 5, and spotted in 5-fold serial cell dilutions on SC agar supplemented with 2% raffinose, 2% galactose to induce tripartite expressions and without (indicated by "No G418") or with a range of G418 concentrations. Representative strains expressing tripartite fusions with prion proteins are spotted on agar supplemented with 0.15 mg mL^{-1} G418 (indicated by "+ G418" in left panel) and representative tripartite fusions with neuropathologic proteins are spotted on agar supplemented with 0.1 mg mL^{-1} (indicated by "+ G418" in right panel). The figure is adapted with permission from Sachsenhauser, V., Deng, X., Kim, H.-H., Jankovic, M., C.A. Bardwell, J., and Bardwell, J. C. A. (2020) Yeast tripartite biosensors sensitive to protein stability and aggregation propensity. ACS Chem. Biol. *XXXX*, XXX, XXX–XXX, https://doi.org/10.1021/acschembio.0c0008. Copyright 2020 American Chemical Society.[97]

Cells expressing fusions with full length Sup35 and the Sup35NM domain conferred decreased antibiotic resistance levels relative to strains expressing the GS linker-only control (Figure 14b, c). Antibiotic resistance conferred by the full length Sup35 fusions was lower than that conferred by the Sup35NM fusions. Although the full length Sup35 tripartite protein levels seemed lower than those of the Sup35NM fusions in western blotting (Figure 14e), their respective mRNA expression levels were comparable (Figure 9). Additionally, both tripartite fusion variants appeared equally proteolytically stable (Figure 14e, f). Consistent with the antibiotic resistance phenotypes, the full length Sup35 tripartite fusions formed a higher proportion of insoluble aggregates in the cell (Figure 12c) and were more prevalent in cellular foci (Figure 14d) than the Sup35NM tripartite fusions. In contrast to the Sup35 full length fusions, aggregates formed by Sup35NM fusions showed amyloid-like structures (Figure 12b). As with the Rnq1 tripartite expression strains, we found no evidence of preexisting [*PSI*+] or [*PIN*+] prions in our strains that might affect the aggregation propensity of the tripartite fusions with prion proteins (Figure 15).

Based on the results from our *in vitro* characterization, we think that differences in the antibiotic resistance phenotypes of the Sup35 variant fusions are probably due to the differential aggregation propensities of the Sup35 variants. However, we cannot make this conclusion with a high degree of certainty, since the antibiotic resistance readout of the full length Sup35 fusions was confounded by cytotoxicity. The cytotoxicity was observed in the absence of antibiotics but not when the tripartite fusion was uninduced, indicating that the transient overexpression of full length Sup35 in the fusion context produced the toxic effect (Figure 14b, c). Although such protein-dependent cytotoxicity negatively affects the antibiotic readout of the tripartite fusion system, such cytotoxic effects are readily detectable by the growth phenotypes of cells expressing the tripartite fusions in the absence of antibiotics.

Consistent with our observations, such Sup35-mediated cytotoxicity has previously been observed when the prion protein was overexpressed.[114,174,181,183] The resulting Sup35 aggregates had amyloid-like structures, and additional expression of Sup35's essential C-terminal domain could mitigate toxicity.[114,174,184] The observed cytotoxicity was attributed to the sequestration of

the endogenous Sup35 into aggregates, which obliterated its essential function.[114,174] Although no Sup35-positive amyloid-like aggregates were detectable in cells expressing the cytotoxic full length Sup35 tripartite fusions (Figure 12b, d), co-expression with Sup35's essential C-terminal domain was able to alleviate cytotoxicity. This result led us to conclude that the observed cytotoxicity of cells expressing the full length Sup35 fusion is likely due to the functional sequestration of the endogenous Sup35 (Figure 16).

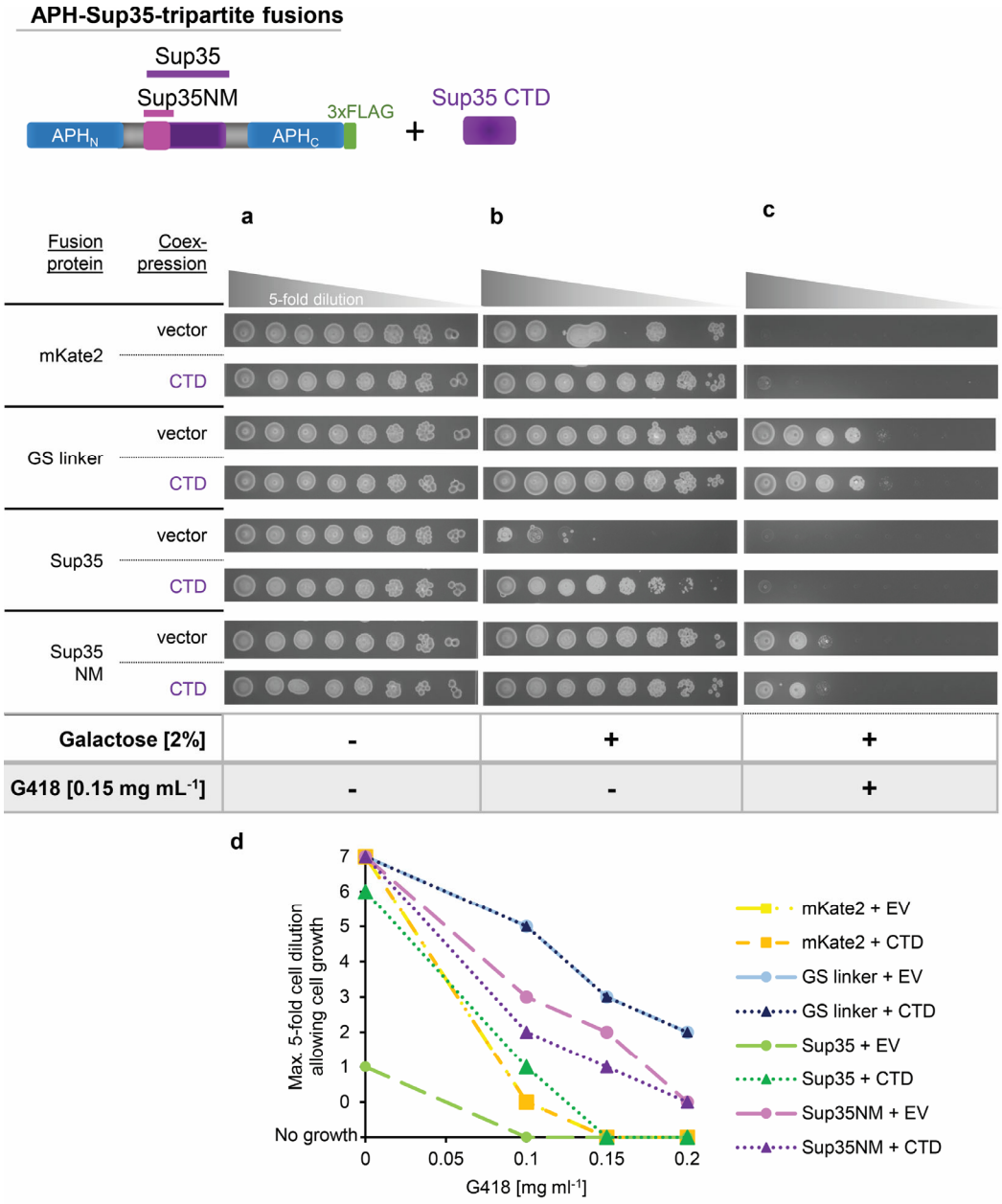

Figure 16. Co-expression of Sup35's essential C-terminal translation termination domain alleviates cytotoxicity of the full length Sup35 tripartite biosensor. Antibiotic resistance of cells co-expressing Sup35's C-terminal translation termination domain (abbreviated as CTD) or an empty vector control together with APH tripartite fusions containing a GS linker or additional insertion of full length Sup35 or Sup35NM was determined in spot titer assays. Mid-log phase yeast cells carrying an empty vector control plasmid or a plasmid encoding Sup35's CTD together with genome encoded APH tripartite fusions with full length Sup35 (VES1035, VES1037), Sup35NM (VES1039, VES1041), or just a GS linker (VES1031, VES1033), or yeast cells expressing just the non-G418 resistant red fluorescent protein control mKate2 (VES1027, VES1029) were spotted in 5-fold serial dilutions onto SC agar media supplemented with 2%

raffinose plus: (a) 2% glucose to control for accurate cell dilution (indicated by a "–" in the galactose row), or (b) 2% galactose to induce the expression of tripartite fusions and the Sup35 CTD (indicated by a "+" in the galactose row), or (c) 2% galactose and 0.15 mg mL^{-1} G418 (indicated by a "+" in the galactose row and in the G418 row). Of note, the strains expressing Sup35 tripartite fusions together with the CTD or empty vector had a different strain background than the ones described in Figure 15 to allow auxotrophy-mediated maintenance of the plasmid encoding the Sup35 CTD. d) Quantification of antibiotic resistance phenotypes of strains described in panels a–c over the range 0 to 0.2 mg mL^{-1} G418. The experiment was performed in duplicate, and error bars indicate ± 1 SD. The figure is reprinted with permission from Sachsenhauser, V., Deng, X., Kim, H.-H., Jankovic, M., C.A. Bardwell, J., and Bardwell, J. C. A. (2020) Yeast tripartite biosensors sensitive to protein stability and aggregation propensity. ACS Chem. Biol. *XXXX*, XXX, XXX–XXX, https://doi.org/10.1021/acschembio.0c0008. Copyright 2020 American Chemical Society.[97]

Overall, our results indicate that the tripartite system provides an aggregation-dependent antibiotic resistance readout and may thus be a valuable approach to conveniently study the aggregation behavior of disease-associated proteins *in vivo*.

5 Conclusions

Changes in protein stability or solubility play a key role in the regulation of many fundamental cellular processes, such as cell signaling and transcription. Conversely, aberrant protein folding and aggregation is a hallmark of many age-related diseases, especially neurodegenerative diseases such as Alzheimer's or Parkinson's disease.[7] Despite the prevalence of these protein misfolding diseases, the underlying principles and factors involved in their pathologies are not yet well understood. *In vitro* studies on the stability of disease-associated proteins cannot fully recapitulate the complex, transiently changing cellular folding environment. Hence, simple, versatile tools that allow one to study protein stability *in vivo* would be of great utility.

Several methods enabling the assessment of the folding status of neuropathogenic proteins *in vivo* have been engineered in *S. cerevisiae* as this species shares significant homology with mammals and is highly amenable to high-throughput screens. Although these yeast models have allowed scientists to gain a better understanding of cellular misfolding events, the existing models have reporter-dependent limitations such as overexpression-induced cytotoxicity effects that are unrelated to the protein's biology, or they suffer from proteolytic artifacts. Hence, it is clear that thus far, no single biosensor can perfectly assess *in vivo* protein folding or solubility.

To provide a complementary biosensor that relies on a different sensor principle, we optimized an antibiotic resistance-based biosensor system in yeast that links protein stability and aggregation propensity to an easily detectable phenotype—antibiotic resistance. The goal of our work was to provide a versatile tool that is sensitive to the protein stability and aggregation propensity of neurodegenerative disease-relevant proteins in *S. cerevisiae*.

We showed a strong correlation between the antibiotic resistance conferred by different Im7 stability variants inserted in our tripartite fusions and the respective thermodynamic stabilities determined for these Im7 variants *in vitro* (Figure 6). The tripartite biosensor approach thus uniquely provides the ability to directly quantify protein stability not only in *E. coli* but also in yeast.[71,119]

In addition, we observed an increase in antibiotic resistance when co-expressing Im7 tripartite fusions with Im7's natural, high-affinity binding partner, colicin E7, but not when co-expressing it with a natural, moderate-affinity Im7 chaperone called Spy (Figure 7). From these data, we conclude that the yeast tripartite system can be used to detect changes in *in vivo* stability resulting from intermolecular interactions with strong binding partners.

Furthermore, fusing the tripartite biosensor with neuropathogenic proteins Aβ42 or α-synuclein allowed us to assess disease-related properties, such as proteolytic sensitivity and propensity to localize at membranes, based on the antibiotic resistance readout (Figure 12). We also applied the tripartite fusion approach to the prion proteins Sup35 and Rnq1 and were able to determine their *in vivo* tendency to aggregate using the antibiotic resistance readouts (Figure 14–16). The yeast tripartite system thus represents a very powerful tool for studying neurodegenerative disease-associated proteins and disease-associated aggregation phenomena in the eukaryotic environment.

To show how our yeast-optimized tripartite folding biosensor approach fits into a bigger picture, in the following sections, I discuss the advantages and limitations of the method compared to other reporter approaches. I also describe how the tripartite sensor could be applied in high-throughput screens in yeast and highlight its potential use as a general tool for investigating various stability and solubility-associated phenomena in yeast.

6 Protein folding sensor perspectives

6.1 Advantages and limitations of the yeast tripartite system for determining protein stability *in vivo*

Our yeast tripartite biosensor system represents a complementary approach to yeast models and biosensors currently used to assay protein stability and solubility. It offers several distinct advantages over these methods due to its simplicity, sensitivity, and selective power.

The functionality of our tripartite system is not strictly dependent on a genetic background, particular growth media, or additional reagents other than readily obtainable antibiotics. Unlike fluorescence-based approaches, the tripartite system does not need specialized lab equipment to detect the reporter readout. Instead, the reporter readout can simply be quantified by evaluating cell growth in the presence of antibiotics. Since the tripartite system is an *in vivo* tool, it does not introduce artifacts associated with cell lysis or reconstitution of components outside of a cellular context. The split resistance markers and test protein are expressed as one tripartite fusion protein. This is an advantage over bimolecular fluorescence complementation (BiFC) approaches in which separate fusions for each marker half must be expressed in the same ratio to work effectively.[92] In addition, the tripartite design should avoid the generation of proteolytic artifacts that are frequently observed with bipartite reporter fusions.[21,22,85]

The readout of the cytosolic tripartite fusions relies on the addition of aminoglycoside antibiotics, which have been shown to induce increased protein aggregation, oxidative damage, and upregulation of the unfolded protein response in *E. coli*.[124–126] Potential aminoglycoside-induced side effects are minimized in our system since the vast majority of our *in vitro* tripartite characterizations were performed in the absence of aminoglycoside. Further experiments are needed to determine if there are effects dependent on the G418 concentration used in our experiments and on the possible effects of the split marker fusion. In order to minimize aminoglycoside-induced side effects, we optimized the APH tripartite sensor so it provides a sensitive readout at relatively low G418 concentrations compared to the standard G418

concentrations used for selection in yeast. Hence, we think that potential aminoglycoside-induced effects are likely to be minor when using our biosensors.

Like other fusion-based approaches, the tripartite fusion partner could affect the solubility of the fused protein.[21,22,136] Similarly, these methods share the requirement for validation of the biosensor readout, which entails follow-up *in vitro* characterization of the conferred phenotype for the tripartite fusions. Both of the antibiotic resistance markers used in our split biosensor designs function in the cytosol. As is the case for several other reporter systems, this cytosolic functionality might limit the compatibility of the tripartite system to proteins of interest that can be expressed in this compartment.[86–88,92]

Tripartite expression was designed to be tunable in order to make the biosensor more amenable to investigating misfolded proteins that exhibit a dose-dependent fitness effect or aggregation susceptibility. Indeed, no cytotoxicity was observed for tripartite fusions with neurodegenerative disease-associated proteins. Furthermore, the deliberately moderate expression level of the tripartite system may make our results more physiologically relevant compared to yeast models that rely on an overexpression-induced toxicity readout.[77,81,82,149,185]

Lastly, the APH and NAT marker genes function in cells of other species, which for NAT includes more than 100 different species.[121] This could make the orthogonal components of the tripartite fusion approach widely transferrable to other organisms.

6.2 The yeast tripartite fusion as a genetic tool for high-throughput screens or selections to identify modifiers of protein stability or aggregation susceptibility

Our biosensor features a tripartite design that directly couples protein folding or solubility to a distinct phenotypic readout—antibiotic resistance. This is a key advantage, as it makes it possible to conduct genome-wide high-throughput screens or even selections for genetic perturbations that affect protein stability or protein aggregation phenomena. The powerful genetics of yeast provides the possibility of screening a plethora of different genetic variants.[13]

Yeast allows the facile combination of the biosensor with systematic gene deletion or overexpression libraries through mating-based synthetic genetic array (SGA) technology.[186] Using transformation techniques, it should be easy to generate plasmid-based gene overexpression libraries, CRISPR/Cas9-based gene (in)activation libraries, or yeast transposon libraries together with the biosensor.[187–189] Hence, comprehensive and diverse genome-wide screens with the yeast biosensor should be possible.[187,190] Similarly, exogenous factors, such as chemical compound libraries, could be systematically screened in high throughput for their impact on protein stability or solubility in yeast. One can also imagine that full genome ORF libraries could be screened for changes in antibiotic resistance conferred by variants of the tripartite sensor system. ORF-dependent changes in sensor aggregation or solubility could allow us to decipher and map out entire implicated biological pathways and aggregation networks. This research could yield a comprehensive insight into the cellular protein quality control machinery.[88]

To generate a more sensitive readout for the stability or aggregation susceptibility of tripartite fused test proteins in such screens, one could optimize the cellular folding environment. Many yeast genes are functionally redundant, and the protein quality control machinery efficiently copes with folding stresses.[128,191,192] Hence, deletion of major endogenous chaperones could make the cellular folding environment more sensitive to changes. These strategies may improve the dynamic range of the sensor readout and possibly allow us to capture weaker stability- or solubility-modifying effects.

The β-lactamase-based tripartite biosensor system was successfully applied in the *E. coli* periplasm in a directed evolution approach to optimize and study the stability of Im7 and to select for Spy variants with improved chaperone function for Im7.[71,145] Thus, the yeast-optimized tripartite system could serve to address similar research questions in the eukaryotic environment. Applications of this type could greatly benefit the biotechnology industry. The biosensor could be applied in high-throughput screens or selections to evolve the folding environment, stability, or expression level of recombinant proteins of biomedical or biotechnological importance. Such optimization steps are often critical during the upstream bioprocessing of valuable bioproducts to ensure their high quality and efficient production.[193]

In summary, the quantifiable antibiotic resistance readout of the tripartite biosensor in the powerful yeast model system may allow its broad application in high-throughput screens or selections to identify modifiers of protein stability or aggregation propensity.

6.3 The yeast tripartite system as a general tool to study protein stability and aggregation susceptibility

As demonstrated in this work, the tripartite system enabled the study of the stability/solubility of a variety of test proteins. It allowed us to determine the relative stabilities of Im7 variants (Figure 6), the proteolytic susceptibility of Aβ variants (Figure 10), the propensity to localize at the membrane of α-synuclein variants (Figure 12), and the aggregation propensities of yeast prions Sup35 and Rnq1 (Figure 14) *in vivo*, based on their antibiotic resistance readout.

The versatile compatibility of our biosensor with different test proteins underscores the advantage of the standardized, tripartite design, which avoids the need to construct new assays for each protein of interest. The yeast biosensor doesn't seem to require prior knowledge of the stability or aggregation propensities of the test protein inserted, which has already been recognized as a key feature of the tripartite system in *E. coli*.[71,119] Depending on selection marker compatibilities, this genetic tool could be customized with independent genetic or enzyme-based reporters. Even the combination of two different tripartite biosensors in one cell may be possible, since the established tripartite designs are based on different antibiotic resistance markers. Such biosensor combinations could provide a rigorous readout for protein stability or solubility and would be highly desirable for screens and selections.

The readout for the stability and solubility of disease-associated test proteins inserted in the tripartite fusions suggests that the system can be extended to study other misfolding disease-associated proteins. It would be interesting to explore whether yeast-optimized tripartite fusions could serve to study neurodegenerative disease-associated RNA binding proteins that contain prion-like domain structures and may undergo liquid-liquid phase separation, such as proteins FUS (fused in sarcoma) or TDP43.[194] Mutations in either of these genes have been linked to amyotrophic lateral sclerosis (ALS) in which these proteins can form cytoplasmic inclusions.[195]

Yeast models for FUS aggregation involve massive overexpression of mutant FUS to induce a cytotoxicity readout.[196] Genome-wide screens for suppressors or enhancers of FUS toxicity have identified factors that seem to indirectly compensate or restore FUS-associated toxicity.[196–198] Our yeast tripartite system could be used to address remaining challenges, such as the identification of proteins that directly affect FUS aggregation, or to study genetic susceptibility and environmental triggers of the disease.[197]

The identification of solubility-modulating mutations in the amino acid sequence of prion proteins and pathologically misfolded proteins has been crucial to our understanding of prion domains and amyloidogenic sequence compositions.[87,104,199,200] Tripartite biosensors may advance this work further by helping us study the effect of point mutations or truncations in pathologically misfolded and aggregated proteins.

It has been suggested that new prion proteins evolve via duplication of aggregation prone segments and selective propagation of prion variants.[201,202] The tripartite system could be applied in rational prion design studies or screening approaches to further explore possible mechanisms of prion evolution.

The tripartite system may also allow us to address a related question—namely, how prion formation in cells is associated with memory effects. Since prion proteins adopt a reproducibly self-perpetuating, heritable conformational change, prions can be considered to be molecular memory devices.[203] Meta-stable prion formation of yeast protein Lsb2 has been linked to heritable thermotolerance in yeast. Another fascinating example of prion-associated memory effects is provided by oligomers of the CPEB protein, which have been shown to polymerize in amyloid-like structures that are linked to long-term memory in humans.[203–205] If a tripartite biosensor fused with prion proteins is sensitive to preexisting prion structures, the system may allow us to investigate prion-mediated memory effects in response to environmental stress.

Clearly, there are a wide range of exciting research questions on the mechanistic and functional aspects associated with both pathologic and beneficial changes in protein stability and aggregation. The yeast-optimized tripartite system provides a flexible framework to explore these questions.

7 Acknowledgments

Writing of my thesis is just the last step of an ambitious and challenging but at the same time highly gratifying and enjoyable educational path. Along my way, I got support from many people who I would like to thank at this point.

First of all, I would like to thank Prof. Jim Bardwell, who gave me the opportunity to advance my scientific career, first during an internship and then as a PhD student in his laboratory. I would like to thank Jim for the exciting project he has offered me and for the trust he has placed in my work. I am very grateful for his advice and guidance and his support of my growth by sending me to excellent training opportunities such as the CSH yeast course.

I would like to thank Prof. Buchner for giving me the opportunity to do my doctorate with him at the TU Munich in collaboration with Jim, and for his continuous support.

I would like to thank Prof. Charlie Boone and his lab members for their valuable advice on yeast genetics and introduction to high-throughput screening approaches.

A big thank you also goes to Prof. Ursula Jakob for her advice on my project.

Special thanks are also going to my colleagues Xiexiong and Hyun-hee, who have contributed to my project, especially in relation to the *in vitro* characterization of tripartite biosensors and cloning. I would also like to thank Maja, Hannah, Franziska and Seb, whom I was able to supervise during my doctorate, for their work and great cooperation. Furthermore, I would like to thank all former and current members of the Bardwell and Jakob Laboratory for their scientific help, ideas and discussions and the non-scientific fun in the lab and at our get togethers.

I would also like to take this opportunity to thank all the friends from Ann Arbor for the great time we spent together and for the fun trips we took. A big thank you also goes to my friends in Germany, Switzerland and Austria, who have always supported me and stayed in touch despite the thousands of kilometers between us.

I would also like to thank a very special person, Scott Scholz, who has enriched my life in a unique way over the past few years. He has always been enthusiastic, understanding and

supportive of my work and decisions. I am grateful for our shared passion for the life sciences, which connects us on a very special level. Many thanks also to the Scholz family for their support.

Zu guter Letzt möchte ich meinen Eltern Irene und Helmut und meinen Brüdern Julian und Michael von ganzem Herzen danken, dass sie mich während des gesamten Studiums stets unterstützt, motiviert und immer ein offenes Ohr für mich gehabt haben. Meinen Eltern bin ich unendlich dankbar, dass sie es mir ermöglicht haben, meine Interessen zu verfolgen.

8 Bibliography

(1) Taverna, D. M., and Goldstein, R. A. (2002) Why are proteins marginally stable? *Proteins Struct. Funct. Genet. 46*, 105–109.

(2) Chakrabortee, S., Byers, J. S., Jones, S., Garcia, D. M., Bhullar, B., Chang, A., She, R., Lee, L., Fremin, B., Lindquist, S., and Jarosz, D. F. (2016) Intrinsically Disordered Proteins Drive Emergence and Inheritance of Biological Traits. *Cell 167*, 369-381.e12.

(3) Tokuriki, N., and Tawfik, D. S. (2009) Chaperonin overexpression promotes genetic variation and enzyme evolution. *Nature 459*, 668–673.

(4) Ulrich Hartl, F. (2017) Protein misfolding diseases. *Annu. Rev. Biochem. 86*, 21–26.

(5) Klaips, C. L., Jayaraj, G. G., and Hartl, F. U. (2018) Pathways of cellular proteostasis in aging and disease. *J. Cell Biol. 217*, 51–63.

(6) Balchin, D., Hayer-Hartl, M., and Hartl, F. U. (2016) In vivo aspects of protein folding and quality control. *Science. 353*, aac4354.

(7) Hipp, M. S., Kasturi, P., and Hartl, F. U. (2019) The proteostasis network and its decline in ageing. *Nat. Rev. Mol. Cell Biol. 20*, 421–435.

(8) Sweeney, P., Park, H., Baumann, M., Dunlop, J., Frydman, J., Kopito, R., McCampbell, A., Leblanc, G., Venkateswaran, A., Nurmi, A., and Hodgson, R. (2017) Protein misfolding in neurodegenerative diseases: implications and strategies. *Transl. Neurodegener. 6*, 6.

(9) Chiti, F., and Dobson, C. M. (2017) Protein Misfolding, Amyloid Formation, and Human Disease: A Summary of Progress Over the Last Decade. *Annu. Rev. Biochem. 86*, 27–68.

(10) Hingorani, K. S., and Gierasch, L. M. (2014) Comparing protein folding in vitro and in vivo: foldability meets the fitness challenge. *Curr. Opin. Struct. Biol. 24*, 81–90.

(11) Gershenson, A., and Gierasch, L. M. (2011) Protein folding in the cell: Challenges and progress. *Curr. Opin. Struct. Biol. 21*, 32–41.

(12) Botstein, D. (1997) GENETICS: Yeast as a Model Organism. *Science. 277*, 1259–1260.

(13) Khurana, V., and Lindquist, S. (2010) Modelling neurodegeneration in Saccharomyces cerevisiae: Why cook with baker's yeast? *Nat. Rev. Neurosci. 11*, 436–449.

(14) Pereira, C., Bessa, C., Soares, J., Leão, M., and Saraiva, L. (2012) Contribution of Yeast Models to Neurodegeneration Research. *J. Biomed. Biotechnol. 2012*, 1–12.

(15) Tenreiro, S., Munder, M. C., Alberti, S., and Outeiro, T. F. (2013) Harnessing the power of yeast to unravel the molecular basis of neurodegeneration. *J. Neurochem. 127*, 438–452.

(16) Oliveira, A. V., Vilaça, R., Santos, C. N., Costa, V., and Menezes, R. (2017) Exploring the power of yeast to model aging and age-related neurodegenerative disorders. *Biogerontology 18*, 3–34.

(17) Winderickx, J., Delay, C., De Vos, A., Klinger, H., Pellens, K., Vanhelmont, T., Van Leuven, F., and Zabrocki, P. (2008) Protein folding diseases and neurodegeneration: Lessons learned from yeast. *Biochim. Biophys. Acta - Mol. Cell Res. 1783*, 1381–1395.

(18) Rencus-Lazar, S., DeRowe, Y., Adsi, H., Gazit, E., and Laor, D. (2019, March 22) Yeast models for the study of amyloid-associated disorders and development of future therapy. *Front. Mol. Biosci.* Frontiers Media S.A.

(19) França, M. B., Lima, K. C., and Eleutherio, E. C. A. (2017) Oxidative stress and amyloid toxicity: insights from yeast. *J. Cell. Biochem. 118*, 1442–1452.

(20) Braun, R. J. (2012) Mitochondrion-mediated cell death: dissecting yeast apoptosis for a better understanding of neurodegeneration. *Front. Oncol. 2*, 1–14.

(21) Cabantous, S., Terwilliger, T. C., and Waldo, G. S. (2005) Protein tagging and detection with engineered self-assembling fragments of green fluorescent protein. *Nat. Biotechnol. 23*, 102–107.

(22) Alberti, S., Halfmann, R., and Lindquist, S. (2010) Biochemical, Cell Biological, and Genetic Assays to Analyze Amyloid and Prion Aggregation in Yeast, in *Methods in Enzymology* 2nd ed., pp 709–734. Elsevier Inc.

(23) Schneider, K. L., Nyström, T., and Widlund, P. O. (2018) Studying spatial protein quality control, proteopathies, and aging using different model misfolding proteins in S. cerevisiae. *Front. Mol. Neurosci. 11*, 1–13.

(24) Alberts, B., Bray, D., Johnson, A., Lewis, J., Raff, M., Roberts, K., and Walter, P. (2013) Essential Cell Biolog. *Essent. Cell Biol.* Garland Science.

(25) Zhang, G., and Ignatova, Z. (2011) Folding at the birth of the nascent chain: coordinating translation with co-translational folding. *Curr. Opin. Struct. Biol. 21*, 25–31.

(26) Anfinsen, C. B. (1972) The formation and stabilization of protein structure. *Biochem. J. 128*, 737–749.

(27) Vecchi, G., Sormanni, P., Mannini, B., Vandelli, A., Tartaglia, G. G., Dobson, C. M., Hartl, F. U., and Vendruscolo, M. (2020) Proteome-wide observation of the phenomenon of life on the edge of solubility. *Proc. Natl. Acad. Sci. 117*, 1015–1020.

(28) Shrivastava, S. (2017) Protein Folding, in *Introduction to Biomolecular Structure and Biophysics*, pp 33–56. Springer Singapore, Singapore.

(29) Beckerman, M. (2015) Fundamentals of Neurodegeneration and Protein Misfolding Disorders. Springer International Publishing, Cham.

(30) Rothman, J. E., and Schekman, R. (2011) Molecular mechanism of protein folding in the cell. *Cell 146*, 851–854.

(31) Kubelka, J., Hofrichter, J., and Eaton, W. A. (2004) The protein folding 'speed limit.' *Curr. Opin. Struct. Biol. 14*, 76–88.

(32) Tycko, R. (2015) Amyloid Polymorphism: Structural Basis and Neurobiological Relevance *86*, 632–645.

(33) Chakravarty, A. K., and Jarosz, D. F. (2018) More than Just a Phase: Prions at the Crossroads of Epigenetic Inheritance and Evolutionary Change. *J. Mol. Biol. 430*, 4607–4618.

(34) Abeliovich, A., and Gitler, A. D. (2016) Defects in trafficking bridge Parkinson's disease pathology and genetics. *Nature 539*, 207–216.

(35) Chen, S. W., Drakulic, S., Deas, E., Ouberai, M., Aprile, F. A., Arranz, R., Ness, S., Roodveldt, C., Guilliams, T., De-Genst, E. J., Klenerman, D., Wood, N. W., Knowles, T. P. J., Alfonso, C., Rivas, G., Abramov, A. Y., Valpuesta, J. M., Dobson, C. M., and Cremades, N. (2015) Structural characterization of toxic oligomers that are kinetically trapped during α-synuclein fibril formation. *Proc. Natl. Acad. Sci. 112*, E1994–E2003.

(36) Cremades, N., Cohen, S. I. A., Deas, E., Abramov, A. Y., Chen, A. Y., Orte, A., Sandal, M., Clarke, R. W., Dunne, P., Aprile, F. A., Bertoncini, C. W., Wood, N. W., Knowles, T. P. J., Dobson, C. M., and Klenerman, D. (2012) Direct Observation of the Interconversion of Normal and Toxic Forms of α-Synuclein. *Cell 149*, 1048–1059.

(37) Shin, Y., and Brangwynne, C. P. (2017) Liquid phase condensation in cell physiology and disease. *Science. 357*, eaaf4382.

(38) Banani, S. F., Lee, H. O., Hyman, A. A., and Rosen, M. K. (2017) Biomolecular condensates: Organizers of cellular biochemistry. *Nat. Rev. Mol. Cell Biol. 18*, 285–298.

(39) Elbaum-Garfinkle, S. (2019) Matter over mind: Liquid phase separation and neurodegeneration. *J. Biol. Chem. 294*, 7160–7168.

(40) Polymeropoulos, M. H., Lavedan, C., Leroy, E., Ide, S. E., Dehejia, A., Dutra, A., Pike, B., Root, H., Rubenstein, J., Boyer, R., Stenroos, E. S., Chandrasekharappa, S., Athanassiadou, A., Papapetropoulos, T., Johnson, W. G., Lazzarini, A. M., Duvoisin, R. C., Di Iorio, G., Golbe, L. I., and Nussbaum, R. L. (1997) Mutation in the α-synuclein gene identified in families with Parkinson's disease. *Science. 276*, 2045–2047.

(41) Krüger, R., Kuhn, W., Müller, T., Woitalla, D., Graeber, M., Kösel, S., Przuntek, H., Epplen, J. T., Schöls, L., and Riess, O. (1998) Ala30Pro mutation in the gene encoding α-synuclein in Parkinson's disease. *Nat. Genet. 18*, 106–108.

(42) Selkoe, D. J. (2004) Cell biology of protein misfolding: The examples of Alzheimer's and Parkinson's diseases. *Nat. Cell Biol. 6*, 1054–1061.

(43) Kim, Y. E., Hipp, M. S., Bracher, A., Hayer-Hartl, M., and Ulrich Hartl, F. (2013) Molecular Chaperone Functions in Protein Folding and Proteostasis. *Annu. Rev. Biochem. 82*, 323–355.

(44) van Leeuwen, F. W., and Kampinga, H. H. (2018) Heat shock proteins and protein quality control in Alzheimer's disease, in *The Molecular and Cellular Basis of Neurodegenerative Diseases* (M. S. Wolfe, Ed.), pp 269–298. Elsevier.

(45) Ciechanover, A., and Kwon, Y. T. (2017) Protein Quality Control by Molecular Chaperones in Neurodegeneration. *Front. Neurosci. 11*.

(46) Balchin, D., Hayer-Hartl, M., and Hartl, F. U. (2016) In vivo aspects of protein folding and quality control. *Science. 353*, aac4354.

(47) Geiler-Samerotte, K. A., Dion, M. F., Budnik, B. A., Wang, S. M., and Hartl, D. L. (2010) Misfolded proteins impose a dosage-dependent fitness cost and trigger a cytosolic unfloded protein response in yeast. *Proc. Natl. Acad. Sci. U. S. A. 108*, 680–685.

(48) Verghese, J., Abrams, J., Wang, Y., and Morano, K. A. (2012) Biology of the Heat Shock Response and Protein Chaperones: Budding Yeast (Saccharomyces cerevisiae) as a Model System. *Microbiol. Mol. Biol. Rev. 76*, 115–158.

(49) Sontag, E. M., Samant, R. S., and Frydman, J. (2017) Mechanisms and Functions of Spatial Protein Quality Control. *Nat. Rev. Mol. Cell Biol. 86*, 97–122.

(50) Kaganovich, D., Kopito, R., and Frydman, J. (2008) Misfolded proteins partition between two distinct quality control compartments. *Nature 454*, 1088–1095.

(51) Samant, R. S., Livingston, C. M., Sontag, E. M., and Frydman, J. (2018) Distinct proteostasis circuits cooperate in nuclear and cytoplasmic protein quality control. *Nature 563*, 407–411.

(52) Nollen, E. A. A., Brunsting, J. F., Roelofsen, H., Weber, L. A., and Kampinga, H. H. (1999) In Vivo Chaperone Activity of Heat Shock Protein 70 and Thermotolerance. *Mol. Cell. Biol. 19*, 2069–2079.

(53) Joazeiro, C. A. P. (2019) Mechanisms and functions of ribosome-associated protein quality control. *Nat. Rev. Mol. Cell Biol. 20*, 368–383.

(54) Kundra, R., Ciryam, P., Morimoto, R. I., Dobson, C. M., and Vendruscolo, M. (2017) Protein homeostasis of a metastable subproteome associated with Alzheimer's disease. *Proc. Natl. Acad. Sci. 114*, E5703–E5711.

(55) David, D. C., Layfield, R., Serpell, L., Narain, Y., Goedert, M., and Spillantini, M. G. (2002) Proteasomal degradation of tau protein. *J. Neurochem. 83*, 176–185.

(56) Lopez Salon, M., Pasquini, L., Besio Moreno, M., Pasquini, J. ., and Soto, E. (2003) Relationship between β-amyloid degradation and the 26S proteasome in neural cells. *Exp. Neurol. 180*, 131–143.

(57) Manavalan, A., Mishra, M., Feng, L., Sze, S. K., Akatsu, H., and Heese, K. (2013) Brain site-specific proteome changes in aging-related dementia. *Exp. Mol. Med. 45*, 1–17.

(58) Boland, B., Yu, W. H., Corti, O., Mollereau, B., Henriques, A., Bezard, E., Pastores, G. M., Rubinsztein, D. C., Nixon, R. A., Duchen, M. R., Mallucci, G. R., Kroemer, G., Levine, B., Eskelinen, E. L., Mochel, F., Spedding, M., Louis,

C., Martin, O. R., and Millan, M. J. (2018) Promoting the clearance of neurotoxic proteins in neurodegenerative disorders of ageing. *Nat. Rev. Drug Discov. 17*, 660–688.

(59) Finka, A., and Goloubinoff, P. (2013) Proteomic data from human cell cultures refine mechanisms of chaperone-mediated protein homeostasis. *Cell Stress Chaperones 18*, 591–605.

(60) Lindberg, I., Shorter, J., Wiseman, R. L., Chiti, F., Dickey, C. A., and McLean, P. J. (2015) Chaperones in neurodegeneration. *J. Neurosci. 35*, 13853–13859.

(61) Kurtishi, A., Rosen, B., Patil, K. S., Alves, G. W., and Møller, S. G. (2019) Cellular Proteostasis in Neurodegeneration. *Mol. Neurobiol. 56*, 3676–3689.

(62) Saibil, H. (2013) Chaperone machines for protein folding, unfolding and disaggregation. *Nat. Rev. Mol. Cell Biol. 14*, 630–642.

(63) Rizzolo, K., Huen, J., Kumar, A., Phanse, S., Vlasblom, J., Kakihara, Y., Zeineddine, H. A., Minic, Z., Snider, J., Wang, W., Pons, C., Seraphim, T. V., Boczek, E. E., Alberti, S., Costanzo, M., Myers, C. L., Stagljar, I., Boone, C., Babu, M., and Houry, W. A. (2017) Features of the Chaperone Cellular Network Revealed through Systematic Interaction Mapping. *Cell Rep. 20*, 2735–2748.

(64) Wentink, A., Nussbaum-Krammer, C., and Bukau, B. (2019) Modulation of Amyloid States by Molecular Chaperones. *Cold Spring Harb. Perspect. Biol. 11*, a033969.

(65) Tanaka, K., and Matsuda, N. (2014) Proteostasis and neurodegeneration: The roles of proteasomal degradation and autophagy. *Biochim. Biophys. Acta - Mol. Cell Res. 1843*, 197–204.

(66) Fleming, A., Vicinanza, M., Renna, M., Puri, C., Ricketts, T., Füllgrabe, J., Lopez, A., de Jager, S. M., Ashkenazi, A., Pavel, M., Licitra, F., Caricasole, A., Andrews, S. P., Skidmore, J., and Rubinsztein, D. C. (2018) Neurodegenerative Diseases and Autophagy, in *The Molecular and Cellular Basis of Neurodegenerative Diseases*, pp 299–343. Elsevier.

(67) Vidal, R. L., Matus, S., Bargsted, L., and Hetz, C. (2014) Targeting autophagy in neurodegenerative diseases. *Trends Pharmacol. Sci. 35*, 583–591.

(68) Paul, S., and Mahanta, S. (2014) Association of heat-shock proteins in various neurodegenerative disorders: Is it a master key to open the therapeutic door? *Mol. Cell. Biochem. 386*, 45–61.

(69) Gomes, C. M. (2019) Protein Misfolding Diseases. Methods and Protocols. *Methods Mol. Biol.*

(70) Meier, B. H., Riek, R., and Böckmann, A. (2017) Emerging Structural Understanding of Amyloid Fibrils by Solid-State NMR. *Trends Biochem. Sci. 42*, 777–787.

(71) Foit, L., Morgan, G. J., Kern, M. J., Steimer, L. R., von Hacht, A. A., Titchmarsh, J., Warriner, S. L., Radford, S. E., and Bardwell, J. C. A. (2009) Optimizing protein stability in vivo. *Mol. Cell 36*, 861–871.

(72) Fruhmann, G., Seynnaeve, D., Zheng, J., Ven, K., Molenberghs, S., Wilms, T., Liu, B., Winderickx, J., and Franssens, V. (2017) Yeast buddies helping to unravel the complexity of neurodegenerative disorders. *Mech. Ageing Dev. 161*, 288–305.

(73) Di Gregorio, S. E., and Duennwald, M. L. (2018) Yeast as a model to study protein misfolding in aged cells. *FEMS Yeast Res. 18*, 1–8.

(74) Tenreiro, S., and Outeiro, T. F. (2010) Simple is good: Yeast models of neurodegeneration. *FEMS Yeast Res. 10*, 970–979.

(75) Menezes, R., Tenreiro, S., Macedo, D., Santos, C. N., and Outeiro, T. F. (2015) From the baker to the bedside: Yeast models of parkinson's disease. *Microb. Cell 2*, 262–279.

(76) Willingham, S., Outeiro, T. F., DeVit, M. J., Lindquist, S. L., and Muchowski, P. J. (2003) Yeast Genes that Enhance the Toxicity of a Mutant Huntingtin Fragment or α-Synuclein. *Science. 302*, 1769–1772.

(77) Antony A. Cooper, Aaron D. Gitler, Anil Cashikar, Cole M. Haynes, Kathryn J. Hill, Bhupinder Bhullar,

Kangning Liu, Kexiang Xu, Katherine E. Strathearn, Fang Liu, Songsong Cao, Kim A. Caldwell, Guy A. Caldwell, Gerald Marsischky, R. D., and Kolodner, Joshua LaBaer, Jean-Christophe Rochet, N. M. B. and S. L. (2006) α-Synuclein Blocks ER-Golgi Traffic and Rab1 Rescues Neuron Loss in Parkinson's Models. *Science. 313*, 324–328.

(78) Klein, C., and Westenberger, A. (2012) Genetics of Parkinson ' S Disease. *Cold Spring Harb. Perspect. Med. 2*, a008888.

(79) Khurana, V., Chung, C. Y., and Tardiff, D. F. (2017) From Yeast to Patients: The Audacity and Vision of Susan Lindquist. *Cell Syst.*

(80) Treusch, S., Hamamichi, S., Goodman, J. L., Matlack, K. E. S. S., Chung, C. Y., Baru, V., Shulman, J. M., Parrado, A., Bevis, B. J., Valastyan, J. S., Han, H., Lindhagen-Persson, M., Reiman, E. M., Evans, D. A., Bennett, D. A., Olofsson, A., DeJager, P. L., Tanzi, R. E., Caldwell, K. A., Caldwell, G. A., and Lindquist, S. (2011) Functional links between Aβ toxicity, endocytic trafficking, and Alzheimer's disease risk factors in yeast. *Science. 334*, 1241–1245.

(81) Outeiro, T. F., and Lindquist, S. (2003) Yeast cells provide insight into alpha-synuclein biology and pathobiology. *Science. 302*, 1772–1775.

(82) Tyedmers, J., Madariaga, M. L., and Lindquist, S. (2008) Prion switching in response to environmental stress. *PLoS Biol. 6*, 2605–2613.

(83) D'Angelo, F., Vignaud, H., Di Martino, J., Salin, B., Devin, A., Cullin, C., and Marchal, C. (2013) A yeast model for amyloid-aggregation exemplifies the role of membrane trafficking and PICALM in cytotoxicity. *Dis. Model. Mech. 6*, 206–216.

(84) Sachsenhauser, V., and Bardwell, J. C. (2018) Directed evolution to improve protein folding in vivo. *Curr. Opin. Struct. Biol. 48*, 117–123.

(85) Nair, S., Traini, M., Dawes, I. W., and Perrone, G. G. (2014) Genome-wide analysis of Saccharomyces cerevisiae identifies cellular processes affecting intracellular aggregation of Alzheimer's amyloid-β42: Importance of lipid homeostasis. *Mol. Biol. Cell 25*, 2235–2249.

(86) Morell, M., de Groot, N. S., Vendrell, J., Avilés, F. X., and Ventura, S. (2011) Linking amyloid protein aggregation and yeast survival. *Mol. Biosyst. 7*, 1121–1128.

(87) Bagriantsev, S., and Liebman, S. (2006) Modulation of Aβ42 low-n oligomerization using a novel yeast reporter system. *BMC Biol. 4*, 1–12.

(88) Newby, G. A., Kiriakov, S., Hallacli, E., Kayatekin, C., Tsvetkov, P., Mancuso, C. P., Bonner, J. M., Hesse, W. R., Chakrabortee, S., Manogaran, A. L., Liebman, S. W., Lindquist, S., and Khalil, A. S. (2017) A genetic tool to track protein aggregates and control prion inheritance. *Cell 171*, 966-979.e18.

(89) Philipps, B., Hennecke, J., and Glockshuber, R. (2003) FRET-based in vivo screening for protein folding and increased protein stability. *J. Mol. Biol. 327*, 239–249.

(90) Ahmed, M., Koo, K. M., Mainwaring, P. N., Carrascosa, L. G., and Trau, M. (2019) Phosphoprotein Biosensors for Monitoring Pathological Protein Structural Changes. *Trends Biotechnol.* 1–12.

(91) Khan, T., Gama, A. R., Kandola, T. S., Wu, J., Venkatesan, S., Ketter, E., Lange, J. J., Rodríguez Gama, A., Box, A., Unruh, J. R., Cook, M., and Halfmann, R. (2018) Quantifying nucleation in vivo reveals the physical basis of prion-like phase behavior. *Mol. Cell 71*, 155-168.e7.

(92) Lázaro, D. F., Rodrigues, E. F., Langohr, R., Shahpasandzadeh, H., Ribeiro, T., Guerreiro, P., Gerhardt, E., Kröhnert, K., Klucken, J., Pereira, M. D., Popova, B., Kruse, N., Mollenhauer, B., Rizzoli, S. O., Braus, G. H., Danzer, K. M., and Outeiro, T. F. (2014) Systematic comparison of the effects of alpha-synuclein mutations on its oligomerization and aggregation. *PLoS Genet.* (Kaganovich, D., Ed.) *10*, e1004741.

(93) Swanson, R., Locher, M., and Hochstrasser, M. (2001) degradation signal. Doa10 functions with two E2s, Ubc6 and Ubc7, to ubiquitinate. *Genes Dev. 15*, 2660–2674.

(94) Capaldi, A. P., Kleanthous, C., and Radford, S. E. (2002) Im7 folding mechanism: Misfolding on a path to the native state. *Nat. Struct. Biol. 9*, 209–216.

(95) Spence, G. R., Capaldi, A. P., and Radford, S. E. (2004) Trapping the on-pathway folding intermediate of Im7 at equilibrium. *J. Mol. Biol. 341*, 215–226.

(96) Pashley, C. L., Morgan, G. J., Kalverda, A. P., Thompson, G. S., Kleanthous, C., and Radford, S. E. (2012) Conformational Properties of the Unfolded State of Im7 in Nondenaturing Conditions. *J. Mol. Biol. 416*, 300–318.

(97) Sachsenhauser, V., Deng, X., Kim, H.-H., Jankovic, M., C.A. Bardwell, J., and Bardwell, J. C. A. (2020) Yeast tripartite biosensors sensitive to protein stability and aggregation propensity. *ACS Chem. Biol. XXXX,* XXX, XXX–XXX, https://doi.org/10.1021/acschembio.0c0008.

(98) Green, M. R., and Sambrook, J. (2018) Caring for Escherichia coli. *Cold Spring Harb. Protoc. 2018*, pdb.prot101337.

(99) Sambrook, J., and Russell, D. W. (2006) The Inoue Method for Preparation and Transformation of Competent E. Coli : "Ultra-Competent" Cells. *Cold Spring Harb. Protoc.* (Sambrook, J., and Russell, D., Eds.) *2006*, pdb.prot3944.

(100) Dunham, M., Gartenberg, M., and Brown, G. (2015) Methods in Yeast Genetics and Genomics, 2015 Edition: A CSHL Course Manual. 2015th ed. Cold Spring Harbor Laboratory Press, Cold Spring Harbor.

(101) Sambrook, J., and Russel, D, W. (2000) Molecular Cloning, 3-Volume Set : A Laboratory Manual. *Cold Spring Harboc Lab. Press*.

(102) Park, S.-K. S. K., Pegan, S. D., Mesecar, A. D., Jungbauer, L. M., LaDu, M. J. J., and Liebman, S. W. (2011) Development and validation of a yeast high-throughput screen for inhibitors of A 42 oligomerization. *Dis. Model. Mech. 4*, 822–831.

(103) Marshall, K. E., Vadukul, D. M., Dahal, L., Theisen, A., Fowler, M. W., Al-Hilaly, Y., Ford, L., Kemenes, G., Day, I. J., Staras, K., and Serpell, L. C. (2016) A critical role for the self-assembly of Amyloid-beta1-42 in neurodegeneration. *Sci. Rep. 6*, 1–13.

(104) Bateman, D. A., and Wickner, R. B. (2012) [PSI+] prion transmission barriers protect Saccharomyces cerevisiae from infection: Intraspecies "species barriers." *Genetics 190*, 569–579.

(105) Douglas, P. M., Treusch, S., Ren, H. Y., Halfmann, R., Duennwald, M. L., Lindquist, S., and Cyr, D. M. (2008) Chaperone-dependent amyloid assembly protects cells from prion toxicity. *Proc. Natl. Acad. Sci. U. S. A. 105*, 7206–7211.

(106) Huang, H., and Yuan, H. S. (2007) The conserved asparagine in the HNH motif serves an important structural role in metal finger endonucleases. *J. Mol. Biol. 368*, 812–821.

(107) Akada, R., Kitagawa, T., Kaneko, S., Toyonaga, D., Ito, S., Kakihara, Y., Hoshida, H., Morimura, S., Kondo, A., and Kida, K. (2006) PCR-mediated seamless gene deletion and marker recycling in Saccharomyces cerevisiae. *Yeast 23*, 399–405.

(108) Wallace, E. W. J., Kear-Scott, J. L., Pilipenko, E. V., Schwartz, M. H., Laskowski, P. R., Rojek, A. E., Katanski, C. D., Riback, J. A., Dion, M. F., Franks, A. M., Airoldi, E. M., Pan, T., Budnik, B. A., and Drummond, D. A. (2015) Reversible, specific, active aggregates of endogenous proteins assemble upon heat stress. *Cell 162*, 1286–1298.

(109) Tran, J. R., and Brodsky, J. L. (2012) Assays to measure ER-associated degradation in yeast. *Methods Mol Biol. 832*, 505–518.

(110) Rose, M. D., Winston, F., and Hieter, P. (1990) Methods in Yeast Genetics, A Laboratory Course Manual. Cold Spring Harbor Laboratory, in *Biochemistry and Molecular Biology Education*.

(111) Halfmann, R., and Lindquist, S. (2008) Screening for amyloid aggregation by semi-denaturing detergent-agarose gel electrophoresis. *J. Vis. Exp.* e838.

(112) Chakrabortee, S., Byers, J. S., Jones, S., Garcia, D. M., Bhullar, B., Chang, A., She, R., Lee, L., Fremin, B., Lindquist, S., and Jarosz, D. F. (2016) Intrinsically disordered proteins drive emergence and inheritance of biological traits. *Cell 167*, 369-381.e12.

(113) Derkatch, I., Bradley, M.; Zhou, P., Chernoff, Y. and Liebman, S. (1997) Genetic and Environmental Factors Affecting the de novo Appearance of the [PSI+] Prion in Saccharomyces cerevisiae. *Genetics 147*, 507–519.

(114) Chernoff, Y. O., Derkach, I. L., and Inge-Vechtomov, S. G. (1993) Multicopy SUP35 gene induces de-novo appearance of psi-like factors in the yeast Saccharomyces cerevisiae. *Curr. Genet. 24*, 268–270.

(115) Bradley, M. E., Edskes, H. K., Hong, J. Y., Wickner, R. B., and Liebman, S. W. (2002) Interactions among prions and prion "strains" in yeast. *Proc. Natl. Acad. Sci. U. S. A. 99*, 16392–16399.

(116) Arslan, F., Hong, J. Y., Kanneganti, V., Park, S.-K., and Liebman, S. W. (2015) Heterologous Aggregates Promote De Novo Prion Appearance via More than One Mechanism. *PLoS Genet.* (True-Krob, H. L., Ed.) *11*, e1004814.

(117) Foit, L., Morgan, G. J., Kern, M. J., Steimer, L. R., von Hacht, A. A., Titchmarsh, J., Warriner, S. L., Radford, S. E., and Bardwell, J. C. A. (2009) Optimizing protein stability and folding in vivo. *Mol. Cell 36*, 861–871.

(118) Lennon, C. W., Thamsen, M., Friman, E. T., Cacciaglia, A., Sachsenhauser, V., Sorgenfrei, F. A., Wasik, M. A., and Bardwell, J. C. A. (2015) Folding Optimization In Vivo Uncovers New Chaperones. *J. Mol. Biol. 427*, 2983–2994.

(119) Malik, A., Mueller-Schickert, A., and Bardwell, J. C. A. (2014) Cytosolic selection systems to study protein stability. *J. Bacteriol. 196*, 4333–4343.

(120) Mingeot-Leclercq, M.-P., Glupczynski, Y., and Tulkens, P. M. (1999) Aminoglycosides: Activity and Resistance. *Antimicrob. Agents Chemother. 43*, 727–737.

(121) Jena Bioscience. (2020) Nourseothricin Additional Information and List of Selectable Organisms. *https://www.jenabioscience.com/images/b3e879b381/Nourseothricin_information.pdf*.

(122) Van Rosmalen, M., Krom, M., and Merkx, M. (2017) Tuning the Flexibility of Glycine-Serine Linkers to Allow Rational Design of Multidomain Proteins. *Biochemistry 56*, 6565–6574.

(123) Erickson, H. P. (2009) Size and shape of protein molecules at the nanometer level determined by sedimentation, gel filtration, and electron microscopy. *Biol. Proced. Online 11*, 32–51.

(124) Ling, J., Cho, C., Guo, L. T., Aerni, H. R., Rinehart, J., and Söll, D. (2012) Protein Aggregation Caused by Aminoglycoside Action Is Prevented by a Hydrogen Peroxide Scavenger. *Mol. Cell 48*, 713–722.

(125) Kohanski, M. A., Dwyer, D. J., Hayete, B., Lawrence, C. A., and Collins, J. J. (2007) A Common Mechanism of Cellular Death Induced by Bactericidal Antibiotics. *Cell 130*, 797–810.

(126) Kohanski, M. A., Dwyer, D. J., Wierzbowski, J., Cottarel, G., and Collins, J. J. (2008) Mistranslation of Membrane Proteins and Two-Component System Activation Trigger Antibiotic-Mediated Cell Death. *Cell 135*, 679–690.

(127) Kumar, D., Ghosh, A., Taneja, B., and Chakraborty, K. Crystal structure of Nourseothricin acetyltransferase. *submitted*.

(128) Morano, K. A., Grant, C. M., and Moye-Rowley, W. S. (2012) The response to heat shock and oxidative stress in saccharomyces cerevisiae. *Genetics 190*, 1157–1195.

(129) Tomala, K., and Korona, R. (2013) Evaluating the fitness cost of protein expression in saccharomyces cerevisiae. *Genome Biol. Evol. 5*, 2051–2060.

(130) Ferrone, F. (1999) Analysis of protein aggregation kinetics. *Methods Enzymol. 309*, 256–274.

(131) Fink, A. L. (1998) Protein aggregation: Folding aggregates, inclusion bodies and amyloid. *Fold. Des. 3*, 9–23.

(132) Cohen, S. I. A., Vendruscolo, M., Dobson, C. M., and Knowles, T. P. J. (2012) From macroscopic measurements to microscopic mechanisms of protein aggregation. *J. Mol. Biol. 421*, 160–171.

(133) McIsaac, R. S., Silverman, S. J., McClean, M. N., Gibney, P. A., Macinskas, J., Hickman, M. J., Petti, A. A., and Botstein, D. (2011) Fast-acting and nearly gratuitous induction of gene expression and protein depletion in Saccharomyces cerevisiae. *Mol. Biol. Cell 22*, 4447–59.

(134) Roney, I. J., Rudner, A. D., Couture, J. F., and Kærn, M. (2016) Improvement of the reverse tetracycline transactivator by single amino acid substitutions that reduce leaky target gene expression to undetectable levels. *Sci. Rep. 6*, 1–8.

(135) Bellí, G., Garí, E., Piedrafita, L., Aldea, M., and Herrero, E. (1998) An activator/repressor dual system allows tight tetracycline-regulated gene expression in budding yeast. *Nucleic Acids Res. 26*, 942–947.

(136) Ho, B., Baryshnikova, A., and Brown, G. W. (2018) Unification of Protein Abundance Datasets Yields a Quantitative Saccharomyces cerevisiae Proteome. *Cell Syst. 6*, 192-205.e3.

(137) Bartlett, A. I., and Radford, S. E. (2010) Desolvation and Development of Specific Hydrophobic Core Packing during Im7 Folding. *J. Mol. Biol. 396*, 1329–1345.

(138) Ghaemmaghami, S., and Oas, T. G. (2001) Quantitative protein stability measurement in vivo. *Nat. Struct. Biol. 8*, 879–882.

(139) Ignatova, Z., and Gierasch, L. M. (2004) Monitoring protein stability and aggregation in vivo by real-time fluorescent labeling. *Proc. Natl. Acad. Sci. U. S. A. 101*, 523–528.

(140) DePristo, M. A., Weinreich, D. M., and Hartl, D. L. (2005) Missense meanderings in sequence space: a biophysical view of protein evolution. *Nat Rev Genet 6*, 678–687.

(141) Du, X., Li, Y., Xia, Y. L., Ai, S. M., Liang, J., Sang, P., Ji, X. L., and Liu, S. Q. (2016) Insights into protein–ligand interactions: Mechanisms, models, and methods. *Int. J. Mol. Sci. 17*, 1–34.

(142) Wallis, R., Moore, G. R., James, R., and Kleanthous, C. (1995) Protein-Protein Interactions in Colicin E9 DNase-Immunity Protein Complexes. 1. Diffusion-Controlled Association and Femtomolar Binding for the Cognate Complex. *Biochemistry 34*, 13743–13750.

(143) Quan, S., Koldewey, P., Tapley, T., Kirsch, N., Ruane, K. M., Pfizenmaier, J., Shi, R., Hofmann, S., Foit, L., Ren, G., Jakob, U., Xu, Z., Cygler, M., and Bardwell, J. C. A. (2011) Genetic selection designed to stabilize proteins uncovers a chaperone called Spy. *Nat. Struct. Mol. Biol. 18*, 262–269.

(144) Chen, J., Sawyer, N., and Regan, L. (2013) Protein-protein interactions: General trends in the relationship between binding affinity and interfacial buried surface area. *Protein Sci. 22*, 510–515.

(145) Quan, S., Wang, L., Petrotchenko, E. V., Makepeace, K. A. T., Horowitz, S., Yang, J., Zhang, Y., Borchers, C. H., and Bardwell, J. C. A. (2014) Super Spy variants implicate flexibility in chaperone action. *Elife 2014*, e01584.

(146) Stull, F., Koldewey, P., Humes, J. R., Radford, S. E., and Bardwell, J. C. A. (2015) Substrate protein folds while it is bound to the ATP-independent chaperone Spy. *Nat. Struct. Mol. Biol. 23*, 53–58.

(147) Jarosz, D. F., and Khurana, V. (2017) Specification of physiologic and disease states by distinct proteins and protein conformations. *Cell 171*, 1001–1014.

(148) Brookmeyer, R., Johnson, E., Ziegler-Graham, K., and Arrighi, H. M. (2007) Forecasting the global burden of Alzheimer's disease. *Alzheimer's Dement. 3*, 186–191.

(149) Caine, J., Sankovich, S., Antony, H., Waddington, L., Macreadie, P., Varghese, J., and Macreadie, I. (2007) Alzheimer's Aβ fused to green fluorescent protein induces growth stress and a heat shock response. *FEMS Yeast Res. 7*, 1230–1236.

(150) Treusch, S., Hamamichi, S., Goodman, J. L., Matlack, K. E. S. S., Chung, C. Y., Baru, V., Shulman, J. M., Parrado, A., Brooke, J., Valastyan, J. S., Han, H., Lindhagen-Persson, M., Reiman, E. M., Evans, D. A., Bennett, D. A.,

Olofsson, A., Dejager, P. L., Rudolph, E., Caldwell, K. A., Caldwell, G. A., Lindquist, S., Bevis, B. J., Valastyan, J. S., Han, H., Lindhagen-Persson, M., Reiman, E. M., Evans, D. A., Bennett, D. A., Olofsson, A., Dejager, P. L., Tanzi, R. E., Caldwell, K. A., Caldwell, G. A., and Lindquist, S. (2011) Functional links between Aβ toxicity, endocytic trafficking, and Alzheimer's disease risk factors in yeast. *Science. 334*, 1241–1245.

(151) Chen, X., and Petranovic, D. (2015) Amyloid-ß peptide-induced cytotoxicity and mitochondrial dysfunction in yeast. *FEMS Yeast Res. 15*, 1–10.

(152) Keller, J. N., Hanni, K. B., and Markesbery, W. R. (2000) Impaired proteasome function in Alzheimer's disease. *J. Neurochem. 75*, 436–439.

(153) Cohen, S. I. A., Linse, S., Luheshi, L. M., Hellstrand, E., White, D. A., Rajah, L., Otzen, D. E., Vendruscolo, M., Dobson, C. M., and Knowles, T. P. J. (2013) Proliferation of amyloid-β42 aggregates occurs through a secondary nucleation mechanism. *Proc. Natl. Acad. Sci. U. S. A. 110*, 9758–9763.

(154) Opoku-Nsiah, K. A., and Gestwicki, J. E. (2018) Aim for the core: suitability of the ubiquitin-independent 20S proteasome as a drug target in neurodegeneration. *Transl. Res. 198*, 48–57.

(155) Lashuel, H. A., Overk, C. R., Oueslati, A., and Masliah, E. (2013) The many faces of α-synuclein: From structure and toxicity to therapeutic target. *Nat. Rev. Neurosci. 14*, 38–48.

(156) Yeger-Lotem, E., Riva, L., Su, L. J., Gitler, A. D., Cashikar, A. G., King, O. D., Auluck, P. K., Geddie, M. L., Valastyan, J. S., Karger, D. R., Lindquist, S., and Fraenkel, E. (2009) Bridging high-throughput genetic and transcriptional data reveals cellular responses to alpha-synuclein toxicity. *Nat. Genet. 41*, 316–323.

(157) Gitler, A. D., Bevis, B. J., Shorter, J., Strathearn, K. E., Hamamichi, S., Su, L. J., Caldwell, K. A., Caldwell, G. A., Rochet, J. C., McCaffery, J. M., Barlowe, C., and Lindquist, S. (2008) The Parkinson's disease protein α-synuclein disrupts cellular Rab homeostasis. *Proc. Natl. Acad. Sci. U. S. A. 105*, 145–150.

(158) Tardiff, D. F., Jui, N. T., Khurana, V., Tambe, M. A., Thompson, M. L., Chung, C. Y., Kamadurai, H. B., Kim, H. T., Lancaster, A. K., Caldwell, K. A., Caldwell, G. A., Rochet, J.-C., Buchwald, S. L., and Lindquist, S. (2013) Yeast Reveal a "Druggable" Rsp5/Nedd4 Network that Ameliorates -Synuclein Toxicity in Neurons. *Science. 342*, 979–983.

(159) Conway, K. A., Lee, S.-J., Rochet, J.-C., Ding, T. T., Williamson, R. E., and Lansbury, P. T. (2000) Acceleration of oligomerization, not fibrillization, is a shared property of both alpha -synuclein mutations linked to early-onset Parkinson's disease: Implications for pathogenesis and therapy. *Proc. Natl. Acad. Sci. 97*, 571–576.

(160) Fredenburg, R. A., Rospigliosi, C., Meray, R. K., Kessler, J. C., Lashuel, H. A., Eliezer, D., and Lansbury, P. T. (2007) The impact of the E46K mutation on the properties of α-synuclein in its monomelic and oligomeric states. *Biochemistry 46*, 7107–7118.

(161) Lemkau, L. R., Comellas, G., Kloepper, K. D., Woods, W. S., George, J. M., and Rienstra, C. M. (2012) Mutant protein A30P α-synuclein adopts wild-type fibril structure, despite slower fibrillation kinetics. *J. Biol. Chem. 287*, 11526–11532.

(162) Li, J., Uversky, V. N., and Fink, A. L. (2001) Effect of familial Parkinson's disease point mutations A30P and A53T on the structural properties, aggregation, and fibrillation of human α-synuclein. *Biochemistry 40*, 11604–11613.

(163) Lashuel, H. A., Petre, B. M., Wall, J., Simon, M., Nowak, R. J., Walz, T., and Lansbury, P. T. (2002) A-Synuclein, Especially the Parkinson'S Disease-Associated Mutants, Forms Pore-Like Annular and Tubular Protofibrils. *J. Mol. Biol. 322*, 1089–1102.

(164) Flagmeier, P., Meisl, G., Vendruscolo, M., Knowles, T. P. J., Dobson, C. M., Buell, A. K., and Galvagnion, C. (2016) Mutations associated with familial Parkinson's disease alter the initiation and amplification steps of α-synuclein aggregation. *Proc. Natl. Acad. Sci. U. S. A. 113*, 10328–10333.

(165) Dixon, C., Mathias, N., Zweig, R. M., Davis, D. A., and Gross, D. S. (2005) alpha-synuclein targets the plasma membrane via the secretory pathway and induces toxicity in yeast. *Genetics 170*, 47–59.

(166) Jo, E., Fuller, N., Rand, R. P., St George-Hyslop, P., and Fraser, P. E. (2002) Defective membrane interactions of familial Parkinson's disease mutant A30P α-Synuclein. *J. Mol. Biol. 315*, 799–807.

(167) Laine, R. F., Sinnige, T., Ma, K. Y., Haack, A. J., Poudel, C., Gaida, P., Curry, N., Perni, M., Nollen, E. A. A., Dobson, C. M., Vendruscolo, M., Kaminski Schierle, G. S., and Kaminski, C. F. (2019) Fast fluorescence lifetime imaging reveals the aggregation processes of α-synuclein and polyglutamine in aging Caenorhabditis elegans. *ACS Chem. Biol. 14*, 1628–1636.

(168) Chen, S. W., Drakulic, S., Deas, E., Ouberai, M., Aprile, F. A., Arranz, R., Ness, S., Roodveldt, C., Guilliams, T., De-Genst, E. J., Klenerman, D., Wood, N. W., Knowles, T. P. J., Alfonso, C., Rivas, G., Abramov, A. Y., Valpuesta, J. M., Dobson, C. M., and Cremades, N. (2015) Structural characterization of toxic oligomers that are kinetically trapped during α-synuclein fibril formation. *Proc. Natl. Acad. Sci. 112*, E1994–E2003.

(169) Shin, Y., and Brangwynne, C. P. (2017) Liquid phase condensation in cell physiology and disease. *Science. 357*, eaaf4382.

(170) Soto, C. (2012) Transmissible Proteins: Expanding the Prion Heresy. *Cell 149*, 968–977.

(171) Harvey, Z. H., Chen, Y., and Jarosz, D. F. (2018) Protein-based inheritance: epigenetics beyond the chromosome. *Mol. Cell 69*, 195–202.

(172) Doronina, V. A., Staniforth, G. L., Speldewinde, S. H., Tuite, M. F., and Grant, C. M. (2015) Oxidative stress conditions increase the frequency of de novo formation of the yeast [PSI+] prion. *Mol. Microbiol. 96*, 163–174.

(173) Wickner, R. B., Shewmaker, F. P., Bateman, D. A., Edskes, H. K., Gorkovskiy, A., Dayani, Y., and Bezsonov, E. E. (2015) Yeast Prions: Structure, Biology, and Prion-Handling Systems. *Microbiol. Mol. Biol. Rev. 79*, 1–17.

(174) Derkatch, I. L., Chernoff, Y. O., Kushnirov, V. V., Inge-Vechtomov, S. G., and Liebman, S. W. (1996) Genesis and variability of [PSI] prion factors in Saccharomyces cerevisiae. *Genetics 144*, 1375–1386.

(175) Bagriantsev, S. N., Kushnirov, V. V., and Liebman, S. W. (2006) Analysis of Amyloid Aggregates Using Agarose Gel Electrophoresis. *Methods Enzymol. 412*, 33–48.

(176) Sondheimer, N., and Lindquist, S. (2000) Rnq1: An epigenetic modifier of protein function in yeast. *Mol. Cell 5*, 163–172.

(177) Alberti, S., Halfmann, R., King, O., Kapila, A., and Lindquist, S. (2009) A Systematic Survey Identifies Prions and Illuminates Sequence Features of Prionogenic Proteins. *Cell 137*, 146–158.

(178) Liebman, S. W., and Chernoff, Y. O. (2012) Prions in yeast. *Genetics 191*, 1041–1072.

(179) Tyedmers, J., Mogk, A., and Bukau, B. (2010) Cellular strategies for controlling protein aggregation. *Nat. Rev. Mol. Cell Biol. 11*, 777–788.

(180) Franzmann, T. M., Jahnel, M., Pozniakovsky, A., Mahamid, J., Holehouse, A. S., Nüske, E., Richter, D., Baumeister, W., Grill, S. W., Pappu, R. V, Hyman, A. A., and Alberti, S. (2018) Phase separation of a yeast prion protein promotes cellular fitness. *Science. 359*, eaao5654.

(181) Derkatch, I. L., Bradley, M. E., Hong, J. Y., and Liebman, S. W. (2001) Prions Affect the Appearance of Other Prions : The Story of [PIN] University of Illinois at Chicago. *Cell 106*, 171–182.

(182) Huang, V. J., Stein, K. C., and True, H. L. (2013) Spontaneous Variants of the [RNQ+] Prion in Yeast Demonstrate the Extensive Conformational Diversity Possible with Prion Proteins. *PLoS One 8*, 1–14.

(183) Zhou, P., Derkatch, I. L., and Liebman, S. W. (2001) The relationship between visible intracellular aggregates that appear after overexpression of Sup35 and the yeast prion-like elements [PSI+] and [PIN+]. *Mol. Microbiol. 39*, 137–46.

(184) McGlinchey, R. P., Kryndushkin, D., and Wickner, R. B. (2011) Suicidal [PSI+] is a lethal yeast prion. *Proc. Natl. Acad. Sci. U. S. A. 108*, 5337–5341.

(185) Treusch, S., and Lindquist, S. (2012) An intrinsically disordered yeast prion arrests the cell cycle by sequestering a spindle pole body component. *J. Cell Biol. 197*, 369–379.

(186) Tong, A. H. Y. (2001) Systematic Genetic Analysis with Ordered Arrays of Yeast Deletion Mutants. *Science. 294*, 2364–2368.

(187) Michel, A. H., Hatakeyama, R., Kimmig, P., Arter, M., Peter, M., Matos, J., De Virgilio, C., and Kornmann, B. (2017) Functional mapping of yeast genomes by saturated transposition. *Elife 6*, 1–28.

(188) Guo, X., Chavez, A., Tung, A., Chan, Y., Kaas, C., Yin, Y., Cecchi, R., Garnier, S. L., Kelsic, E. D., Schubert, M., DiCarlo, J. E., Collins, J. J., and Church, G. M. (2018) High-throughput creation and functional profiling of DNA sequence variant libraries using CRISPR–Cas9 in yeast. *Nat. Biotechnol. 36*, 540–546.

(189) Ho, C. H., Magtanong, L., Barker, S. L., Gresham, D., Nishimura, S., Natarajan, P., Koh, J. L. Y., Porter, J., Gray, C. A., Andersen, R. J., Giaever, G., Nislow, C., Andrews, B., Botstein, D., Graham, T. R., Yoshida, M., and Boone, C. (2009) A molecular barcoded yeast ORF library enables mode-of-action analysis of bioactive compounds. *Nat. Biotechnol. 27*, 369–377.

(190) Guo, X., Chavez, A., Tung, A., Chan, Y., Kaas, C., Yin, Y., Cecchi, R., Garnier, S. L., Kelsic, E. D., Schubert, M., DiCarlo, J. E., Collins, J. J., and Church, G. M. (2018) High-throughput creation and functional profiling of DNA sequence variant libraries using CRISPR–Cas9 in yeast. *Nat. Biotechnol. 36*, 540–546.

(191) Musso, G., Costanzo, M., Huangfu, M. Q., Smith, A. M., Paw, J., San Luis, B. J., Boone, C., Giaever, G., Nislow, C., Emili, A., and Zhang, Z. (2008) The extensive and condition-dependent nature of epistasis among whole-genome duplicates in yeast. *Genome Res. 18*, 1092–1099.

(192) Li, J., Yuan, Z., and Zhang, Z. (2010) The Cellular Robustness by Genetic Redundancy in Budding Yeast. *PLoS Genet.* (Zhang, J., Ed.) *6*, e1001187.

(193) Tripathi, N. K., and Shrivastava, A. (2019) Recent Developments in Bioprocessing of Recombinant Proteins: Expression Hosts and Process Development. *Front. Bioeng. Biotechnol. 7*.

(194) King, O. D., Gitler, A. D., and Shorter, J. (2012) The tip of the iceberg: RNA-binding proteins with prion-like domains in neurodegenerative disease. *Brain Res. 1462*, 61–80.

(195) Kwiatkowski, T. J., Bosco, D. A., LeClerc, A. L., Tamrazian, E., Vanderburg, C. R., Russ, C., Davis, A., Gilchrist, J., Kasarskis, E. J., Munsat, T., Valdmanis, P., Rouleau, G. A., Hosler, B. A., Cortelli, P., de Jong, P. J., Yoshinaga, Y., Haines, J. L., Pericak-Vance, M. A., Yan, J., Ticozzi, N., Siddique, T., McKenna-Yasek, D., Sapp, P. C., Horvitz, H. R., Landers, J. E., and Brown, R. H. (2009) Mutations in the FUS/TLS Gene on Chromosome 16 Cause Familial Amyotrophic Lateral Sclerosis. *Science. 323*, 1205–1208.

(196) Sun, Z., Diaz, Z., Fang, X., Hart, M. P., Chesi, A., Shorter, J., and Gitler, A. D. (2011) Molecular Determinants and Genetic Modifiers of Aggregation and Toxicity for the ALS Disease Protein FUS/TLS. *PLoS Biol.* (Weissman, J. S., Ed.) *9*, e1000614.

(197) Lindström, M., and Liu, B. (2018) Yeast as a Model to Unravel Mechanisms Behind FUS Toxicity in Amyotrophic Lateral Sclerosis. *Front. Mol. Neurosci. 11*, 1–10.

(198) Ju, S., Tardiff, D. F., Han, H., Divya, K., Zhong, Q., Maquat, L. E., Bosco, D. A., Hayward, L. J., Brown, R. H., Lindquist, S., Ringe, D., and Petsko, G. A. (2011) A Yeast Model of FUS/TLS-Dependent Cytotoxicity. *PLoS Biol.* (Weissman, J. S., Ed.) *9*, e1001052.

(199) Ter-Avanesyan, M. D., Dagkesamanskaya, A. R., Kushnirov, V. V., and Smirnov, V. N. (1994) The SUP35 omnipotent suppressor gene is involved in the maintenance of the non-Mendelian determinant [psi+] in the yeast Saccharomyces cerevisiae. *Genetics 137*, 671–676.

(200) Parham, S. N., Resende, C. G., and Tuite, M. F. (2001) Oligopeptide repeats in the yeast protein Sup35p stabilize intermolecular prion interactions. *EMBO J. 20*, 2111–2119.

(201) Paul, K. R., Hendrich, C. G., Waechter, A., Harman, M. R., and Ross, E. D. (2015) Generating new prions by

targeted mutation or segment duplication. *Proc. Natl. Acad. Sci. U. S. A. 112*, 8584–8589.

(202) Wickner, R. B., and Kelly, A. C. (2016) Prions are affected by evolution at two levels. *Cell. Mol. Life Sci. 73*, 1131–1144.

(203) Chernova, T. A., Chernoff, Y. O., and Wilkinson, K. D. (2017) Prion-based memory of heat stress in yeast. *Prion 11*, 151–161.

(204) Fowler, D. M., Koulov, A. V., Balch, W. E., and Kelly, J. W. (2007) Functional amyloid – from bacteria to humans. *Trends Biochem. Sci. 32*, 217–224.

(205) Fioriti, L., Myers, C., Huang, Y.-Y., Li, X., Stephan, J. S., Trifilieff, P., Colnaghi, L., Kosmidis, S., Drisaldi, B., Pavlopoulos, E., and Kandel, E. R. (2015) The Persistence of Hippocampal-Based Memory Requires Protein Synthesis Mediated by the Prion-like Protein CPEB3. *Neuron 86*, 1433–1448.